

<https://doi.org/10.15388/vu.thesis.725>

<https://orcid.org/0009-0001-6568-0428>

VILNIUS UNIVERSITY

Rapolas Jamontas

Demodification by TudS Proteins: from Individual Thionucleobases to Intact tRNA

DOCTORAL DISSERTATION

Natural Sciences,
Biochemistry (N 004)

VILNIUS 2025

This dissertation was prepared between 2020 and 2024 at Vilnius University, Life Sciences Center, Institute of Biochemistry, Department of Molecular Microbiology and Biotechnology.

Academic Supervisors:

Dr. Agota Aučynaitė (Vilnius University, Natural Sciences, Biochemistry – N 004); from 2023-12-19 to 2024-09-30.

Prof. Dr. Rolandas Meškys (Vilnius University, Natural Sciences, Biochemistry – N 004); from 2020-10-01 to 2023-12-18.

Academic consultants:

Prof. Dr. Rolandas Meškys (Vilnius University, Natural Sciences, Biochemistry – N 004); from 2023-12-19 to 2024-09-30.

Dr. Agota Aučynaitė (Vilnius University, Natural Sciences, Biochemistry – N 004); from 2020-10-01 to 2023-12-18.

Chairman – Prof. Dr. Eglė Lastauskienė (Vilnius University, Natural Sciences, Biology – N 010).

Members:

Dr. Dukas Jurėnas (Free University of Brussels, Belgium, Natural Sciences, Biochemistry – N 004);

Dr. Patrick Pausch (Vilnius University, Natural Sciences, Biochemistry – N 004);

Dr. Jūratė Skerniškytė (Vilnius University, Natural Sciences, Biochemistry – N 004);

Dr. Miglė Tomkuvienė Vilnius University, Natural Sciences, Biochemistry – N 004).

The dissertation shall be defended at a public meeting of the Dissertation Defence Panel at 10:00 AM on 6th February 2025 in Room R401 of the Vilnius University Life Sciences Centre.

Address: Saulėtekio al. 7-R401, Vilnius, LT-10257

Tel. +37065639405; e-mail: rapolas.jamontas@gmc.vu.lt

The text of this dissertation can be accessed at the library of Vilnius University, as well as on the website of Vilnius University:

www.vu.lt/lt/naujienos/ivykiu-kalendorius

<https://doi.org/10.15388/vu.thesis.725>

<https://orcid.org/0009-0001-6568-0428>

VILNIAUS UNIVERSITETAS

Rapolas Jamontas

TudS baltymai: nuo tionukleobazių iki tRNR demodifikacijos

DAKTARO DISERTACIJA

Gamtos mokslai,
Biochemija (N 004)

VILNIUS 2025

Disertacija rengta 2020–2024 metais Vilniaus universiteto Gyvybės mokslų centre, Biochemijos institute, Molekulinės mikrobiologijos ir biotechnologijos skyriuje.

Moksliniai vadovai:

dr. Agota Aučynaitė (Vilniaus universitetas, gamtos mokslai, biochemija – N 004). Nuo 2023-12-19 iki 2024-09-30;

prof. dr. Rolandas Meškys (Vilniaus universitetas, gamtos mokslai, biochemija – N 004) Nuo 2020-10-01 iki 2023-12-18.

Moksliniai konsultantai:

prof. dr. Rolandas Meškys (Vilniaus universitetas, gamtos mokslai, biochemija – N 004). Nuo 2023-12-19 iki 2024-09-30;

dr. Agota Aučynaitė (Vilniaus universitetas, gamtos mokslai, biochemija – N 004) Nuo 2020-10-01 iki 2023-12-18.

Gynimo taryba:

Pirmininkė – prof. dr. Eglė Lastauskienė (Vilniaus universitetas, gamtos mokslai, biologija – N 010).

Nariai:

dr. Dukas Jurėnas (Laisvasis Briuselio Universitetas, Belgija, gamtos mokslai, biochemija – N 004),

dr. Patrick Pausch (Vilniaus universitetas, gamtos mokslai, biochemija – N 004),

dr. Jūratė Skerniškytė (Vilniaus universitetas, gamtos mokslai, biochemija – N 004,)

dr. Miglė Tomkuvienė (Vilniaus universitetas, gamtos mokslai, biochemija – N 004).

Disertacija ginama viešame Gynimo tarybos posėdyje 2025 m. vasario mėn. 6 d. 10:00 val. Vilniaus universiteto Gyvybės mokslų centro R401 auditorijoje. Adresas: Saulėtekio al. 7-R401, Vilnius, LT-10257, tel. +37065639405 el. paštas rapolas.jamontas@gmc.vu.lt

Disertaciją galima peržiūrėti Vilniaus universiteto bibliotekoje ir Vilniaus universiteto interneto svetainėje adresu: <https://www.vu.lt/naujienos/ivykiu-kalendorius>

CONTENTS

CONTENTS	5
ABBREVIATIONS.....	8
INTRODUCTION.....	9
SCIENTIFIC NOVELTY AND PRACTICAL VALUE	10
Major findings presented for defence of this thesis.....	11
1. LITERATURE OVERVIEW	12
1.1 tRNA life cycle	12
1.1.1 tRNA gene structure and processing in bacteria	12
1.1.2 tRNA modifications	13
1.1.3 tRNA modification erasers and editors	16
1.1.4 tRNA degradation	18
1.1.5 RNA recycling	19
1.1.6 The fate of modified nucleosides	19
1.2 4-Thiouridine	21
1.2.1 4-Thiouridine impact on tRNA stability	21
1.2.2 4-Thiouridine impact on incorporation of other modifications.....	22
1.2.3 4-Thiouridine and tRNA quality control.....	22
1.2.4 4-Thiouridine as a bacterial UV sensor.....	24
1.2.5 Applications of 4-thiouridine	27
1.2.6 4-thiouridine synthesis	29
1.2.7 Diversity of ThiI enzymes.....	31
1.3 Iron-sulfur proteins	35
1.3.1 Iron-sulfur proteins	35
1.3.2 Iron-sulfur cluster biogenesis.....	36
1.3.3 Regulation of iron-sulfur cluster synthesis by IscR	37
1.3.4 [4Fe-4S] proteins in non-redox catalysis	38
1.4 TudS desulfidases	40
1.4.1 Discovery of TudS desulfidases.....	40

1.4.2	Catalysis by TudS	40
1.4.3	Distribution of TudS domain-containing proteins	41
2.	MATERIALS AND METHODS	43
2.1	Materials.....	43
2.1.1.	Nucleic acids	43
2.1.2.	Proteins, kits and chemicals	43
2.1.3.	Bacterial strains.....	43
2.2	Methods.....	45
2.2.1.	Construction of bacterial expression vectors	45
2.2.2.	Cultivation of bacteria and overexpression of recombinant proteins.	45
2.2.3.	<i>Pseudomonas putida</i> KT2440 mutant strains.....	48
2.2.4.	Purification of recombinant proteins.....	48
2.2.5.	Enzymatic activity assays	50
2.2.6.	Bulk tRNA isolation.....	51
2.2.7.	tRNA nucleoside analysis	51
2.2.8.	Western blot.....	52
2.2.9.	Electrophoretic mobility shift assay (EMSA).....	53
2.2.10.	Ultraviolet A (UVA) irradiation experiments.....	53
2.2.11.	Phylogenetic analysis.....	54
2.2.12.	Modelling and molecular dynamic simulations	54
3.	RESULTS AND DISCUSSION.....	56
3.1.	Function of stand-alone TudS domain-containing proteins	56
3.1.1.	TudS orthologs share a phenotype in vivo.....	56
3.1.2.	Uracil auxotrophic <i>Pseudomonas putida</i> KT2440 utilize exogenous 4-thiouracil(uridine).....	58
3.1.3.	TudS-deficient cell growth is inhibited by 4-thiouracil(uridine)	60
3.1.4.	TudS enzymes are monomeric 4-thio-UMP desulfidases	61
3.1.5.	TudS does not affect 4-thiouridine content in tRNA	65
3.2.	Function of RudS (TudS-DUF1722) proteins.....	68
3.2.1	TudS and RudS do not share phenotypes in vivo.....	68

3.2.2	Phylogenetic analysis indicates a link between ThiI and RudS	71
3.2.3	tRNA desulfidation activity of RudS in vivo	73
3.2.4	The [4Fe-4S] cluster is necessary for RudS function.....	75
3.2.5	Recombinant RudS_KT is active in vitro	77
3.2.6	RudS_KT-tRNA interaction mechanism	80
3.2.7	Overexpression of RudS_KT in <i>E. coli</i> diminishes UVA-triggered growth delay	89
4.	DISCUSSION.....	90
	CONCLUSIONS	96
	REFERENCES	97
	APPENDICES.....	113
	ACKNOWLEDGEMENTS	120
	LIST OF PUBLICATIONS.....	121
	CONFERENCE PRESENTATIONS	121
	CURRICULUM VITAE	122
	SANTRAUKA	125
1.	SANTRUMPOS	125
2.	ĮVADAS	126
3.	METODAI.....	129
4.	REZULTATAI	130
4.2	TudS funkcijos tyrimas	130
4.2	RudS funkcijos tyrimas	135
5.	IŠVADOS.....	141
	NOTES	142

ABBREVIATIONS

4-thio-UMP	4-thiouridine-5'-monophosphate
4-thio-UTP	4-thiouridine-5'-triphosphate
DEPC	Diethyl pyrocarbonate
DUF1722	Domain of unknown function 1722
DUF523	Domain of unknown function 523
EMSA	Electrophoretic mobility shift assay
FeS	Iron-sulfur (cluster)
FNR	Fumarate and nitrate reductase transcriptional activator
FOA	5-fluoroorotic acid
FPLC	Fast protein liquid chromatography
HPLC-MS/MS	High performance liquid chromatography-tandem mass spectrometry
HRP	Horseradish peroxidase
IPTG	Isopropyl β -D-1-thiogalactopyranoside
ISC	Iron-sulfur cluster (synthesis pathway)
NFLD	N-terminal ferredoxin-like domain
PDBID	Protein Data Bank ID
PNPase	Polynucleotide phosphorylase
ppGpp	Guanosine tetraphosphate
pppGpp	Guanosine pentaphosphate
RBS	Ribosome-binding site
RHD	C-terminal rhodanese-like domain
s4U	4-thiouridine
THUMP	Thiouridine synthase, RNA methylase, and pseudouridine synthase tRNA binding domain
TRAMP	Trf4/Air2/Mtr4p polyadenylation complex
UHPLC	Ultra high-performance liquid chromatography
UPLC	Ultra performance liquid chromatography
UVA	320-400 nm UV radiation
UVB	280-320 nm UV radiation
UVC	100-280 nm UV radiation

INTRODUCTION

The diversity of functions and structural features of nucleic acids requires them to extend beyond canonical components and interactions. One of the most remarkable examples of this phenomenon is the transfer RNA (tRNA) molecules. As an integral part of protein synthesis, these diverse yet structurally similar molecules exhibit unique properties, allowing them to participate in multiple highly specific interactions, thereby contributing to the continuous maintenance of life. The uniqueness of different tRNAs is largely attributed to nucleotide modifications, of which more than 100 are known to date. These post-transcriptional modifications enable tRNA molecules to achieve proper folding, maintain thermodynamic stability, decode messenger RNA (mRNA) codons with high accuracy, and act as discriminating factors for interacting molecules.

In addition to the common functions mentioned above, some post-transcriptional modifications equip tRNA with unique properties beyond simply being a workhorse of protein translation. One such modification, 4-thiouridine (s4U), is conserved in prokaryotes. Like many other modifications, it enhances tRNA stability, contributing to proper folding and function. Additionally, it also plays a role in bacterial tRNA quality control mechanisms, and s4U's unique photoreactivity enables it to act as a UV sensor, absorbing UVA light and triggering bacterial stress responses. This ability emphasizes the adaptive significance of s4U in bacterial survival under varying environmental conditions.

Although tRNA molecules are not the most abundant RNA species by mass, they outnumber any other known RNA species. Despite their relative stability, tRNA molecules can undergo degradation, releasing a plethora of modified nucleosides. Unlike the well-established degradation and salvage pathways for canonical nucleosides, the metabolic fate of modified nucleosides remains largely understudied. However, new pathways and enzymes involved in modified nucleotide catabolism are being discovered.

TudS, which catalyzes the conversion of 4-thiouracil to canonical uracil, is one of the recently discovered enzymes (previously – Domain of Unknown Function 523) involved in modified nucleotide catabolism. Up until the experiments presented in this thesis, neither the physiological functions nor the substrate spectrum of TudS were known. Furthermore, TudS is often fused with DUF1722 – another domain of formerly unknown function.

The aim of this work was to provide insight into the biochemical properties of both TudS and TudS-DUF1722 (RudS) proteins and their possible physiological functions.

The objectives of this study were:

1. To identify the substrate preference of TudS proteins.
2. To establish a possible physiological role of TudS in bacteria.
3. To identify the activity of RudS (TudS-DUF1722) proteins.
4. To identify the catalytic mechanism of RudS proteins.
5. To identify the RudS-tRNA binding mechanism.
6. To establish a possible physiological role of RudS in bacteria.

SCIENTIFIC NOVELTY AND PRACTICAL VALUE

In the present thesis, two widespread prokaryotic TudS domain-containing proteins, TudS and RudS, were biochemically characterized and their physiological roles in thiomodified nucleotide recycling and the bacterial UV-stress response were suggested. Additionally, a tRNA binding function was proposed for the previously uncharacterized Domain of Unknown Function 1722 (DUF1722) domain, which is part of the RudS protein. These findings expand our understanding of enzymes involved in modified nucleotide catabolism and tRNA de-modification.

The widespread prokaryotic stand-alone TudS domain proteins were identified as 4-thio-UMP desulfidases, contributing to the understudied field of modified nucleotide catabolism. To the best of our knowledge, no other enzymes involved in the salvage of thiomodified nucleotides were known to date. Moreover, it was demonstrated that TudS supports bacterial growth by utilizing exogenous 4-thiouracil-containing compounds as a uracil source, some of which are toxic to bacteria, thereby concurrently detoxifying their environment.

The antimicrobial properties of 4-thiouridine have been previously established (1). In this study, it was demonstrated that while 4-thiouracil and 4-thiouridine can inhibit the growth of certain wild-type bacteria, the knockout of the *tudS* gene completely abolishes the bacterial growth in the presence of 4-thiouridine. A combination of a yet-to-be-discovered TudS inhibitor and 4-thiouridine may be applied as a broad-spectrum antimicrobial or bacteriostatic agents in the future.

RudS, a fusion protein containing TudS and DUF1722 domains, was identified as a tRNA 4-thiouridine de-modifying enzyme. This is the first identified bacterial tRNA de-modifying enzyme that acts on a specific site. Furthermore, RudS proteins are the first tRNA de-modifying enzymes possessing non-demethylase activity across all domains of life. Proof-of-concept experiments conducted in this study indicated that RudS is

involved in the prokaryotic UV-stress response and may well contribute to bacterial adaptation to UV radiation.

Ultraviolet radiation is a widely used disinfection technique. Along with monochromatic UVC disinfection, a combination of UVA, UVB, and UVC is also applied (2). The fundamental knowledge of the regulation of s4U, a bacterial UVA sensor located in tRNA, by RudS proteins should be considered when employing UV radiation for disinfection of certain bacterial species.

MAJOR FINDINGS PRESENTED FOR DEFENCE OF THIS THESIS

1. TudS proteins catalyze the desulfidation of 4-thiouracil derivatives, with the highest activity towards 4-thio-UMP.
2. TudS proteins allow bacteria to salvage 4-thiouracil containing compounds as a source of uracil.
3. RudS (TudS-DUF1722) functions as a tRNA 4-thiouridine de-modification enzyme.
4. RudS activity depends on [4Fe-4S] cluster and the catalytic mechanism is shared with TudS.
5. The DUF1722 domain of RudS mediates tRNA-binding, by interacting with the anticodon arm, while the TudS domain interacts with the variable loop, acceptor stem, and D arm of the tRNA.
6. RudS allows bacteria to overcome UVA-caused growth delay.

1. LITERATURE OVERVIEW

1.1 tRNA life cycle

Transfer RNA (tRNA) is a molecule found across all domains of life that acts as a direct link between messenger RNA (mRNA) and the amino acid sequence of translated proteins. tRNA transports specific amino acids to the ribosome, where it recognizes the appropriate codon of mRNA, resulting in the elongation of the ribosome-associated polypeptide chain (3).

1.1.1 tRNA gene structure and processing in bacteria

Genes encoding tRNAs in the bacterial chromosome are often found in clusters. In addition to clusters containing just tRNA genes, they can also contain ribosomal RNA genes or code for translation-associated proteins such as elongation factor Tu. Besides the genes encoding different tRNA species, it is also common for bacteria to have multiple copies of a single tRNA species.

tRNA genes range from 75 to 90 base pairs in length, and the transcribed precursors are typically longer than a mature molecule. Nucleotide sequences between different tRNA species vary significantly; however, all of them contain four or five inverted repeats (Figure 1A) that form stem-loop elements within the secondary cloverleaf structure (Figure 1B). Additionally, unlike in eukaryotes, bacterial tRNA precursors already contain a 3' CCA sequence acting as an aminoacylation site (4). To take their final shape, become recognizable by aminoacyl-tRNA synthetases, and participate in translation, tRNA transcripts must undergo maturation (5).

tRNA transcripts may be polycistronic and contain multiple tRNAs. Additionally, each tRNA precursor usually contains extra nucleotides at both the 5' and 3' termini. The endonucleolytic cleavage of these fragments occurs even before transcription is terminated (5). If the transcript contains a single tRNA, the ribozyme RNase P alone is sufficient for the maturation of the 5' end. However, if the transcript contains multiple tRNA sequences, other endoribonucleases such as RNase E and RNase III may be required to generate smaller tRNA precursors (4). Maturation of the 3' end typically involves multiple steps. First, the transcript is endonucleolytically cleaved downstream of the CCA terminus, followed by exonucleolytic trimming of the 3' end by a combination of RNase E and RNase III (6). A simplified bacterial tRNA maturation scheme is depicted in Figure 1C.

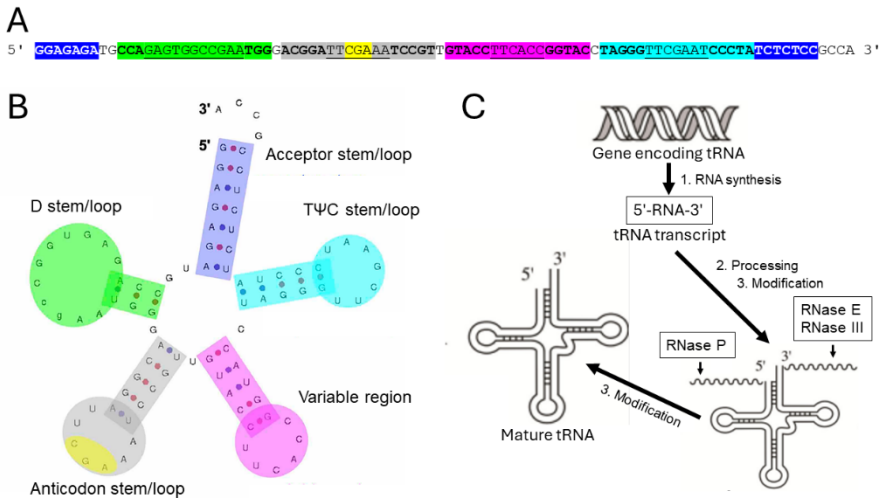


Figure 1. A: tRNA gene of *Pseudomonas fluorescens* SBW24 tRNA-Ser(CGA). Nucleotides in bold represent inverted repeats forming stems in the secondary structure; underlined nucleotides represent loop-forming nucleotides. Colors represent structural features of the secondary structure (blue: acceptor stem; green: D stem/loop; grey: anticodon stem/loop; yellow: anticodon; pink: variable region; turquoise: TΨC stem/loop). **B:** Secondary structure of *Pseudomonas fluorescens* SBW24 tRNA-Ser(CGA). Colors of structural features correspond to those depicted in A. **C:** Simplified bacterial tRNA biogenesis scheme. A and B were adapted from (7), C was adapted from (4).

1.1.2 tRNA modifications

There are over 140 known tRNA sequences across bacteria, most of which share a high level of structural conservation (8). However, the complexity of processes involving tRNA requires these molecules to interact very specifically with a wide diversity of molecules, such as ribosomes, elongation factors, mRNAs, and aminoacyl-tRNA synthetases (9). To achieve this, nucleotides in tRNA molecules are modified post-transcriptionally by altering their bases and/or sugar moieties, thus diversifying their structures (9). In fact, tRNAs are the most modified molecules among all nucleic acids. Over 100 different modified nucleosides found in tRNA across all domains of life have been identified to date (10), with bacterial tRNAs usually containing 6-10 modifications and an average of 8 modifications per molecule (Figure 2) (11). These modifications contribute to proper mRNA decoding, serve as determinants for tRNA recognition, and maintain tRNA structure (12).

The anticodon stem-loop is the most frequently modified element of the tRNA. It is directly involved in the translation process and is responsible for codon recognition within mRNA, enabling the ribosome to accurately synthesize proteins (13). The standard 20 proteinogenic amino acids are

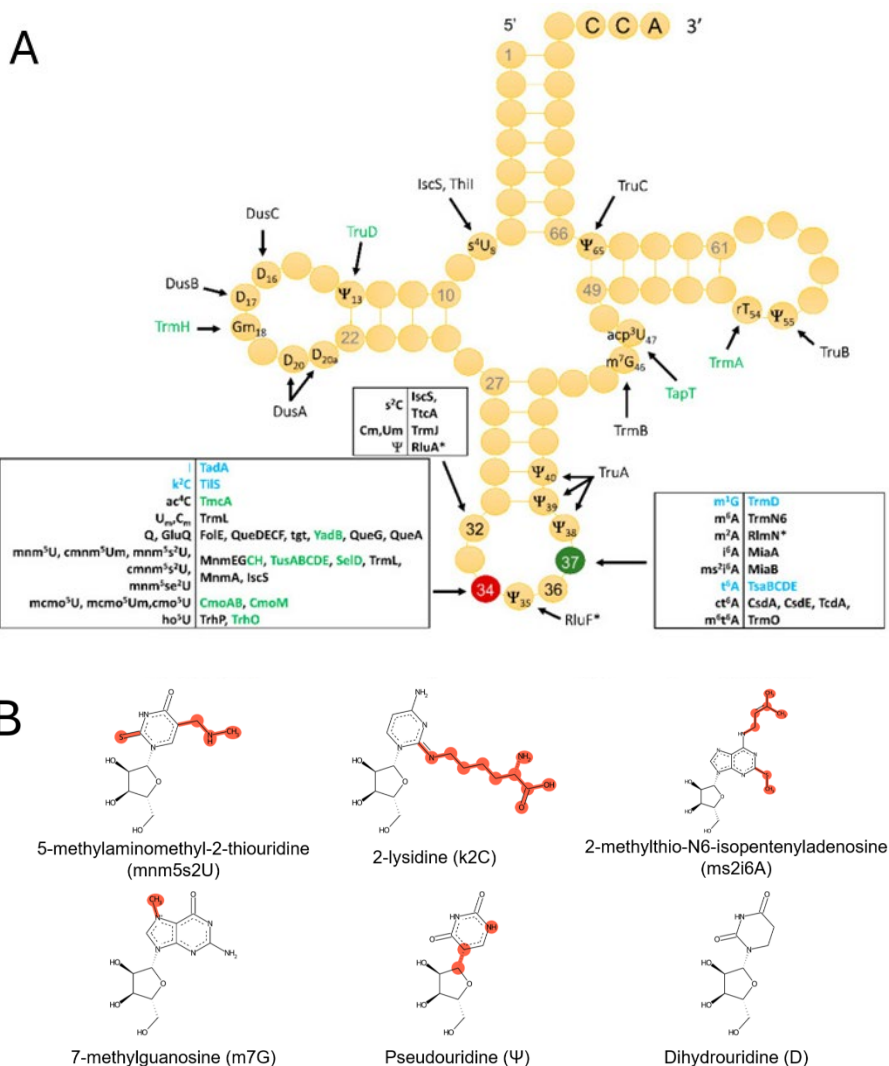


Figure 2. A: Positions of *Escherichia coli* tRNA modifications, modification types, and responsible modifying enzymes. **B:** Structures of modified nucleosides referred to in text. A reproduced from (14), nucleoside structures in B reproduced from (10).

encoded by 61 codons, and in most cases, there are two or more synonymous triplets coding for the same amino acid, except for methionine and tryptophan. Although the 36th and 35th tRNA bases, which interact with the 1st and 2nd codon bases, strictly follow the standard rules of Watson-Crick pairing, modifications of the 34th position of the tRNA allow for nonstandard wobble interactions, thus enabling a single tRNA species to decode different yet synonymous codons (12). As of 2021, 16 different modifications of the 34th position have been identified in *E. coli*, including various 2-thiouridine

derivatives (e.g., mnm5s2U, Figure 2B) and lysidine – a modified nucleoside unique to bacteria (Figure 2B) (9).

Another commonly modified position within the anticodon stem-loop is the 37th position, located at the 3' end of the anticodon, which often contains a hypermodified purine (e.g., ms2i6A¹, Figure 2B). Modifications at this position tend to be bulky next to U or A in the anticodon and are hypothesized to stabilize intrinsically weaker anticodon-codon interactions (15). Additionally, modifications at this particular position are known to positively impact reading frame maintenance (16). At least six modified nucleosides are known to act as tRNA recognition determinants for aminoacyl-tRNA synthetases and they are all located within the anticodon stem-loop, with five located at the 34th wobble position and one at the 37th position (17).

Another important role of tRNA modifications is the maintenance of its unique and rigorous L-shaped tertiary structure. The major interactions ensuring the correct folding and tertiary structure of the molecule occur at the elbow region, where the D-loop and TΨC loop meet (12). The simplest mechanism for adjusting the molecule's structure is base methylation (e.g., m7G, Figure 2B). These modifications are the most common and can occur at every position of the target nucleoside. Thus, the alternative fold is restricted by blocking possible interactions (18). Uridine isomerization to pseudouridine (Figure 2B) introduces an additional hydrogen bond donor, capable of participating in novel pairing interactions, as well as bridging interactions with the sugar-phosphate backbone by utilizing a water molecule. Additionally, pseudouridine enhances base stacking and overall contributes to the molecule's stability (19). On the other hand, dihydrouridine (Figure 2B) is the sole known nucleoside with a non-planar base. This feature disturbs the stacking interactions in helices, thus destabilizing the tRNA structure and allowing for greater conformational flexibility in tRNA regions that require the simultaneous accommodation of tertiary interactions and loop formation (20).

Although extensive modification of tRNA allows the formation of unique tertiary structures, RNA molecules, including tRNA, are known to become kinetically “trapped” in alternative folds. Additionally, the correct tertiary

¹ Key principles for modification abbreviation nomenclature: capital letter denotes canonical nucleoside (A, C, G, U) or special nucleosides (Ψ – pseudouridine, Q – queuosine, I – inosine, rT – ribothymidine, D – dihydrouridine); numbers specify the carbon or nitrogen atom position in the base or ribose where the modification occurs (e.g., s4U for 4-thiouridine); prefixes indicate the specific chemical modification of the nucleoside (m – methylation, s – sulfur substitution, ac – acetylation, n – amination, etc.).

structure may not be thermodynamically strongly favored over other possible structures (21). To overcome this, some tRNA-modifying enzymes have been shown to act as tRNA chaperones. For example, the pseudouridine synthase TruB, in addition to its modification ability, assists in correctly folding tRNA into its proper tertiary structure (22). Another known tRNA chaperone, TrmA, has been shown to have tRNA folding activity that is independent of its enzymatic catalytic activity. The presence of functional tRNA-modifying chaperones is critical for bacterial cellular fitness (23).

1.1.3 tRNA modification erasers and editors

Although tRNAs are relatively stable, the tRNA pool in bacteria is dynamically regulated (24). The modification content of bacterial tRNAs is regulated as well. A study on *Mycobacterium bovis* revealed, that under environmental stress conditions, significant changes in tRNA modifications at the 34th wobble position are triggered. These changes in modifications influence codon usage, favoring the translation of specific proteins that support bacterial survival under environmental stress. Although this demonstrates that tRNA modification patterns are dynamically regulated, it is not yet clear how these changes are introduced (25).

One type of enzymes that could contribute to changes in tRNA modification composition is called tRNA modification erasers. However, such specifically acting enzymes have so far been reported only in humans. Currently, three modification eraser enzymes are known, all of them acting as demethylases: ALKBH1, ALKBH3, and FTO. These enzymes carry out the demethylation of N1-methyladenosine (m1A) located at the 58th position of the tRNA (Figure 3A) (11). It is worth noting, that bacteria possess an *alkB* gene, coding for a homolog of the abovementioned enzymes, which is induced during the adaptive response. Bacterial AlkB is involved in the reversal of alkylation damage to DNA and RNA (26). In addition to the demethylation of a broad spectrum of damaged nucleosides in DNA and RNA, AlkB has been shown to demethylate and repair 2-methylthiocytidine (ms2C) within tRNA – an unnatural nucleoside at the 32nd position formed from 2-thiocytidine after bacterial exposure to antibiotics and methylation agents (Figure 3B1) (27). Similarly, AlkB was shown to repair 4-methylthiouridine (ms4U), another unnatural modification formed from 4-thiouridine at the 8th position after stress induced by methylating agents (Figure 3B2) (28).

Another type of enzymes capable of altering tRNA by changing its sequence is called tRNA editors. The most studied example of tRNA editing is the deamination of adenosine, resulting in inosine at the 34th wobble

position (Figure 3C1), which is present in eukaryotes and bacteria, but not in archaea. Editing of adenosine allows target tRNAs to decode three different codons (ending in U, C, or A). In bacteria, this process is carried out by tRNA-specific adenosine deaminase TadA (29). Another type of editing by deamination is the C-to-U conversion occurring in eukaryotes and archaea. An unusual example of this process occurs at tRNA position 8 in the archaeon *Methanopyrus kandleri* (Figure 3C2). Although all canonical tRNAs possess a uridine at this position, 30 of 34 tRNAs of this hyperthermophile contain cytidine. During the tRNA maturation cytidine is edited by tRNA-specific cytidine deaminase CDAT8, resulting in canonical uridine. It is hypothesized that cytosine at the tRNA gene might stabilize the genome under extreme temperatures (30).

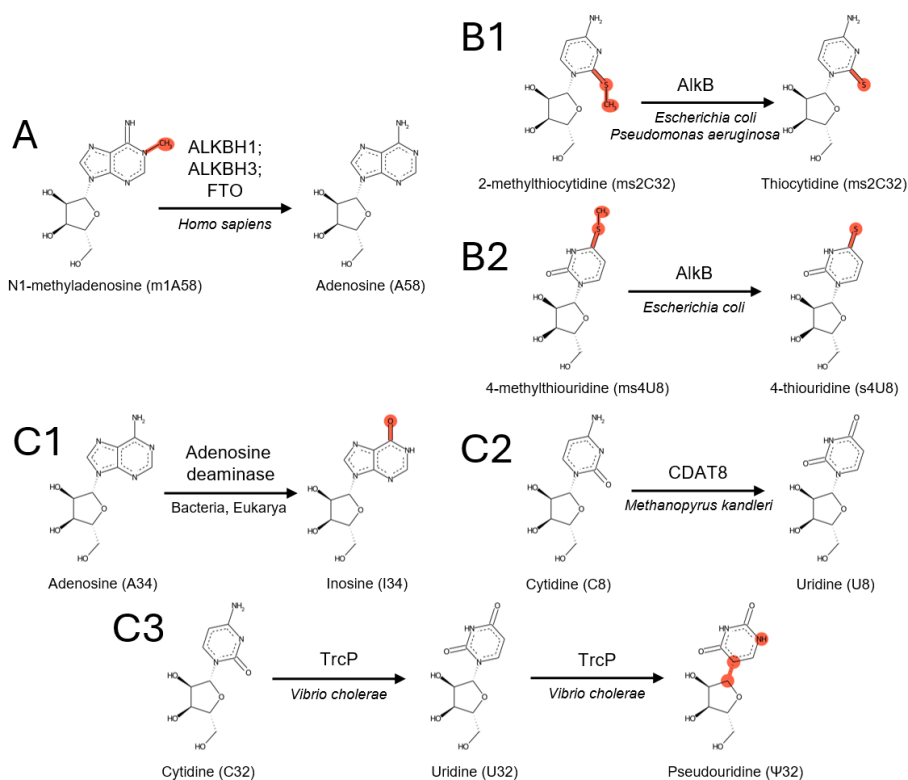


Figure 3. Reported nucleoside modification erasing, repair, and editing reactions in tRNA with corresponding enzymes and organisms. Nucleoside abbreviations and positions within tRNA are indicated in parentheses. **A:** Modification erasing reaction. **B1** and **B2:** Modification repair reactions. **C1-C3:** base editing reactions. Nucleoside structures reproduced from (10).

Recently, a unique and more complex editing process was discovered in *Vibrio cholerae*. A three-domain protein, TrcP, consisting of cytidine

deaminase and pseudouridylase domains connected by a long helical domain catalyzes cytidine-to-pseudouridine editing at the 32nd position of tRNA (Figure 3C3). The editing occurs through two subsequent reactions: cytidine to uridine and uridine to pseudouridine conversions. It is hypothesized that this process may contribute to bacterial adaptation to iron availability (31).

1.1.4 tRNA degradation

rRNA and tRNA are the main non-coding RNAs, commonly referred to as "stable RNA" because they have significantly longer half-lives compared to short-lived mRNA. However, when misprocessed or under unfavorable growth conditions, these molecules can undergo degradation (32). Two main degradation pathways for tRNAs have been established in yeast: the nuclear surveillance pathway and the rapid tRNA decay pathway (33).

The nuclear surveillance pathway works as a quality control system during tRNA processing. It is carried out by the nuclear RNA exosome, a 3'–5' exonuclease complex, and the TRAMP polyadenylation complex. This pathway eliminates incorrectly spliced tRNA and precursors with improperly processed 3' ends by polyadenylation via the TRAMP complex and subsequent degradation by the nuclear RNA exosome. It is hypothesized that higher eukaryotes (e.g., humans), which possess homologues of aforementioned enzymes, may utilize this pathway as well (34).

The rapid tRNA decay pathway in yeast relies on two 5'–3' exonucleases, Rat1 and Xrn1, and acts on mature but hypomodified tRNAs. The lack of at least four different tRNA modifications is known to cause degradation. However, substrate recognition *in vivo* does not necessarily depend on modifications but rather on tRNA structural integrity and the stability of the acceptor and T-stems (35).

Unlike in yeast, bacterial tRNA quality control and subsequent degradation pathways are understudied. However, some instances of the elimination of hypomodified and unstable tRNAs have been observed (33). Temperature-sensitive tRNA mutant precursors have been shown to be polyadenylated by poly(A) polymerase and degraded by polynucleotide phosphorylase (PNPase) in *E. coli* (36). In the extreme thermophile *Thermus thermophilus*, *trmB* gene knockouts lacking the m7G modification at the 46th position lead to the degradation of some tRNAs by a yet unidentified pathway (37). Nevertheless, a mechanism for the elimination of hypomodified tRNAs lacking 4-thiouridine by the RNA degradosome was elucidated in *Vibrio cholerae* (38). This process is further reviewed in paragraph 1.2.3.

1.1.5 RNA recycling

Mature stable RNA species like rRNA and tRNA are generally not degraded during exponential bacterial growth. Only defective precursors become polyadenylated and subsequently degraded (39). However, the median half-life of mRNA in *E. coli* cultivated under standard laboratory conditions is 4.7 minutes, a duration multiple times shorter than cell doubling time, indicating rapid mRNA turnover (40). RNA recycling and nucleotide salvage are essential activities that allow restocking of the nucleotide pool to maintain mRNA turnover and persistently changing protein expression, enabling bacteria to rapidly divide and quickly adapt to environmental changes (41).

Out of 20 RNases identified in *E. coli*, at least 9 are known to participate in mRNA decay, both by exonucleolytic and endonucleolytic activities (42). Additionally, 2 RNases are known to carry out sRNA and nanoRNA decay. However, it is complicated to generalize RNA decay in bacteria because the enzymes involved in this process vary between microorganisms. For example, *Bacillus subtilis* possesses 23 RNases, of which only 9 are shared with *E. coli*. Moreover, no 5'-to-3' exonucleolytic activity is known for *E. coli* exoribonucleases, while *B. subtilis* possesses RNase J1 which exhibits such activity and participates in mRNA decay as well as in 16S rRNA maturation (43).

After RNA decay, nucleotides can be hydrolysed by nucleotidases to form ribonucleoside and phosphate, or by nucleotide nucleosidases and nucleotide phosphorylases to form ribose phosphate and base, which can be salvaged and reused in RNA synthesis or further degraded (44).

1.1.6 The fate of modified nucleosides

The degradation of various RNAs, especially tRNA, releases a plethora of modified nucleotides. However, unlike canonical nucleotides, the metabolic fate of most modified nucleotides is unknown. Nevertheless, there are some examples. A recycling pathway for the most abundant modified nucleoside, pseudouridine, has been identified in bacteria and eukaryotes (Figure 4A). This pathway involves two enzymes: pseudouridine kinase (PsuK in *E. coli*), which catalyzes pseudouridine phosphorylation, and pseudouridine monophosphate glycosidase (PsuG in *E. coli*), which catalyzes hydrolysis, resulting in uracil and ribose 5-phosphate (45).

A small 103-amino acid-containing amidohydrolase from *E. coli*, YqfB, was shown to hydrolyze N4-acetylcytidine (ac4N) (Figure 4B) and

N⁴-acetylcytosine to cytidine and cytosine (46). ac⁴N is a highly conserved nucleoside present in tRNA, rRNA, and mRNA of prokaryotes and eukaryotes (47). A 5-methylcytosine deaminase has been discovered in some bacterial species, catalyzing 5-methylcytosine deamination to thymine (Figure 4C) (48). Primarily, 5-methylcytosine is found in DNA as a result of DNA methylation; however, it is also identified in RNAs including tRNA (48).

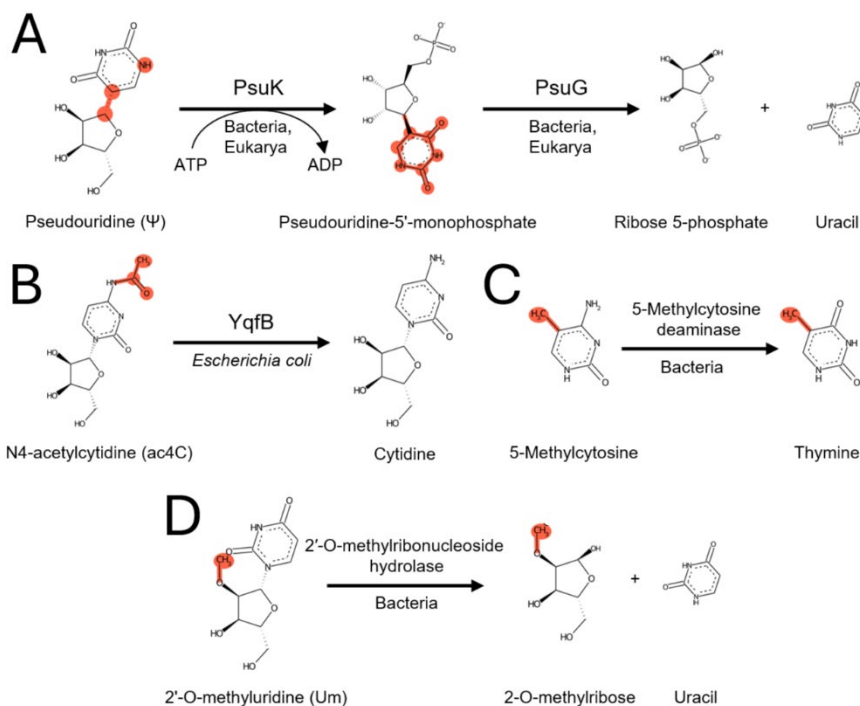


Figure 4. **A:** pseudouridine recycling pathway. **B:** cytidine recovery from N⁴-acetylcytidine by *E. coli* YqfB amidohydrolase. **C:** thymine recovery from 5-methylcytosine by bacterial 5-methylcytosine deaminases. **D:** uracil recovery by bacterial 2'-O-methyluridine hydrolases. Structures reproduced and adapted from (10).

Modified nucleoside hydrolases in bacteria are known to catalyze 2'-O-methyluridine hydrolysis to uracil and 2-O-methyl ribose (Figure 4D) (49). Interestingly, the function of 2'-O-methyluridine is not yet well established, but it is present in high abundances in various RNAs, including tRNA (50). Moreover, multispecific cytidine deaminases targeting the fourth position of N⁴-acyl-cytidines, N⁴-alkyl-cytidines, and N⁴-alkyloxycarbonyl-cytidines, and S⁴-alkylthio-uridines as well as O⁴-alkyl-uridines, converting them to uridine and corresponding amide, amine, carbamate, thiol, or alcohol as leaving groups, have been reported recently (51).

1.2 4-Thiouridine

4-thiouridine (s4U) in tRNA was discovered in 1966 when it was observed that this unconventional nucleoside found in *E. coli* tRNA absorbs longer wavelengths than other then-known nucleobases (52). Unlike most other frequent tRNA modifications, 4-thiouridine (s4U) is conserved in bacteria and archaea (10). It has been demonstrated that approximately 70% of *E. coli* bulk tRNA contains s4U modifications (53). However, this fraction can vary in some tRNA species dependent on bacterial growth rate (54). Generally, this modification is located at the 8th position of the tRNA (55), although some bacterial and archaeal tRNA species may exhibit a second modification at position 9, resulting in two adjacent s4U moieties (56–58).

1.2.1 4-Thiouridine impact on tRNA stability

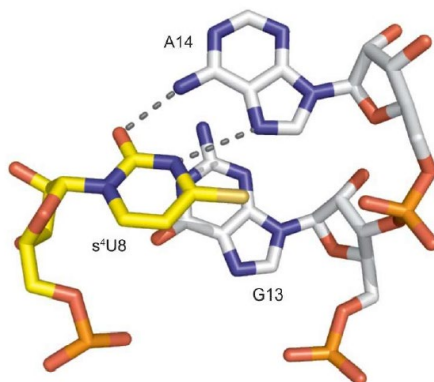


Figure 5. Interactions of 4-thiouridine (s4U) at tRNA position 8 with nucleosides at positions 13 and 14. Figure reproduced from (59).

Contrary to nitrogen and oxygen, sulfur typically does not form hydrogen bonds. However, sulfur in s4U can indirectly influence hydrogen bonds by altering the conformation and polarity of the molecule itself, thereby affecting potential hydrogen bonds with nearby molecules (60). Structural analysis of *E. coli* tRNA-Tyr shows that the s4U participates in stacking interactions with the residue at the 13th position and in reverse Hoogsteen base pair formation with the nucleoside at the 14th position (59). The presence of sulfur is hypothesized to strongly reinforce the latter interaction (33). This is strongly supported by the fact that the absence of s4U in *E. coli* tRNA-Ser reduces its melting temperature by 4.7 °C, while the lack of the other most common tRNA body modifications reduces the melting temperature by 1.3 to 2.7 °C (61). A more drastic difference is observed in *Vibrio cholerae* tRNA-Tyr and

tRNA-Ser with, melting temperature differences of 5.9 and 6 °C, respectively (38). The presence of s4U may contribute to bacterial thermotolerance. A comparative study of closely related psychrophilic, mesophilic, and thermophilic Bacillales has shown that thermophilic species exhibit strikingly higher occurrence of s4U in tRNA when compared to non-thermophilic bacteria (62).

1.2.2 4-Thiouridine impact on incorporation of other modifications

The presence of s4U in tRNA affects the incorporation of other modifications. A positive effect has been observed for tRNA guanosine-2'-methyltransferase in *Thermus thermophilus* in the formation of 2'-O-methylguanosine. The 4-thiouridine residue has been shown to influence the proper recognition of the tRNA substrate. In the absence of a 4-thiouridine residue, the activity of guanosine methyltransferase was reduced more than twofold in vitro (63). Conversely, an opposite effect was observed with archaeosine found in archaeal tRNA. The stability and melting temperature of the tRNA were shown to be the main determinants for the activity of archaeal tRNA-guanine transglycosylase (ArcTGT). The presence of 4-thiouridine, along with other modifications, negatively influenced the catalytic activity of this enzyme (61).

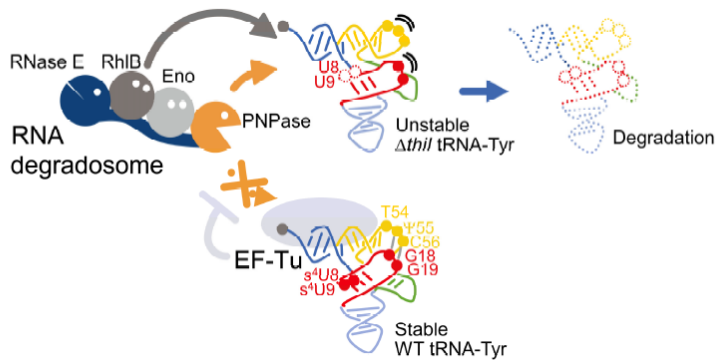
1.2.3 4-Thiouridine and tRNA quality control

Studies in rabbits used as cholera disease models have shown that *thiI*, among several other tRNA anticodon loop-modifying enzyme genes, is required for optimal growth of *Vibrio cholerae* in the host during infection (64). Further studies revealed that tRNA levels are modulated by the presence of s4U during the stationary growth phase. A substantial decrease in the abundance of 12 species of tRNAs during the stationary growth phase of *V. cholerae* mutants defective in tRNA s4U synthesis was observed in comparison to wild-type bacteria. However, such a phenotype was not pronounced during the exponential growth stage. This phenomenon was attributed to the bacterial RNA degradosome (38).

Bacterial RNA degradosomes are multienzyme complexes that participate in bulk mRNA degradation, sRNA processing, and maturation of 16S and 5S rRNAs and tRNAs. In *E. coli* as well as in *V. cholerae*, it consists of endoribonuclease RNase E, RNA helicase RhlB, glycolytic enzyme enolase, and the phosphorolytic 3'-5' exoribonuclease PNPase (65). The s4U-deficient tRNAs in *V. cholerae* were shown to be processed by the RNA degradosome

which is carried out by RNase E's C-terminus and PNPase catalytic activity. Interestingly, the RhIB double-stranded RNA unwinding activity of the degradosome is required for the decay of tRNA-Tyr, but not tRNA-Ser, indicating two different processes, although the determinants for these are unknown. The degradosome-mediated decay seems to be able to target both aminoacylated and non-aminoacylated tRNAs. However, EF-Tu protects aminoacyl-tRNAs from decay by competing with the degradosome, although it is not known whether EF-Tu has a lower affinity for hypomodified tRNAs. The model of RNA degradosome-mediated tRNA quality control of s4U deficient tRNAs is depicted in Figure 6 (38).

tRNA-Tyr



tRNA-Ser1

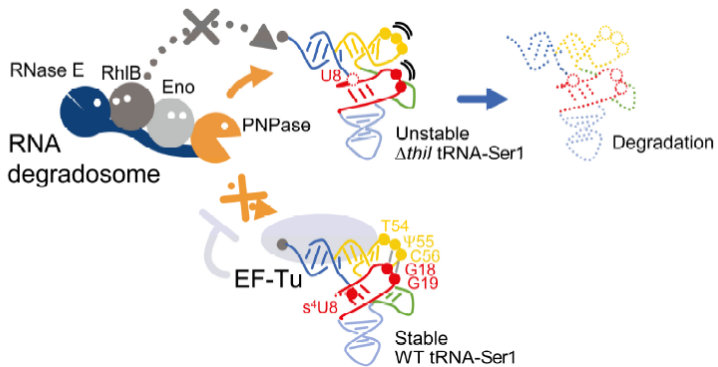


Figure 6. Model of RNA degradosome-mediated tRNA quality control in *Vibrio cholerae*. s4U deficient unstable tRNA(Tyr) is degraded in RhIB-dependent manner, while tRNA(Ser) is degraded in RhIB-independent manner. EF-Tu bound (grey oval) tRNAs are protected from degradation. Figure reproduced from (57).

1.2.4 4-Thiouridine as a bacterial UV sensor

s4U photoreactivity. The substitution of oxygen with sulfur at the C4 position of the uracil ring drastically shifts the absorption spectrum of the nucleoside (Figure 7). Unlike canonical uridine, which absorbs shorter wavelengths of UVC (100-280 nm) and UVB (280-320 nm) in the electromagnetic spectrum, s4U efficiently absorbs UVA (320-400 nm) wavelengths, with an absorption maximum at 331 nm compared to 259 nm for canonical uridine (66). Although this nucleoside is stable in the dark, upon illumination, s4U undergoes intersystem crossing from its singlet state to a reactive triplet state. These alterations make s4U highly reactive and are responsible for its photochemical properties (67).

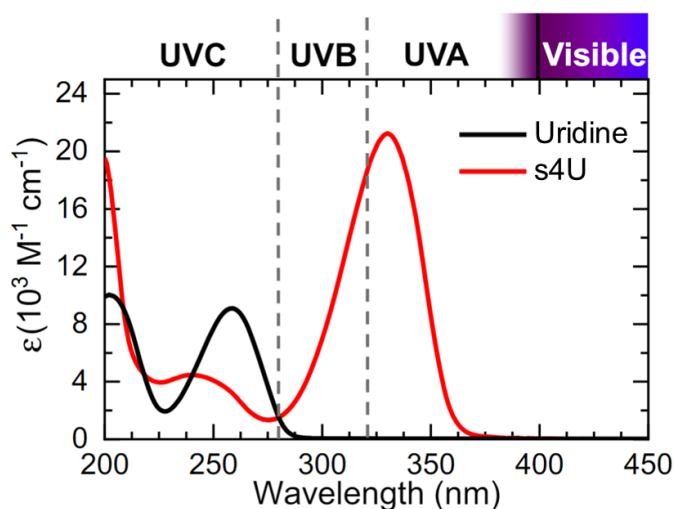


Figure 7. Absorbance spectra of uridine and 4-thiouridine (s4U). Figure reproduced from (66).

s4U reactivity effects on tRNA. Illumination of bacterial tRNA containing s4U with UVA results in a crosslinking reaction between s4U at the 8th position and cytidine at the 13th position (Figure 8) (68). The formation of a covalent bond between these two nucleosides causes conformational changes in the tRNA tertiary structure around the s4U, including the stem of the dihydrouracil arm (69). Although irradiated tRNAs can be fully aminoacylated, their affinity for tRNA-aminoacyltransferases drops threefold. Furthermore, while the ability of irradiated tRNA to bind ribosomes is not affected, the incorporation of amino acids into polypeptide chains is twofold slower when the amino acid is attached to irradiated tRNA (70).

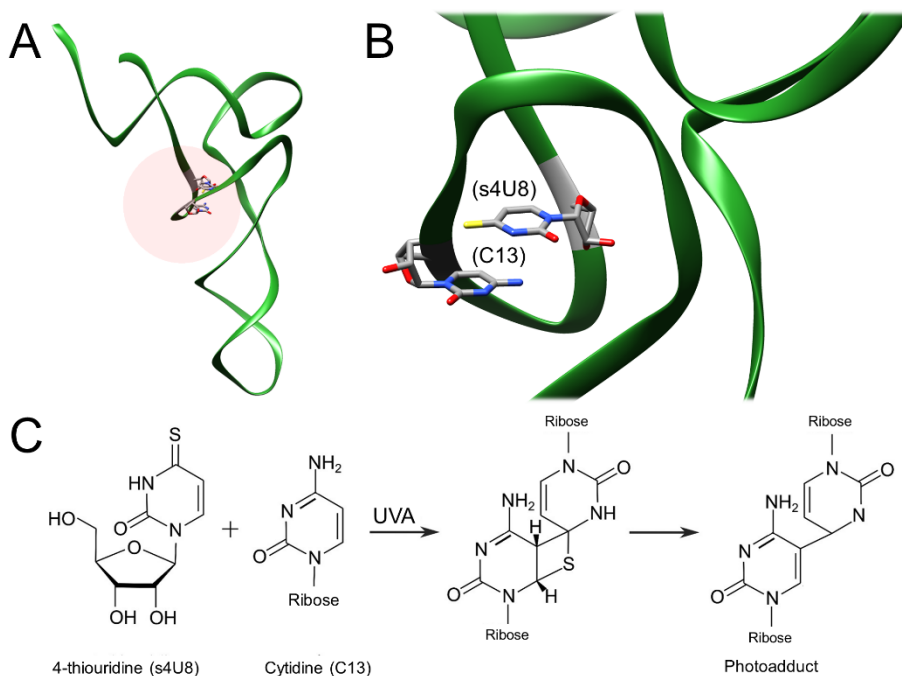


Figure 8. **A:** location of s4U at the 8th position and cytidine at the 13th position within *E. coli* tRNA(Phe) (highlighted in red). **B:** close up of s4U at 8th position and cytidine at 13th position within *E. coli* tRNA(Phe). **C:** UVA-mediated crosslink reaction between s4U and cytidine. A and B adapted from *E. coli* tRNA(Phe) crystal structure (PDBID:6y3g) (71). C reproduced from (72).

UV radiation effects on bacteria. The majority of short-wavelength solar UV is filtered out by the ozone layer, making UVA the most energetic fraction that reaches the ground. While short-wavelength UV represents a minor fraction, it is harmful to bacteria, causing DNA damage through the formation of pyrimidine cyclobutane dimers or other adducts, which are repaired by lesion-repair enzymes such as photolyases or excision nucleases. In contrast, UVA requires multiple orders of magnitude more energy to achieve the same lethality rate in bacteria compared to UVC (73). However, UVA is known to cause sub-lethal effects on bacteria. Particularly in *E. coli*, these effects include inhibition of catabolic amino acid gene induction (e.g. tryptophanase) and transient growth inhibition (74). The latter example of transient growth inhibition has also been observed in other bacterial species, such as *Salmonella typhimurium* (75) and *Enterobacter cloacae* (76).

UVA irradiation causes a stringent response. Experiments with *E. coli* have shown that irradiation by UVA leads to reduced levels of charged tRNAs, which mimic amino acid starvation, subsequently slowing down protein synthesis. The accumulation of uncharged tRNAs triggers an increase

in the bacterial alarmone guanosine tetraphosphate (ppGpp) levels, leading to a significant reduction in RNA production and causing a delay in cell growth (77).

The elevation of ppGpp levels due to uncharged-tRNA is known as the stringent response, which occurs during amino acid starvation and other stress conditions in bacteria. Under these conditions in *E. coli*, a complex of uncharged tRNA and inactive ppGpp synthetase RelA enters the vacant ribosomal A-site, activating RelA and resulting in ppGpp production by transferring a pyrophosphate group from ATP to GTP or GDP (78). The accumulation of the alarmone ppGpp leads to bacterial metabolic reprogramming: downregulation of nucleotide synthesis, replication, tRNA, and rRNA synthesis, alongside upregulation of nucleotide catabolism, central metabolism, and induction of RpoS general stress response, which regulates the response to various stresses, including oxidative (79), which is known to be caused by general UV radiation (80).

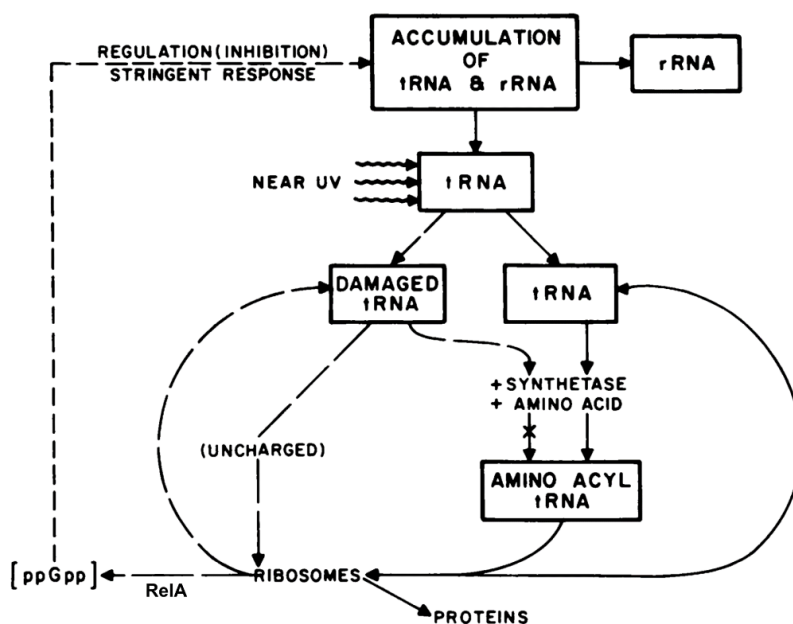


Figure 9. Proposed scheme of events following UVA irradiation of bacteria. Broken lines indicate events during UVA irradiation, solid lines indicate events during normal bacterial growth. Figure reproduced from (77).

According to the proposed model of UVA-caused stringent response, UVA causes a decrease in the level of charged tRNAs by damaging tRNAs, which in turn decreases the rate of protein synthesis. Uncharged tRNAs increase the levels of ppGpp, which in turn decrease the rate of stable RNA accumulation.

To resume normal growth, the cell might either repair its damaged tRNAs or dilute the damage through the synthesis of new tRNA (77). The scheme of the model is depicted in Figure 9.

s4U mediates stringent response. In *Salmonella typhimurium*, deletion of the *thiI* increases sensitivity to low-intensity UVA exposure during prolonged durations, a condition mimicking environmental conditions and resulting in decreased survival rates over time. Mutants lacking s4U also do not demonstrate ppGpp accumulation during exposure, whereas wild-type strain does. Additionally, experiments with *relA* gene knockouts under the same conditions have shown increased sensitivity as well (75). On the other hand, the combination of UVA and UVB has been shown to be more lethal to *E. coli* bacteria possessing s4U than to *thiI* knockouts. The authors of the latter study proposed that crosslinked tRNAs reduce protein synthesis, impairing the cell's ability to repair DNA, thereby making the direct DNA damage caused by UVB irradiation more effective and lethal (81).

The growth delay caused by UVA irradiation differs between bacterial species. A comparative study between *E. cloacae* and *E. coli* demonstrated, that the growth lag in *E. coli* is longer, lasting 90 minutes, while that of *E. cloacae* lasts 45 min under the same experimental conditions. Moreover, the ppGpp levels accumulated in *E. coli* were twice those in *E. cloacae*, and the time required to restore ppGpp content to basal levels in *E. cloacae* was shorter than that in *E. coli* (76).

Pretreatment of *E. cloacae* cultures with UVA almost abolishes the growth delay upon second irradiation carried out after one doubling of bacteria in the dark. The pretreated bacteria exhibit almost 11-fold lower s4U content and only minor levels of photoreaction product. The events involved in the phenomenon remain unknown (82). Although the mechanism is unknown in *E. cloacae*, the study with irradiated *E. coli* extracts has shown approximately 4-fold decreased s4U sulfur transference which may implement lower *thiI* expression or inhibition (83).

1.2.5 Applications of 4-thiouridine

The unique properties of s4U make it a useful tool for molecular biology applications. Moreover, exogenously supplied s4U is effectively utilized for RNA synthesis in both prokaryotes (84) and eukaryotes (85). The efficient uptake of s4U allows for the study of RNA-protein interactions (86), as well as RNA dynamics within the cell (87). Moreover, in addition to its reactive

nature, s4U is conserved in prokaryotes, thus making it attractive for specific applications in eukaryotes (88).

One of the earliest applications of s4U was the photosensitization of eukaryotic RNA. This involved the incorporation of s4U followed by the crosslinking of interacting proteins using UVA radiation, a wavelength spectrum, where other natural nucleotides do not crosslink. This approach overcame issues associated with previously applied UVC crosslinking, which had the drawbacks of being non-selective and lethal to cells (89).

Moreover, s4U can be introduced into RNA through *in vitro* transcription using T7 RNA polymerase. This method allows for the insertion of s4U at specific positions within the RNA product, thus allowing precise localization of RNA-protein interaction (90). PAR-CLIP (Photoactivatable-Ribonucleoside-Enhanced Crosslinking and Immunoprecipitation) is the currently widely applied version of the crosslinking method. It relies on the *in vivo* incorporation of photoreactive nucleosides, such as s4U and 6-thioguanosine, followed by UVA crosslinking. The RNA-protein complex is then isolated via immunoprecipitation, subjected to RNA fragmentation, and analyzed through cDNA sequencing (86).

Another widespread application of s4U is the metabolic labeling of mRNA, which allows for the tracking of mRNA dynamics under certain conditions. Unlike basic RNA-seq, which provides only a snapshot of the transcriptome, metabolic labeling combined with RNA-seq enables monitoring of mRNA turnover for specific transcripts of interest. It is achieved by s4U addition to a cell culture, which is taken up by the cells, phosphorylated, and incorporated into newly transcribed RNA (Figure 10A) (91).

The methods for analyzing labeled RNA continue to improve. Early examples involved biotinylation of s4U-containing transcripts, followed by purification with streptavidin-coated beads and analysis on RNA microarrays (92). To overcome the issue of unspecific biotinylation of other thionucleosides (e.g., 5-methyl-2-thiouridine), techniques utilizing s4U-specific biotin derivatives were developed (93). Nevertheless, biotinylation comes with disadvantages in downstream analysis, including interference of biotinylated RNA with reverse transcription.

Current state-of-art techniques rely on s4U-specific chemical base conversion reactions, typically to cytidine analogs, which alter the base call signal during RNA-seq (88). Current techniques utilizing s4U to cytidine analog conversion are TUC-seq, conversion is done using osmium tetroxide (OsO₄) oxidation, followed by the addition of an amine group with ammonium chloride (NH₄Cl), resulting in canonical cytidine (Figure 10B) (94); SLAM-seq, the s4U group is alkylated with iodoacetamide, and the alkylation

product S⁴-carboxyamidomethyl-thiouridine contains an amine group recognized as cytidine (Figure 10C) (95); TimeLapse-seq, s4U is oxidized by sodium periodate (NaIO₄) and subsequently treated with 2,2,2-trifluoroethylamine (TFEA), resulting in N⁴-trifluoroethylcytidine, another cytidine analog (Figure 10D) (96). The combination of s4U labeling and subsequent conversions to cytidine analogs results in uridine to cytidine change in sequencing data, distinguishing labeled RNA from unlabeled RNA (88).

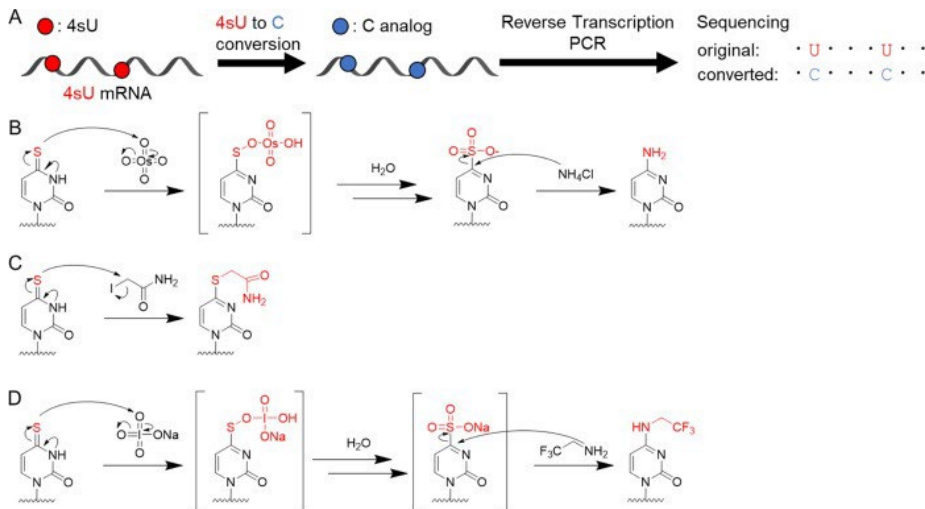


Figure 10. A: Simplified workflow s4U-labeled mRNA sequencing. B: s4U to cytidine conversion reaction applied in TUC-seq. C: s4U to S⁴-carboxyamidomethyl-thiouridine conversion reaction applied in SLAM-seq. D: s4U to N⁴-trifluoroethylcytidine conversion reaction applied in TimeLapse-seq. Figure reproduced from (88).

1.2.6 4-thiouridine synthesis

The synthesis of 4-thiouridine within the tRNA is typically attributed to the product of the *thiI* gene. Initially, ThiI, along with ThiFSGH was identified as essential enzymes for the biosynthesis of the thiazole moiety of thiamin in *Escherichia coli* (97) and *Salmonella typhimurium* (98). Soon after these initial discoveries, an additional role for ThiI in tRNA 4-thiouridine synthesis was identified in *E. coli* (99). Interestingly, further studies have shown that, unlike ThiI in *Escherichia* and *Salmonella*, many orthologs of this enzyme do not participate in thiamine synthesis (100). These orthologs lack the C-terminal rhodanese domain, which is independently sufficient to ensure thiamine synthesis, and generally, the sulfur transfer to 4-thiouridine is conducted via a mechanism distinct from that used in thiazole synthesis (101). In fact, enzymes responsible for 4-thiouridine synthesis vary across species,

exhibiting differing structural features and sulfur transfer mechanisms. To date, 4-thiouridine synthesizing proteins can be divided into three types (Figure 11): *Escherichia coli* type, possessing rhodanese-like domain (RHD); *Methanococcus maripaludis* type, possessing an iron-sulfur cluster and no RHD; and *Bacillus anthracis* type – possessing neither RHD nor an iron-sulfur cluster (102).

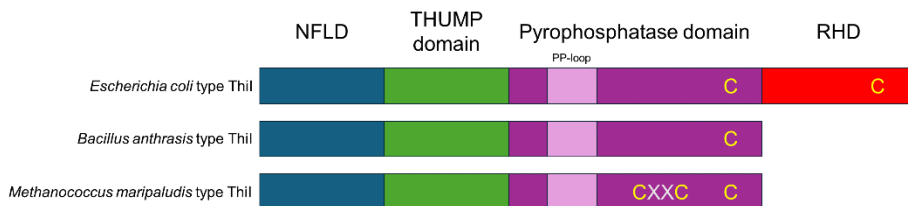


Figure 11. Simplified scheme of the domain organization of ThiI enzymes. Yellow Cs depict conserved cysteines.

The N-terminus of ThiI contains the N-terminal ferredoxin-like domain (NFLD), which, along with the THUMP domain, forms a continuous surface that allows ThiI to bind tRNA by ensuring the correct orientation and distance between residues involved in RNA binding and the enzyme's active site (103). The NFLD is also found in other RNA-interacting proteins, such as RNA polymerase (104) and tRNA methyltransferases, particularly in the bacterial and archaeal TrmN/Trm14 family (105).

Following the NFLD is the THUMP domain (named after THioUridine synthases, RNA Methylases, and Pseudouridine synthases). This domain is often found in other tRNA-interacting enzymes, particularly those modifying tRNA nucleosides in close proximity to the 8th position, such as methyltransferases forming N²-methylguanosine at the 6th (106) or at the 10th position (107) and cytidine deaminases carrying out cytidine to uridine editing at the 8th position of archaeal tRNA (30). Additionally, this domain is found in some pseudouridine synthases that form pseudouridine at the 54th and 55th positions (108). In general, all THUMP-containing tRNA modification enzymes produce nucleosides that are considered to stabilize the L-shaped tRNA structure (109).

The third element present in all ThiI homologs is the pyrophosphatase domain (catalytic domain) containing the PP-loop motif (102). This motif facilitates ATP binding and activates uridine by forming an adenylated tRNA intermediate (110). The PP-loop motif is widespread in various enzymes that catalyze the hydrolysis of the α - β phosphate bond of ATP, such as GMP synthetases, argininosuccinate synthetases, asparagine synthetases, or ATP sulfurylases (111). Additionally, it is found in multiple tRNR sulfurases. These sulfurases catalyze the thiolation of the C2 of uridine. Those targeting

the anticodon loop and thiolating the hypermodified wobble uridine at the 34th position, such as MnmA (112) or NcsA (113), as well as forming non-hypermodified 2-thiouridine at the 54th position in thermophilic bacteria such as TtuA (114).

Some ThiI orthologs possess a fourth, C-terminal rhodanese-like domain (RHD). This domain is present in ThiI of *E. coli* and other Gammaproteobacteria, as well as in some species of the archaeal genus *Thermoplasma* (115). The ThiI from *Escherichia* and *Salmonella* possessing a RHD can facilitate dual function and participate both in 4-thiouridine and thiamine synthesis (100). The RHD in ThiI acts as a sulfur acceptor and forms a persulfide with the assistance of cysteine desulfurase IscS (116). The domain derives its name from the mitochondrial enzyme rhodanese, which is involved in cyanide detoxification by catalyzing the conversion of cyanide to thiocyanate, forming persulfide as a reaction intermediate (117).

Interestingly, recently it was reported that some ThiI from archaea such as *Pyrococcus furiosus* or *Methanococcus maripaludis* possess an $[4\text{Fe}-4\text{S}]^{2+}$ iron-sulfur cluster coordinated by three cysteines within the conserved CXXC + C motif. The iron-sulfur cluster is proposed to catalyze the transfer of sulfur atoms to the activated tRNA substrate (102).

1.2.7 Diversity of ThiI enzymes

***Escherichia coli* type ThiI.** The 4-thiouridine synthesis by *Escherichia coli* type ThiI is facilitated with the help of IscS cysteine desulfidase (118), a protein known to catalyze the formation of alanine and sulfane sulfur from cysteine, resulting in a persulfide formed at the active site of IscS (119). Initially, the conserved cysteine residue (Cys456 in *E. coli* ThiI) of the ThiI RHD accepts the sulfur as a persulfide from IscS (Figure 12B) (118). Concurrently, the uridine at the 8th position of tRNA is activated by adenylation (Figure 12A) (110). The persulfide formed on the RHD then attacks the activated uridine, releasing AMP. This is followed by an attack from a second conservative cysteine in the catalytical domain (Cys344 in *E. coli*), leading to the cleavage of the disulfide bond that couples ThiI to the tRNA, leaving the thiouridine on the tRNA and forming a disulfide bond between Cys344 and Cys456 (102).

Notably, an alternative mechanism involving the persulfide is possible, where Cys344 acts as a nucleophile to liberate the terminal sulfur of the persulfide on Cys456 as hydrogen sulfide (Figure 12C). The hydrogen sulfide then serves as the nucleophile to attack the adenylated intermediate, resulting in the release of AMP and the formation of the 4-thiouracil moiety (120). In

both scenarios, the reduction of the disulfide bond is necessary for the enzyme to achieve multiple turnovers (116).

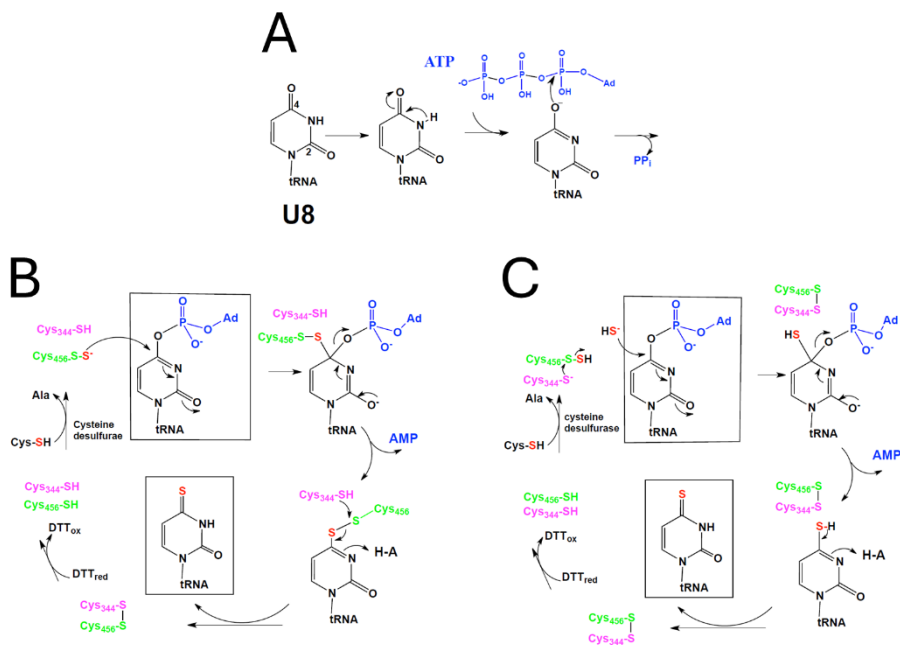


Figure 12. Persulfide-based mechanism proposed for *E. coli* ThiI. **A:** U8 activation by ATP adenylation. **B:** The first scenario, with persulfide formed on Cys456 acting as a nucleophile and directly attacking the C4 of adenylylated uridine at the 8th position of tRNA. **C:** The second scenario, where Cys344 acts as a nucleophile to liberate the terminal sulfur of the persulfide on Cys456 as hydrogen sulfide which then serves as the nucleophile to attack C4 of adenylylated uridine at the 8th position of tRNA. Figure adapted from (102).

To date, no crystal structure has been reported for *E. coli* type ThiI. However, crystal structures of *Bacillus anthracis*-type ThiI suggest a possible dimeric architecture. Nevertheless, biochemical analyses have shown that the disulfide bond likely forms within a single (sub)unit (120).

***Bacillus anthracis* type ThiI.** Another widespread type of ThiI enzymes lacks the RHD, which is involved in the sulfur transfer reaction in *E. coli* type ThiI (102). Interestingly, this type of ThiI does not possess a second conserved cysteine (equivalent to Cys456 in *E. coli*, located within RHD), and the uridine sulfuration mechanism remains unknown. However, adenylation of the substrate is proposed, as AMP is detected during *in vitro* thiolation (121). Moreover, AMP was captured in complex with *Bacillus anthracis* ThiI within the crystal structure (103).

The crystal structure of *Thermotoga maritima* ThiI in complex with tRNA revealed that the physiologically relevant form of the enzyme is a homodimer, capable of catalyzing the thiolation of two tRNAs simultaneously. Each of the

two tRNA molecules interacts with both subunits of ThiI, and the tRNA is primarily bound by the NFLD and THUMP domains (Figure 13) (121).

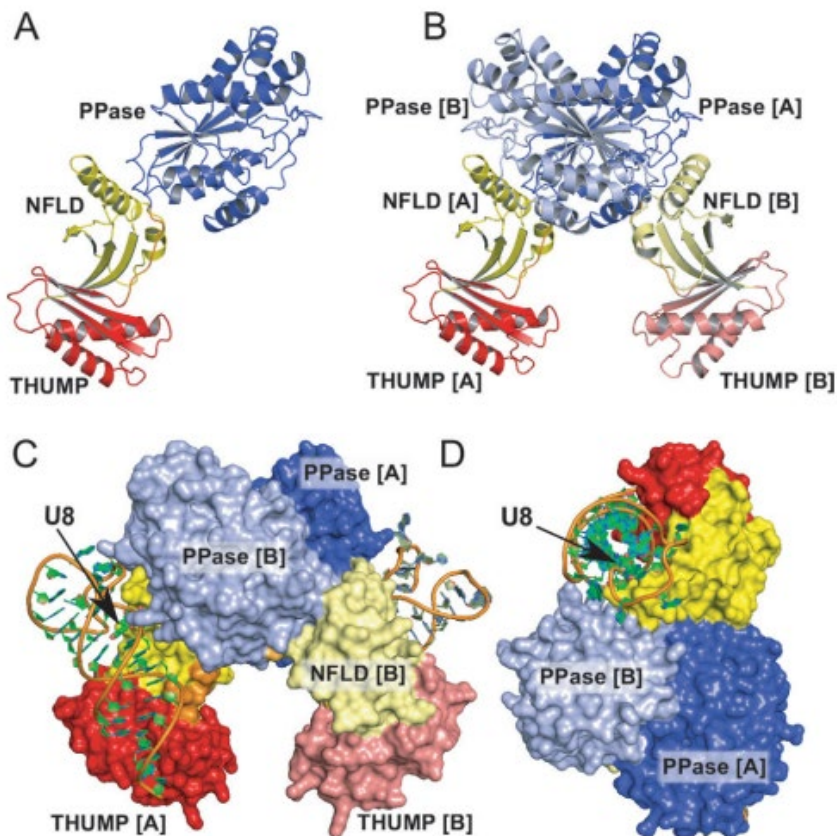


Figure 13. Structure of *Thermotoga maritima* ThiI in complex with tRNA. **A:** monomer structure featuring pyrophosphatase (PPase), NFLD, and THUMP domains. **B:** structure of ThiI homo-dimer A and B represent domains of single monomer. **C:** ThiI homo-dimer in complex with two tRNA molecules. Arrow indicates tRNA-U8 bound by THUMP and NFLD domains of A monomer close to the active site of PPase domain of the B monomer. **D:** perpendicular view of complex depicted in C. Figure reproduced from (121).

***Methanococcus maripaludis* type ThiI.** In contrast to the examples described above, ThiI in various archaea possesses three conserved cysteines within the catalytic pyrophosphatase domain. Initial studies of *Methanococcus maripaludis* ThiI indicated the presence of a [3Fe-4S] cluster within these three cysteines, which was essential for its tRNA thiolation activity, although no reaction mechanism was suggested at the time (122).

However, further research by another group attributed the unusual [3Fe-4S] cluster to be an oxidation product of a [4Fe-4S] cluster. The presence of the latter was confirmed in the archaeal ThiI of *Methanococcus maripaludis*

and *Pyrococcus furiosus*. This finding led to a proposal of a catalytic mechanism for s4U formation utilizing the FeS cluster (Figure 14) (102), based on previously investigated tRNA sulfurtransferases that utilize sulfur donor proteins (123).

The fourth non-protein-bound Fe atom of the FeS cluster is proposed to bind and activate the sulfur atom of the donor in the form of a hydrogen sulfide ligand. After adenylation at O⁴ by ATP and the formation of a [4Fe–5S] cluster intermediate, nucleophilic substitution of O-adenosyl monophosphate by the SH group coordinated by the [4Fe–4S] cluster would generate the final s4U-tRNA product. The reaction mechanism is depicted in Figure 14 (102).

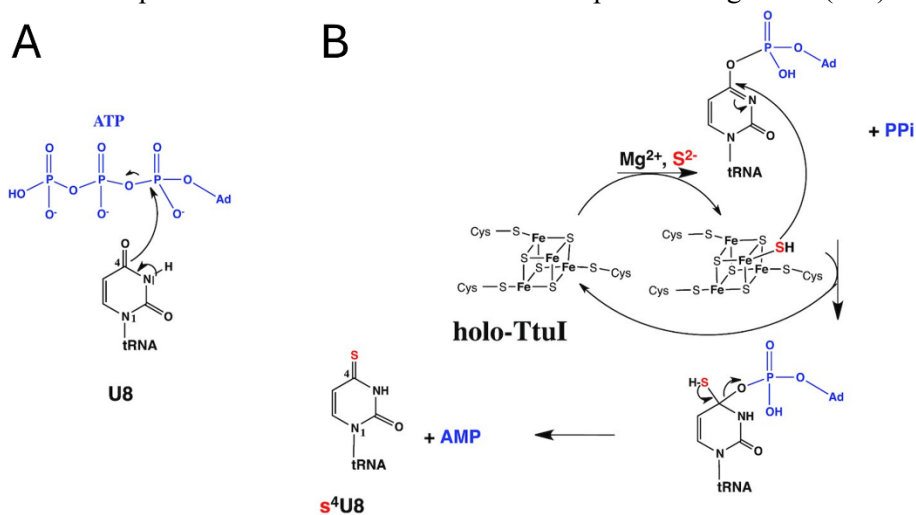


Figure 14. Proposed catalysis mechanism for *Methanococcus maripaludis* ThiI. **A:** U8 activation by ATP adenylation. **B:** formation of a [4Fe–5S] cluster intermediate and nucleophilic substitution of O-adenosyl monophosphate by the SH group coordinated by the [4Fe–4S] cluster. Figure reproduced from (102).

1.3 Iron-sulfur proteins

1.3.1 Iron-sulfur proteins

Iron-sulfur (FeS) proteins are a class of proteins that contain FeS inorganic cofactors and are found ubiquitously in nearly all living organisms. These proteins are highly versatile in their functions and participate in various processes such as electron transfer (e.g., ferredoxins, Rieske proteins, nitrogenases), catalysis (e.g., aconitase, fumarase), and regulation (e.g., IscR, FNR) (124). FeS clusters are assembled from either ferrous (Fe^{2+}) or ferric (Fe^{3+}) iron and, unlike the simplest FeS proteins, rubredoxins (Figure 15A), they contain inorganic sulfide (S^{2-}). These clusters are most often combined in rhombic [2Fe-2S] or cubic [3Fe-4S] and [4Fe-4S] (Figure 15BCD) structures (125). Typically, FeS clusters within proteins are coordinated by the four side chains of cysteine residues. However, in addition to cysteines, coordination by histidine is common for [2Fe-2S] clusters. Occasionally, the coordination of clusters may involve other side chains such as aspartic acid, glutamic acid serine or arginine (126). Apart from the relatively common single-type non-cysteine ligand, only one protein to date has been reported to possess an FeS cluster bound with three different amino acid ligands (127). The diversity of possible coordinating ligands and sequence motifs, similar to other metal cofactor-containing proteins, makes the identification of new FeS proteins challenging (126).

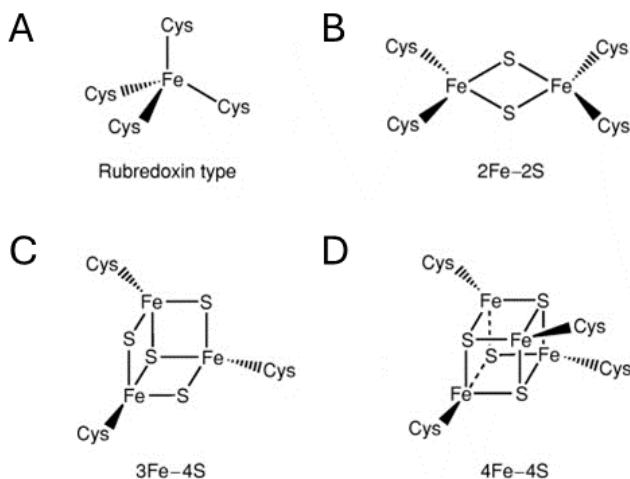


Figure 15. The coordination of Fe and S in the four most common types of FeS proteins. Reproduced from (125).

1.3.2 Iron-sulfur cluster biogenesis

Although FeS clusters can be assembled spontaneously, this process is tightly controlled *in vivo* to prevent the accumulation of toxic levels of Fe^{2+} and S^{2-} (125). The biogenesis of FeS clusters is a complex process involving multiple proteins. Three different FeS cluster assembly systems are known in bacteria: ISC, a common bacterial housekeeping cluster assembly system (124); SUF, a pathway associated with stress response (e. g. iron limitation or oxidative stress in *E. coli*), though some bacteria (e.g. *Bacillus subtilis*) utilize it as a housekeeping system (128); and NIF, a pathway responsible for the specific maturation of nitrogenases in azototrophic bacteria. A common feature of all *de novo* FeS cluster assembly systems is the utilization of cysteine desulfurase (IscS, SufSE, or NifS respectively) by converting L-cysteine to L-alanine to form protein-bound sulfane sulfur in the form of persulfide on the cysteine residue of the protein. Clusters are then combined with iron on scaffold proteins (IscU, SufB, or NifU) and transferred to recipient proteins by energy-dependent chaperones and FeS carrier proteins (for example IscA, SufA) (124).

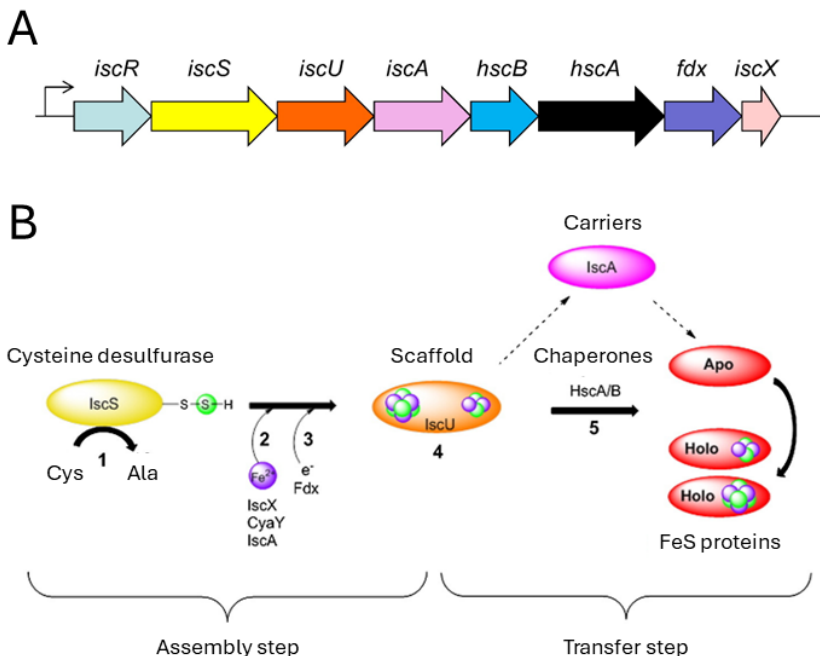


Figure 16. A: operon structure of ISC FeS cluster assembly system. **B:** Schematic view of FeS biogenesis in the ISC system. Ovals represent proteins (IscS, IscU, IscA, and targets). Steps 1-4 correspond to the assembly step and step 5 is the transfer step in which the FeS cluster is transferred directly from IscU to targets with the help of chaperones or indirectly through the IscA FeS transporter. Balls in green represent sulfur atoms; balls in violet represent iron, with both [2Fe-2S] and [4Fe-4S] represented on IscU and on targets. Figure reproduced from (129).

The assembly of FeS clusters by the ISC system relies on an operon consisting of eight genes (Figure 16A) and at least one additional protein encoded outside the operon (129). Cluster biogenesis starts with persulfide formation on IscS (Figure 16B1). Due to the cellular toxicity of free iron, in addition to IscS, IscU, and IscA a protein acting as an iron donor is required for FeS cluster formation. The role of the iron carrier is hypothesized to be carried out by IscX and/or IscA and/or CyaY (Figure 16B2). However, the direct contributions and specific circumstances under which these proteins are utilized remain largely unknown (130). Notably, CyaY is encoded outside the operon and is homologous to eukaryotic frataxin, which is hypothesized to act as an iron chaperone or an iron storage protein (131). To form an FeS cluster utilizing persulfide-bound sulfur, additional electrons must be provided (Figure 16B3). It is hypothesized that this requirement is fulfilled by Fdx, a [2Fe-2S] cluster-containing ferredoxin (132). Once the FeS cluster is formed within the IscU scaffold (Figure 16B4), it must be transferred to apo-targets. This process can be carried out through the IscA FeS transporter or assisted by HscA and HscB chaperone proteins, which promote a rapid and controlled transfer of the cluster through ATP-dependent activation (Figure 16B5) (129).

1.3.3 Regulation of iron-sulfur cluster synthesis by IscR

The operon encoding proteins of the ISC FeS cluster assembly system includes a gene for the transcription regulator IscR. IscR controls the expression of more than 40 genes associated with anaerobic respiration and FeS cluster formation, including its own operon and the SUF system (133). IscR contains a [2Fe-2S] cluster ligated by three cysteine residues and one histidine residue (134). Likely due to its central role in FeS homeostasis, IscR does not require sulfur carrier proteins for its [2Fe-2S] cluster formation and instead receives it directly from scaffold proteins (135).

IscR is sensitive to oxygen; exposure to oxygen results in the destruction of its [2Fe-2S] cluster, producing apo-IscR. Depending on the binding site it targets, IscR can function as both a transcription repressor and an activator. Type I binding sites are primarily targeted by holo-IscR, where it acts as a repressor, while type II binding sites are targeted by apo-IscR, where it acts as a transcription activator. The ISC operon is targeted by holo-IscR at the type I binding site, and its transcription is inhibited during anaerobic growth (Figure 17A). In the presence of oxygen, the damaged IscR dissociates from the binding site, allowing ISC genes to be transcribed (Figure 17B). This regulation is important under anaerobic conditions, when the turnover of FeS

clusters in bacterial proteins is lower than under aerobic conditions due to the susceptibility of FeS clusters to O₂ and/or reactive oxygen species (136).

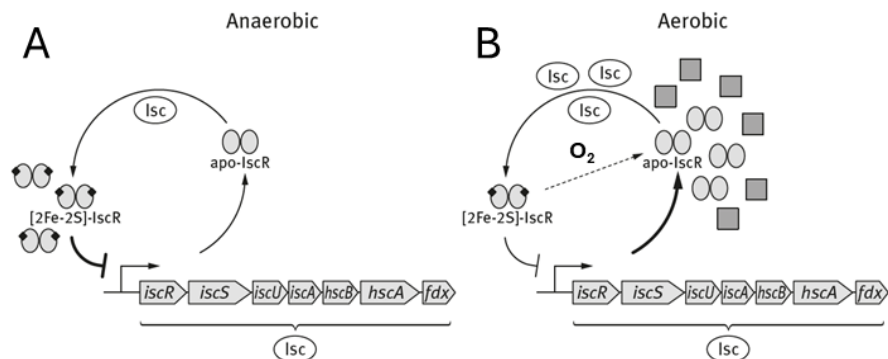


Figure 17. Model of IscR-controlled transcription regulation (ISC operon example). **A:** under anaerobic conditions, the rate of general FeS cluster turnover is decreased, resulting in increased levels of holo-IscR, which is repressing the ISC operon **B:** Under aerobic conditions, holo-IscR loses its FeS cluster and the overall demand of FeS cluster assembly is high. Due to competition for cluster acquisition, apo-IscR levels are elevated resulting in derepression of IscR operon. Figure reproduced from (136).

The deletion of the *iscR* gene can be a useful tool for producing FeS cluster-containing recombinant proteins under anaerobic conditions. In the *E. coli* BL21(DE3) strain, deletion of this gene results in significantly higher yields of recombinant FeS cluster-containing proteins and increased protein iron content, indicating a higher fraction of fully assembled FeS clusters compared to the wild-type laboratory strain (137).

1.3.4 [4Fe-4S] proteins in non-redox catalysis

A significant share of cubane [4Fe-4S] cluster-containing proteins participate in various redox reactions. In nature, [4Fe-4S] is the most common multinuclear metal cofactor involved in electron transfer and storage (138). However, some [4Fe-4S] cluster-containing proteins demonstrate distinct functions, such as regulation. For instance, FNR transcriptional activator uses its [4Fe-4S] cluster as an oxygen sensor (139). Another function includes non-redox catalysis, where the [4Fe-4S] cluster acts as a Lewis acid (140).

Not many examples of [4Fe-4S] cluster-containing enzymes that catalyze non-redox reactions are available. Most of these enzymes belong to hydrolyase class (EC 4.2.1) (e.g., aconitase, 3-Isopropylmalate isomerase, Fumarase A and B) (141) and aconitases stand out as best-studied examples. Aconitases, participating in the citric acid cycle, are present in mammalian cytosol, mitochondria, and bacteria (142). These enzymes catalyze the reversible isomerization of citrate to isocitrate via cis-aconitate. The [4Fe-4S] cluster of

aconitase is coordinated by three cysteine residues, leaving the fourth iron ion exposed to the solvent. During catalysis, this fourth iron binds to the oxygen atoms of citrate, facilitating its dehydration (Figure 18) (143).

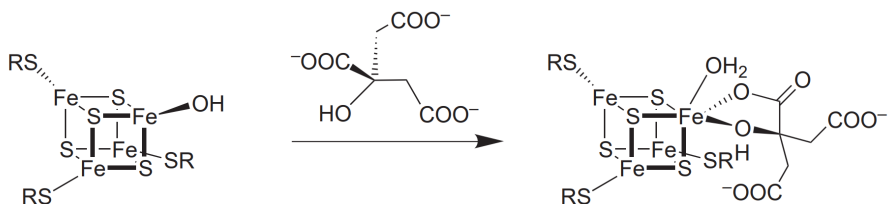


Figure 18. Citrate binding to the active site [4Fe-4S] cluster of aconitase. Reproduced from (144).

Another example of a [4Fe-4S] cluster-containing enzyme catalyzing non-redox reaction is thiouracil desulfidase TudS. TudS is further reviewed in the following paragraph.

1.4 TudS desulfidases

1.4.1 Discovery of TudS desulfidases

TudS is a thiouracil desulfidase, previously known as DUF523 (Domain of Unknown Function 523). TudS was initially identified from metagenomic libraries using the *E. coli* uracil auxotrophic strain. Three different plasmids allowing uracil auxotrophs to grow on 2-thiouridine as the sole source of uracil were isolated. All of these plasmids contained ORFs encoding proteins of the previously uncharacterized DUF523 family (145). It was later shown, that 2-thiouracil could be substituted with 4-thiouracil while maintaining the same growth phenotype (146).

Mutational analysis and in vivo and in vitro tests indicated that the TudS protein possesses an FeS cluster. Aerobically purified recombinant TudS demonstrated spectral properties typical of a [4Fe-4S] cluster-containing proteins, though no in vitro activity was observed, likely due to FeS cluster damage from environmental oxygen (145).

1.4.2 Catalysis by TudS

To elucidate the enzyme's mechanistic properties, a functionally active enzyme was obtained by reconstituting the FeS cluster in anaerobically purified recombinant TudS from *Aeromonas* sp. using ferrous iron, L-cysteine, and the cysteine desulfurase CsdA, resulting in holo-TudS. In vitro activity assays showed a preference for 4-thiouracil over 2-thiouracil. Furthermore, holo-TudS was crystalized (Figure 19A), confirming the [4Fe-4S] cluster was coordinated by three conserved cysteines, with the fourth iron being free, potentially binding other ligands during catalysis. After soaking the crystals with 4-thiouracil, a hydrosulfide, most likely derived from 4-thiouracil, was detected bound to the [4Fe-4S] cluster resulting in [4Fe-5S] cluster intermediate (Figure 19B) (146). The existence of such a structure in nature was previously postulated, although not unambiguously proven (147).

These results suggested a catalytical mechanism for TudS (Figure 19B), which was supported by mutational analysis. Initially, the 4-thiouracil molecule binds to the TudS [4Fe-4S] cluster via its sulfur atom. A water molecule is then activated by hydrogen bonds with Ser101 and Glu45, and becomes nucleophilic enough to attack the C–S bond of thiouracil and this leads to the substitution of sulfur by a hydroxide ion. The resulting hydroxyl group at the C4 atom is deprotonated, releasing hydrosulfide and forming a

[4Fe-5S] cluster. The [4Fe-4S] cluster is then regenerated by a proton, likely from the adjacent water molecule, by releasing H₂S (146).

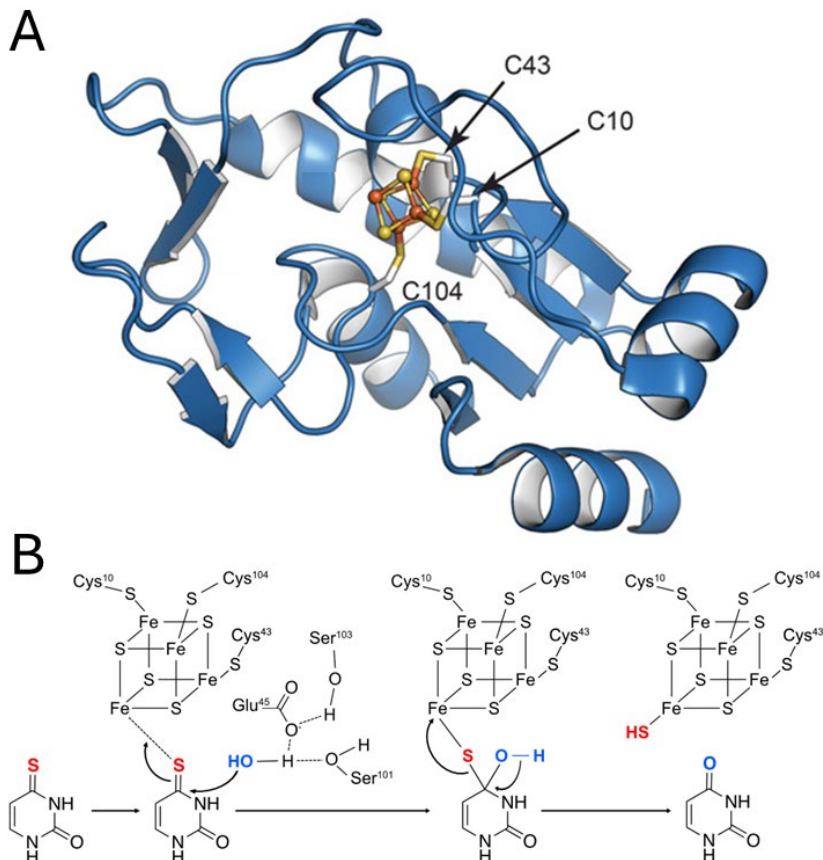


Figure 19. **A:** Crystallographic structure of TudS from *Aeromonas* sp. with FeS cluster. Three conserved cysteines (Cys10, Cys43, and Cys104) are bound to three iron atoms of the [4Fe-4S] cluster. **B:** proposed catalytic mechanism of TudS featuring [4Fe-5S] cluster intermediate. A reproduced and B adapted from (146).

1.4.3 Distribution of TudS domain-containing proteins

Sequences encoding TudS domain-containing proteins are reported across all domains of life, predominantly in bacteria. As of 2024 13934 bacterial-origin sequences are reported, compared to 493, 41, and 14 sequences from archaea, eukaryotes, and viruses, respectively (148). Although the TudS domain functions as a standalone enzyme (146) and is predominant in this family of proteins (58,5% of all reported sequences), a significant portion is found fused with the DUF1722 domain (40.4% of all reported sequences). Additionally, 47 sequences (0.3% of all reported

sequences) are fused with nucleoside phosphorylase, an enzyme involved in the nucleoside salvage pathway (148).

The DUF1722 domain, often fused with TudS in some organisms, is also encoded as a standalone protein (20% of all reported DUF1722 sequences) (148). Notably, *E. coli* lacks both TudS and TudS-DUF1722 but possesses a standalone DUF1722 domain coding gene *ybgA*. This gene is located within the same operon and is co-transcribed with *phr*, which encodes DNA photolyase, an enzyme that repairs UV radiation-induced pyrimidine dimerization in DNA (149). The operon containing the *ybgA* gene is part of the RpoS regulon, which is activated by the alarmone ppGpp during various stress conditions, including amino acid starvation and other forms of nutrient depletion. An isoleucine starvation-based experimental approach has shown that transcription of the *ybgA* gene is indeed activated during the amino acid starvation-induced stringent response (150). Presumably, cotranscribed genes may serve related functions, however, despite *E. coli* being a well-studied organism, the function of YbgA and its relation to DNA damage repair or the stringent response remain unspecified.

Previous studies on TudS suggest that the function of TudS-DUF1722 fusion proteins may differ from that of standalone TudS. Expression of TudS-DUF1722 encoding gene from *Salmonella typhi* LT2 strain (*orf319*) resulted in no growth phenotype of uracil auxotrophs on 2-thiouracil in contrast to TudS (145). The *orf319* gene is located within *Salmonella* pathogenicity island 2 (SPI-2), a gene cluster essential for intracellular survival and proliferation in infected hosts (151). It is situated immediately downstream of the *mlrB* gene, which encodes a MerR-like family transcription regulator that represses *orf319* transcription in vitro under SPI-2-inducing conditions and in vivo when bacteria reside inside macrophages. However, the regulation of MlrB and its physiological role remain unclear (152).

The control of TudS-DUF1722 encoding genes by MerR-like family transcription regulators is observed in other species as well. In *Pseudomonas putida* KT2440, *TudS-DUF1722* is a light-responsive gene. The gene is part of the same operon as the DNA photolyase encoding gene, and their co-transcription is regulated by the MerR-like light-sensitive LitR adenosyl B12-dependent regulator. In the dark, LitR functions as a negative regulator, suppressing the transcription of light-inducible genes. However, upon exposure to 450 nm blue light, LitR is deactivated (153). Similarly, in *Thermus thermophilus*, the *TudS-DUF1722* gene is controlled by adenosyl B12-dependent LitR where it is upregulated along with the light-inducible carotenoid biosynthesis cluster involved in the light-induced oxidative stress response (154).

2. MATERIALS AND METHODS

2.1 Materials

2.1.1. Nucleic acids

DNA primers were synthesized by Metabion International AG (Germany) and Azenta (Germany) and are listed in Appendix 1. Gene synthesis was performed by Thermo Fisher Scientific (USA). Total tRNA from *E. coli* MRE 600 manufactured by Roche (Switzerland). Plasmid vectors used in this study are listed in Appendix 2.

2.1.2. Proteins, kits and chemicals

Enzymes used for molecular biology procedures were obtained from Thermo Fisher Scientific (USA) and tRNA digestion was carried out using Nucleoside Digestion Mix manufactured by New England Biolabs (USA). All these products were used according to the manufacturer's protocols if not otherwise indicated. aLICator LIC Cloning and Expression Kit, GeneJET Plasmid Miniprep Kit and GeneJET Gel Extraction and DNA Cleanup Micro Kit were obtained from Thermo Fisher Scientific (USA) and Quick-DNA Fungal/Bacterial Miniprep Kit was obtained from Zymo Research (USA). Anti-His-Tag primary antibodies were obtained from Thermo Fisher Scientific (USA) and HRP-conjugated anti-mouse secondary antibodies from Carl Roth (Germany). All chemicals used in this study were of the highest quality available.

2.1.3. Bacterial strains

***Escherichia coli* DH5 α** – [F⁻ *endA1 glnV44 thi-1 recA1 relA1 gyrA96 deoR nupG purB20 ϕ 80dlacZ Δ M15 Δ (lacZYA-argF)U169, hsdR17(*r*_K⁻*m*_K⁺), λ -] – Pharmacia, USA.*

***Escherichia coli* BL21(DE3)** – [*E. coli* str. B F⁻ *ompT gal dcm lon hsdS_B*(*r*_B⁻*m*_B⁻) λ (DE3 [*lacI lacUV5-T7p07 ind1 sam7 nin5*]) [*malB*⁺]_{K-12}(λ ^S)] – Avidis, France.

***Pseudomonas* sp. MIL9** – NCBI accession ID: PRJNA698458 – Isolated from soil; Vilnius university Life Sciences Center (155).

***Pseudomonas* sp. MIL19** – NCBI accession ID: PRJNA877084 PRJNA698458 – Isolated from soil; Vilnius university Life Sciences Center.

***Pseudomonas putida* KT2440** – DSM No.: 6125 – Leibniz Institute DSMZ-German Collection of Microorganisms and Cell Cultures GmbH, Germany.

***Salmonella enterica* subsp. *enterica* serovar Typhimurium LT2 Δ pyrF** – a gift from Gunilla Jäger, Umeå University, Sweden.

***Thermus thermophilus* HB8** – DSM No.: 579 – Leibniz Institute DSMZ German Collection of Microorganisms and Cell Cultures GmbH, Germany.

***Escherichia coli* BL21(DE3) Δ iscR** – (137).

***Escherichia coli* HMS174(DE3) Δ pyrF** – (146).

***Bacillus subtilis* subsp. *subtilis* 168** – DSM No.: 23778 – *Bacillus* Genetic Stock Center, USA.

***Bacillus subtilis* subsp. *subtilis* 168 Δ ybbK::erm** – BKE01720 – *Bacillus* Genetic Stock Center, USA.

2.2 Methods

2.2.1. Construction of bacterial expression vectors

Standard DNA manipulation techniques were used (156), and all the kits were utilized according to the manufacturer's recommendations unless otherwise indicated.

E. coli expression vectors were constructed using the aLICator LIC Cloning and Expression Kit. Bacterial genes were either cloned directly from the genomic DNA or plasmid vectors used in previous studies served as templates. For genomic DNA isolation, the Quick-DNA Fungal/Bacterial Miniprep Kit was used. Routine cloning was carried out using the *E. coli* DH5 α strain, and plasmid isolation and PCR product extraction from agarose gels were carried out using GeneJET kits. Site-directed mutagenesis was carried out using Phusion™ Plus DNA polymerase and a single oligonucleotide primer as described in (157). The primers were designed by changing a codon encoding the amino acid of interest to one encoding either methionine (158), phenylalanine, or alanine. An empty pLATE11 vector was generated by PCR amplification of the backbone and blunt end ligation. The parental plasmid was digested by *DpnI* restriction endonuclease, PCR product was gel-purified, phosphorylated using T4 polynucleotide kinase, and blunt ends were ligated using T4 DNA ligase.

Pseudomonas putida KT2440 expression vectors were constructed by amplification of the insert together with RBS from pLATE11 *E. coli* expression vector using primers introducing 5' *XbaI* and 3' *NheI* restriction sites and then cloning it into pJNN vector (159).

2.2.2. Cultivation of bacteria and overexpression of recombinant proteins

Routine cultivation. *E. coli* and *P. putida* KT2440 cultivation was carried out at 37 °C either on agarized LB (1% (w/v) tryptone, 0.5% (w/v) yeast extract, 0.05% NaCl (w/v), 1.5% agar (w/v)) media or in liquid LB (1% (w/v) tryptone, 0.5% (w/v) yeast extract, 0.05% NaCl (w/v)) media with agitation at 180 rpm unless otherwise indicated. Standard antibiotic concentrations were used: 100 μ g/mL ampicillin and 15 μ g/mL kanamycin for *E. coli*, and 100 μ g/mL kanamycin and 20 μ g/mL gentamycin for *P. putida* KT2440, if not otherwise indicated.

***E. coli* growth complementation assay.** The assay utilized the uracil auxotrophic *E. coli* HMS174 Δ *pyrF* strain. Bacteria, either carrying the

pLATE11 vector with an insert or an empty pLATE11 vector as a negative control, were initially cultured in LB medium supplemented with ampicillin overnight at 37 °C, 180 rpm. The overnight cultures were then diluted in M9 minimal media (1× M9 salts, 1 mM MgSO₄, 0.05 mM, CaCl₂, 0.4% glucose, 100 µg/mL ampicillin, 0.1 mM IPTG) to an OD₆₀₀ of 0.001. If necessary, cultures were supplemented with nucleobases at a final concentration of 200 µM. Aliquots of 150 µL were dispensed into the wells of 96-well flat-bottom plate. Bacterial growth was monitored using Infinite M200 PRO (Tecan, Switzerland) microplate reader. Plates were incubated at 37 °C with periodic shaking for 30 s every 5 min and OD₆₀₀ measurements every 15 min.

***P. putida* KT2440 growth complementation assay.** The assay was carried out using wild-type bacteria and uracil auxotrophic *P. putida* KT2440 Δ pyrF and *P. putida* KT2440 Δ pyrF Δ tudS_{KT} strains. The wild-type strain was grown in liquid LB medium, while the uracil auxotrophic strains were grown in liquid LB medium supplemented with 1 mM uracil overnight. Overnight cultures were washed from uracil using 0.9% NaCl, resuspended, and inoculated to an OD₆₀₀ of 0.02 in liquid M9 minimal media (1× M9 salts, 1mM MgSO₄, 0.05mM CaCl₂, 0.2% glucose) supplemented with nucleobases and nucleosides at the final concentration of 200 µM. Aliquots of 150 µL were dispensed into the wells of 96-well flat-bottom plate. Bacterial growth was monitored using the same settings as described above

TudS_PP overexpression for purification. *E. coli* BL21(DE-3) Δ iscR strain (137) carrying the pLATE31-TudS_PP vector was cultivated anaerobically. Bacteria were grown in TB medium (89 mM KH₂PO₄/K₂HPO₄ at pH 7.5, 12 g/L tryptone, 24 g/L yeast extract, 0.2% (v/v) glycerol, 50mM fumaric acid, 760 µM Fe(III)-citrate, 100 µg/mL ampicillin, 75 µg/mL kanamycin). After inoculation, the culture bottles were sealed with rubber stoppers and the air in the headspace was flushed with sterile nitrogen. Cells were incubated at 37 °C, 100 rpm until reaching the log phase (OD₆₀₀ ~0.6). Recombinant gene expression was induced by adding 0.75mM IPTG, and growth medium was supplemented with 1 mL/L vitamin solution VL-73 (160), trace element solution SL-93 (161), 0.1mM CaCl₂, 0.8mM MgSO₄, and 3mM NaNO₃. Cells were incubated for 20 h at 20 °C, 100 rpm. Cells were harvested anaerobically by centrifugation at 4,500 × g (4 °C) for 20 min and used directly or stored at -80 °C in anaerobically sealed bottles.

tRNA isolation from *E. coli*. For tRNA isolation, a single colony of *E. coli* BL21(DE3), either carrying the pLATE11 or pLATE52 vector with an insert or an empty pLATE11 vector as a negative control, was inoculated into 20 mL of LB medium supplemented with ampicillin. Cultures were incubated at 37°C, 180 rpm. Upon reaching the log phase (OD₆₀₀ ~0.6), recombinant

protein production was induced by the adding IPTG to a final concentration of 0.1 mM. Cells were harvested by centrifugation 4 h post-induction and used for tRNA isolation immediately or stored at -20°C until further use.

tRNA isolation from *P. putida* KT2440. For tRNA isolation, a single colony, either carrying the pJNN (159) vector with an insert or an empty pJNN vector as a negative control, was inoculated into 20 mL LB medium supplemented with gentamycin (50 µg/mL) and grown overnight at 30°C, 180 rpm. The overnight culture was added to 50 mL of fresh LB media, and sodium salicylate (1 mM final concentration) was added to induce recombinant protein production at 30°C, 180 rpm. Four hours after induction, cells were harvested by centrifugation and used for tRNA isolation immediately or stored at -20°C until further use. *P. putida* KT2440 strains without vectors were grown overnight in LB medium at 30°C, 180 rpm, harvested by centrifugation and used for tRNA isolation immediately or stored at -20°C until further use.

RudS_KT overexpression for purification. For recombinant RudS_KT production, an auto-induction medium with slight modifications was used (162). The base medium consisted of 10 g tryptone, 10 g yeast extract, and 10 g glycerol per liter. The medium was supplemented with 50× salt solution (1.25 M Na₂HPO₄, 1.25 M KH₂PO₄, 2.5 M NH₄Cl, 0.25M Na₂SO₄), 50× lactose solution (25% glycerol, 2.5% glucose, 10% α-lactose), MgSO₄ (2 mM final concentration), 1000× trace metal solution, and 100 µg/mL ampicillin. A single colony of *E. coli* BL21(DE3) carrying the pLATE52-RudS_KT vector was inoculated into 50 mL of medium and incubated at 37 °C, 180 rpm. After 6 h, the temperature was reduced to 20°C, and incubation continued for an additional 16-20 h. Induction was verified by adding 1 µL of a 2% X-Gal solution to 1 mL of the culture, followed by incubation for 30 min at 37 °C.

TruB overexpression for purification. To serve as a positive EMSA shift control *E. coli* BL21(DE3) pseudouridine synthase gene (NCBI gene locus tag: ECD_03033) was cloned into pLATE31 vector. A single colony of *E. coli* BL21(DE3), carrying pLATE31-TruB, was inoculated into 50 mL of LB medium supplemented with ampicillin. Cultures were incubated at 37°C, 180 rpm. Upon reaching the log phase (OD₆₀₀ ~0.6), recombinant protein production was induced by the adding IPTG to a final concentration of 0.1 mM and incubated 20°C, 180 rpm, overnight. Cells were harvested by centrifugation used immediately or stored at -20°C until further use.

2.2.3. *Pseudomonas putida* KT2440 mutant strains

P. putida KT2440 mutant strains bearing single or double markerless gene disruptions were obtained by double crossover recombination technique according to the modified protocol by Oh et al. (163). Two ~500 bp regions upstream and downstream of the gene of interest were amplified by PCR directly from *P. putida* suspension in water. A kanamycin resistance cassette was amplified from FRT-PGK-gb2-neo-FRT PCR-template (Gene Bridges, Germany). Two genomic DNA fragments and a kanamycin resistance cassette were joined by overlap PCR and the product was cloned into SmaI-digested pUC19_sacB suicide vector (164). *P. putida* cells were transformed by electroporation (165). Kanamycin resistant crossovers were selected on LB agar plates supplemented with 100 µg/mL kanamycin, grown at 30 °C overnight. The first crossover was confirmed by streaking colonies on LB agar plate containing 20% sucrose, grown at 30 °C overnight. The positive clones demonstrated characteristic blurred shape and slower growth. A single sucrose-sensible clone was grown for 6 h in LB media at 37 °C and serial dilutions were plated on LB agar plate containing 1 mg/mL 5-fluoroorotic acid (FOA) or 20% sucrose to detect *pyrF* or *thiI*, *tudS_KT*, *ruds_KT* knockouts, respectively. Sucrose or FOA-resistant, kanamycin-sensitive second crossovers were confirmed by PCR using specific primers covering a region upstream and downstream knocked out gene. Markerless mutations were confirmed by cloning the region of interest into pUC19 vector and sequencing.

2.2.4. Purification of recombinant proteins

Anaerobic purification of TudS_PP. Sample preparation and purification were carried out in a glovebox (Coy, USA) under anaerobic conditions (95% N₂, 5% H₂). For the preparation of crude cell extracts, harvested bacteria were resuspended in buffer A (20mM HEPES pH 7.5, 300mM NaCl, 10mM imidazole) supplemented with ~0.1 mg/L DNase I, ~0.1 mg/L RNase A and ~0.1 mg/L lysozyme. The cell suspension was passed through a chilled French pressure cell, followed by ultra-centrifugation at 150,000 × g for 1h. The supernatant was filtered with a 0.22 µm filter, and the recombinant TudS_PP protein was purified using an AKTA pure FPLC system (Cytiva, USA) with a 5mL HiTrap TALON® crude (Cytiva, USA) protein purification column, previously equilibrated with buffer A. After washing the column with 10 column volumes of buffer A, the adsorbed protein was eluted with a linear gradient of 10–400 mM imidazole over 10 column volumes. The protein was concentrated to 10–35 mg/mL using Vivaspin™ Turbo 15 RC 10000 MWCO

concentrators (Sartorius, Germany), and the buffer was adjusted to 20mM HEPES pH 7.3, 300 mM NaCl and 5 % (v/v) glycerol. The purified enzyme was stored in anaerobically sealed tubes at -80°C .

Aerobic purification of RudS_KT. For the preparation of crude cell extracts, harvested bacteria from 50 mL cultures were resuspended in 7.5 mL of buffer A (50 mM TRIS-HCl pH 8, 500 mM NaCl, 10 mM imidazole, 10% (w/v) glycerol), supplemented with ~ 0.1 mg of DNase I, 15 mM MgSO_4 and 1 mM PMSF. The cells were disrupted using an ultrasonic disintegrator and centrifuged at $30,000 \times g$, 4°C for 10 min. The supernatant was applied to 1 mL HiTrap Chelating HP chromatography column (Cytiva, USA) pre-equilibrated with buffer A using AKTA Pure FPLC system (Cytiva, USA). The protein was eluted by applying a linear gradient (0–100%) of buffer B (50 mM TRIS-HCl pH 8, 500 mM NaCl, 500 mM imidazole, 10% (w/v) glycerol) over 10 min using 10 column volumes. Following elution, the buffer in the fractions was exchanged with buffer S (50 mM TRIS-HCl pH 8, 500 mM NaCl, 10% (w/v) glycerol) using 5 mL HiTrap Sephadex G-25 Desalting columns (Cityva, USA). To minimize the protein's exposure to oxygen, all buffers were degassed under vacuum for 30 min with stirring. The fractions were collected in 0.5 mL aliquots in 0.5 mL tubes and sealed immediately after fractionation.

The molar mass of RudS_KT was determined by analytical gel filtration using a Superose 12 10/300 GL column (Cytiva, USA) previously equilibrated with 50 mM TRIS-HCl pH 8, 500 mM NaCl, 10% (w/v) glycerol, under aerobic conditions. Carbonic anhydrase (29 kDa), bovine serum albumin (66 kDa), alcohol dehydrogenase (150 kDa), and β -Amylase (200 kDa) were used as standards (Sigma-Aldrich, USA) for column calibration. The experiment was repeated three times to determine the standard deviation.

Aerobic purification of TruB. For the preparation of crude cell extracts, harvested bacteria from 50 mL cultures were resuspended in 7.5 mL of buffer A (25 mM TRIS-HCl pH 7, 300 mM NaCl, 10 mM imidazole). The cells were disrupted using an ultrasonic disintegrator and centrifuged at $30,000 \times g$, 4°C for 10 min. The supernatant was applied to 1 mL HiTrap Chelating HP chromatography column (Cytiva, USA) pre-equilibrated with buffer A using AKTA Pure FPLC system (Cytiva, USA). The protein was eluted by applying a linear gradient (0–100%) of buffer B (25 mM TRIS-HCl pH 7, 300 mM NaCl, 500 mM imidazole) over 10 min using 10 column volumes. Following elution, the buffer in the fractions was exchanged with buffer S (25 mM TRIS-HCl pH 7, 300 mM NaCl, 5% (w/v) glycerol) using 5 mL HiTrap Sephadex G-25 Desalting columns (Cityva, USA).

All purified protein samples were analyzed using 14% SDS-PAGE gel. Protein concentration was measured using Bradford method (166). Iron content in protein samples was determined using ferene assay (167).

2.2.5. Enzymatic activity assays

TudS_PP in vitro activity measurements. Enzymatic activity assay of TudS_PP was carried out in a glovebox (Coy, USA) under anaerobic conditions (95% N₂, 5% H₂). The assays were performed in 40–50 μ L of 100 mM MOPS/KOH pH 7.3 and started by adding 0.02–5 μ M of recombinant TudS_PP. Conversion of low substrate concentrations of <150 μ M (4-thiouracil, 4-thiouridine, 4-thio-UMP, and 4-thio-UTP) was assayed using a continuous spectrophotometric assay measuring the specific decrease in substrate absorbance (extinction coefficients provided by the manufacturers). Conversion of high substrate concentrations (0.25–3.75mM) was measured by UPLC. Reactions were started by the addition of the enzyme and stopped by adding 5 μ L of formic acid. The proteins were precipitated, and supernatants were analyzed on an Acquity H-Class UPLC (Waters) by reversed-phase liquid chromatography (Waters Acquity UPLC HSS T3 2.1 \times 100mm column, 1.8 μ m particle size) using a gradient of water/acetonitrile containing 0.1% formic acid. The identity and concentrations of the substrates and products were determined from their retention times and spectra by comparison with standards. The catalytic constants were determined using the Prism software package (GraphPad, USA) by fitting the reaction rates obtained at different substrate concentrations to Michaelis–Menten curves.

RudS_KT in vitro activity measurements. The in vitro tRNA 4-thiouridine desulfidation assay was carried out aerobically using purified RudS_KT and total tRNA from *E. coli* MRE 600 (Roche, Switzerland). Purified RudS_KT concentrations were adjusted to 0.7 mg/mL (17.85 μ M) with buffer S (50 mM Tris-HCl pH 8, 500 mM NaCl, 10% (w/v) glycerol). Reactions were carried out in 100 μ L reaction mixtures containing 5.3 μ M RudS_KT, 0.4 μ M tRNA, 100 mM Tris-HCl pH 7, and 150 mM NaCl at 22 $^{\circ}$ C. Reactions were stopped by heating the samples at 95 $^{\circ}$ C for 5 min, followed by centrifugation at 30,000 \times g, 4 $^{\circ}$ C for 10 min, and ethanol precipitation of tRNA in the supernatant. Samples were digested to single nucleosides and analyzed by HPLC-MS/MS as described in the following section. To test the (p)ppGpp effect on RudS_KT activity, a 10-fold molar excess of guanosine-3',5'-pentaphosphate (pppGpp) (Jena Bioscience, Germany) or guanosine-3',5'-tetraphosphate (ppGpp) (Jena Bioscience, Germany) was added to an equimolar amount of tRNA and RudS_KT.

Reactions were carried out in 100 μ L reaction mixtures at 22 °C containing 4 μ M RudS_KT, 4 μ M tRNA, 100 mM Tris-HCl pH 7, 150 mM NaCl, and 40 μ M of (p)ppGpp. Reactions were stopped by heating and analyzed by HPLC-MS/MS.

2.2.6. Bulk tRNA isolation

Bulk tRNA was prepared with slight modifications to the method described in (168). The harvested bacterial culture was resuspended in 600 μ L of extraction buffer (1 mM Tris-HCl, pH 7.4, 10 mM Mg-acetate) and mixed with 600 μ L of ROTI Aqua-Phenol (Carl Roth, Germany). The mixture was mixed using a vortex mixer at 2000 rpm for 15 min, followed by centrifugation at $30,000 \times g$, 16 °C for 10 min. The aqueous phase was mixed with 0.1 volume of 5 M NaCl and 2 volumes of 100% ethanol, followed by centrifugation at $30,000 \times g$, 4 °C for 10 min. The pellet was resuspended in 550 μ L of 1 M NaCl and centrifuged at $30,000 \times g$, 4 °C for 10 min. Subsequently, 500 μ L of the supernatant was mixed with 1250 μ L of 100% ethanol and incubated at -20 °C overnight. The precipitate was collected by centrifugation at $30,000 \times g$, 4 °C for 10 min and dissolved in 25 mM K-phosphate buffer (pH 6.5).

For the purification step, the sample was applied to a HiTrap DEAE Sepharose FF column (Cytiva, USA) pre-equilibrated with buffer A (25 mM Na-phosphate pH 6.5, 50 mM NaCl, 5 mM MgSO₄) using an AKTA Pure FPLC system (Cytiva, USA). The tRNA was eluted by applying a linear gradient (0-100%) of buffer B (25 mM Na-phosphate pH 6.5, 1 M NaCl) over 10 min using 10 CV. The eluted fractions were precipitated by the addition of 3 volumes of 100% ethanol. The resulting pellet was resuspended in DEPC-treated water.

The nano-tRNAseq of total *E. coli* BL21(DE3) tRNA was performed by Immagina Biotechnology S.r.l. (Italy) using a nanopore-based sequencing approach (169). The bulk tRNA was extracted as indicated above, and s4U was quantified using HPLC-MS/MS.

2.2.7. tRNA nucleoside analysis

For the analysis of modified nucleosides using HPCL-MS/MS, 1 μ g of tRNA was heat denatured for 5 min at 95 °C and subjected to digestion at 37 °C for 16 h using Nucleoside Digestion Mix (New England BioLabs, USA). After digestion, proteins were precipitated by adding an equal volume of acetonitrile to the digested tRNA. The mixture was mixed at 1,400 rpm, 37 °C

for 10 min, and centrifuged at 30,000 g, 4 °C for 20 min. The supernatant was used for nucleoside analysis.

4 μL of the supernatant were analyzed using liquid chromatography-tandem mass spectrometry with a Nexera X2 UHPLC system coupled with LCMS-8050 mass spectrometer (Shimadzu, Japan) equipped with an ESI source. The chromatographic separation was carried out using a 3 × 150 mm YMC-Triart C18 (particle size 3 μm) column (YMC, Japan) at 40 °C and a mobile phase that consisted of 0.1% formic acid (solvent A) and acetonitrile (solvent B) delivered in gradient elution mode at a flow rate of 0.45 mL/min. The following elution program was used: 0 to 1 min, 5% solvent B; 1 to 5 min, 95% solvent B; 5 to 7 min, 95% solvent B; 7 to 8 min, 5% solvent B; 8 to 12 min, 5% solvent B. Modified nucleosides were detected using transitions m/z 247→115 (dihydrouridine), 261→129 (4-thiouridine) at interface temperature of 300 °C and desolvation line temperature of 250 °C. N₂ was used as nebulizing (3L/min) and drying (10L/min) gas, dry air was used as heating (10L/min) gas. The data were analyzed using LabSolutions LCMS software. For quantification, the amount of 4-thiouridine was normalized to the total dihydrouridine content (170).

2.2.8. Western blot

In total, 2 mL of induced bacterial cultures were centrifuged, and the pellets were resuspended in 2 mL Tris-HCl pH 7, 250 mM NaCl buffer. Cells were disrupted using an ultrasonic disintegrator and centrifuged at 30,000 g, 4°C for 10 min. The concentrations of the soluble fractions of the crude extracts were measured using Bradford method. All samples were adjusted to a concentration of 200 ng/μL, and 2 μg of soluble crude extract was loaded onto a 14% SDS-PAGE gel using the Bio-Rad Mini-PROTEAN electrophoresis system and a 10-well or 15-well, 0.75 mm comb (Bio-Rad, USA). Following the electrophoresis, proteins were transferred onto a 0.45 μm nitrocellulose membrane (Thermo Scientific, USA) and blocked using TBST (10 mM Tris-HCl pH 7.5, 150 mM NaCl, 0.1% Tween 20) containing 0.2% I-Block reagent (Thermo Fisher Scientific, USA) for 1 h at room temperature. The membrane was incubated overnight at 4 °C with anti-His-Tag antibodies (Thermo Fisher Scientific, USA) diluted 1:1000 in the blocking solution. The following day, membranes were incubated with the HRP-conjugated anti-mouse secondary antibody (Carl Roth, Germany) diluted 1:10000 in blocking solution for 1 h at room temperature. Detection of protein-antibody complexes was performed using an enhanced chemiluminescence substrate (Thermo Fisher Scientific, USA) and digitally imaged with Azure 280

chemiluminescence detection system (Azure Biosystems, USA). Band intensities were quantified using ImageJ software (National Institutes of Health, USA).

2.2.9. Electrophoretic mobility shift assay (EMSA)

Non-radioactive EMSA was adapted from (171) with slight modifications. The binding reaction was carried out in 20 μ L volume and contained 20 mM Tris-HCl, 10% glycerol, 200 mM NaCl, 0.5 μ g (1 μ M final concentration) total *E. coli* tRNA and 6 μ M his-tagged *E. coli* pseudouridine synthase TruB (positive shift-control) or 1–10 μ M RudS_KT. After 1 min incubation on ice, the whole binding mixture was loaded into 2% agarose gel prepared by using RNase-free TBE buffer (Invitrogen, USA) and DEPC-treated water. Gel and TBE running buffer was supplemented with SYBR™ Green II RNA Gel Stain (Invitrogen, USA). The gel was run at 7 V/cm for 90 min and imaged using Azure 280 fluorescence detection system (Azure Biosystems, USA).

2.2.10. Ultraviolet A (UVA) irradiation experiments

A single colony of *E. coli* BL21(DE3), either carrying the pLATE11 vector with an insert or an empty pLATE11 vector as a negative control, was inoculated into 20 mL of LB medium supplemented with 100 μ g/mL ampicillin and incubated at 37 °C, 180 rpm overnight. The next day 200 μ L of overnight culture was inoculated into 20 mL of fresh of LB medium supplemented with 100 μ g/mL ampicillin and incubated at 37 °C, 180 rpm. Upon reaching the log phase (OD600 ~0.6), the production of recombinant protein was induced by the addition of IPTG to a final concentration of 0.1 mM. Two hours post-induction, the cells were transferred on ice followed by OD600 measurements. The cultures were subsequently diluted in cold M9 minimal media (1 \times M9 salts, 1 mM MgSO₄, 0.05 mM CaCl₂, 0.4% glucose, 100 μ g/mL ampicillin, 0.1 mM IPTG) uniformly to OD600 0.05 and 150 μ L of suspensions were dispensed into the wells of pre-cooled 96-well flat-bottom plate. The UVA irradiation was carried out in UVP C-10 Chromato-Vue cabinet (Analytik Jena, Germany) equipped with 6W, 365 nm UVP UVGL-58 lamp (Analytik Jena, Germany). Bacterial suspensions were irradiated for 120 min (theoretical exposure ~100 kJ/m²), the plate was held on ice throughout the whole procedure. Subsequently, bacterial growth was monitored using Infinite M200 PRO (Tecan, Switzerland) microplate reader. Plates were incubated at 37 °C with periodic shaking for 30 s every 5 min and OD600 measurements every 15 min.

2.2.11. Phylogenetic analysis

Phylogenetic analysis represented in this work was performed by Dr. Audrius Laurynėnas.

The tRNA sulfurtransferase P77718 (172) from *Escherichia coli* was selected as the representative sequence for ThiI, and A0A2L1IC02 (172) from *Pseudomonas* sp. SWI36 was selected as the representative sequence for RudS. These sequences were used to obtain homologous sequences for seed alignments using HMMER (173) with the n70 and nr90 databases (MPI Bioinformatics Toolkit (174)). The initial sequences were split according to domain boundaries identified from AlphaFold2 models, specifically the THUMP, ThiI, and Rhodanese-like domains in ThiI, and the TudS and DUF1722 domains in RudS.

Sequences for each domain obtained from the HMMER search were realigned using T-CoffeeWS with default settings. These alignments were then used to construct hidden Markov models (HMMs). HMMSEARCH was employed to search for homologous sequences using the previously constructed HMMs among complete reference genomes of 332 Archaea, 5042 Bacteria, and 47 viruses. The criteria for the presence of RudS in genomes were an e-value <0.001 and an aligned region length with the HMM >80 amino acids for both the TudS and DUF1722 domains, with these domains appearing in this specific order. The same criteria were applied for the ThiI search, but only the THUMP and ThiI domains were required, instead of all three domains present in P77718.

Found RudS homologues were aligned using HMMALIGN with HMMs produced from the seed alignments obtained with HMMER, as previously described for domain alignments. The resulting alignment was used to produce a phylogenetic tree using Biopython (175) capabilities, with identity fraction as the distance metric and the UPGMA method (176). The resulting tree was visualized using the ETE toolkit (177).

2.2.12. Modelling and molecular dynamic simulations

Modelling and molecular dynamic simulations represented in this work were performed by Dr. Audrius Laurynėnas.

The RudS_KT structures were modeled using Alphafold2 (178) and trRosetta (179) web servers. Both methods utilized multiple sequence alignments generated with mmseqs2 (180) and HHblits (181) for Alphafold2 and trRosetta, respectively. The RudS_KT holoenzyme model was constructed by selecting the best model from Alphafold2 and incorporating

the iron-sulfur cluster from PDBID:6z96 (146). Molecular dynamics calculations were performed using the AMBER20 software package (182). The holoenzyme model was parameterized with the AMBER ff14SB force field (183) and the TIP3P explicit solvent model with a 12 Å protein water solvation box and approximately 150 mM NaCl. The angle and bond parameters for the iron-sulfur cluster were adapted from (184), with charges adjusted for different iron oxidation states.

A crystal structure of *E. coli* phenylalanine tRNA (PDBID:6y3g) (71) served as the model substrate, featuring a 4-thiouridine moiety at the 8th position. As the original structure rendered the thiouridine moiety inaccessible to the enzyme, the base was manually repositioned to obtain an initial substrate structure suitable for enzymatic interaction. Additionally, calcium ions in the crystal structure were replaced with magnesium ions. Both the original and repositioned structures were parameterized using identical water models and ranges as the protein, supplemented with OL3 and modrna8 force field for modified RNA (185–187).

The initial enzyme-substrate structures were docked using default settings on the HDock web server (188). The resulting structures were ranked based on the distance between the sulfur atom in the thiouridine moiety and the relevant iron atom in the iron-sulfur cluster. The structure that performed best in this regard was selected for further calculations. Molecular dynamics simulations, with various restraints detailed in the Supporting Information, were carried out for the holoenzyme, tRNA substrates, and enzyme-substrate complexes.

3. RESULTS AND DISCUSSION

3.1. Function of stand-alone TudS domain-containing proteins

3.1.1. TudS orthologs share a phenotype in vivo

Earlier work by Dr. A. Aučynaitė and colleagues identified the desulfidation activity of a previously uncharacterized protein from *Aeromonas* sp., containing the DUF523 domain, toward 2-thiouracil and 4-thiouracil. Subsequently, the crystal structure of the enzyme was solved, and the enzyme was dubbed TudS, standing for **Thiouracil desulfidaSe** (referred to as TudS_A in this study) (145, 146).

To confirm that thiouracil desulfidation is a common feature of TudS proteins, three putative TudS-encoding genes from *Pseudomonas putida* KT2440 laboratory strain (TudS_KT), *Pseudomonas* sp. MIL9 (TudS_PU), and *Pseudomonas* sp. MIL19 (TudS_PP) soil bacteria (Table 1. TudS encoding genes used in this study.) were cloned to T7 RNA polymerase promoter-based pLATE11 expression vector. All the investigated TudS orthologs possess conserved cysteine residues, previously shown to form an FeS cluster in TudS_A, as well as other conserved amino acids involved in catalysis (Figure 20) (146). Additionally, an empty pLATE11 vector was generated to serve as a negative control, and the previously reported TudS_A was cloned into the pLATE11 vector to ensure consistency with the vectors used in this study.

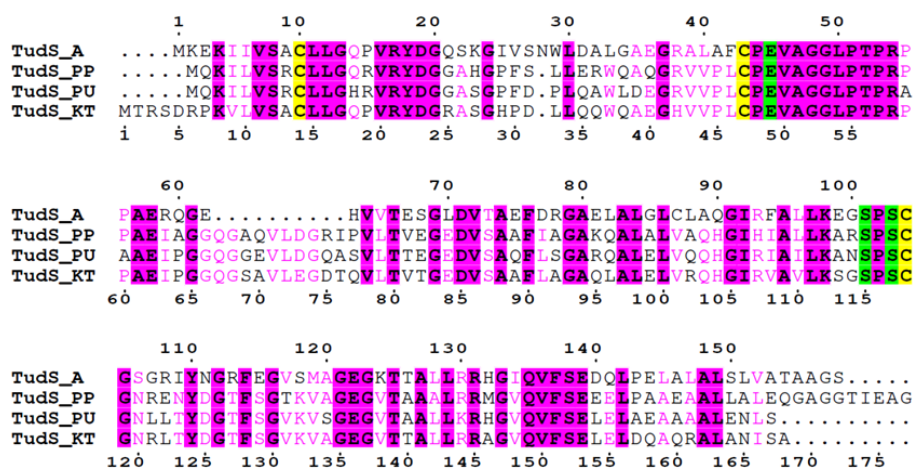


Figure 20. Amino acid sequence alignment of TudS proteins used in this study. All proteins contain the three conserved cysteines (yellow) that ligate the [4Fe-4S] cluster and the catalytic glutamic acid and serine residues (green).

Table 1. TudS encoding genes used in this study.

Insert	Origin	GeneBank accession ID (189)	Gene locus tag
TudS_A	<i>Aeromonas</i> sp.	6Z92_A (146)	-
TudS_PP	<i>Pseudomonas</i> sp. MIL19	JAPPVG010000016	N1078_RS18190
TudS_PU	<i>Pseudomonas</i> sp. MIL9	JAFEHE010000014	JQF37_RS12420
TudS_KT	<i>Pseudomonas putida</i> KT2440	AE015451	PP_5158

The TudS phenotype complementation assay was conducted in the uracil auxotrophic *E. coli* HMS174 $\Delta pyrF$ strain, whose growth is dependent on exogenous uracil (146). Notably, the genome of *E. coli* does not contain a gene encoding a native TudS enzyme. TudS_A was previously reported to support the growth of uracil auxotrophic strain on 2-thiouracil and 4-thiouracil as the sole source of uracil. Therefore, the three TudS orthologs were heterologously overexpressed in the same strain and cultured in a defined minimal liquid medium supplemented with 2-thiouracil and 4-thiouracil, with bacteria expressing TudS_A serving as a positive control.

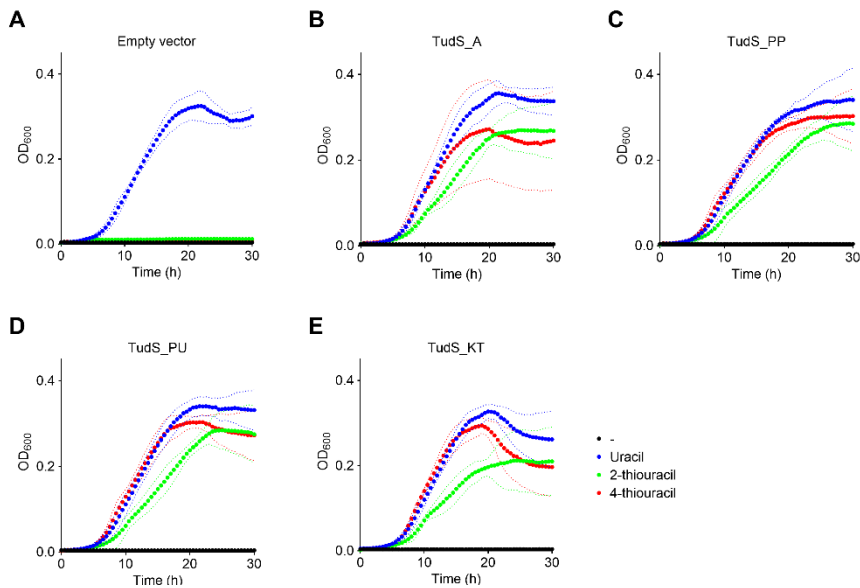


Figure 21. Growth curves of uracil auxotrophic *E. coli* HMS 174 $\Delta pyrF$ producing TudS orthologs in the presence of uracil (positive control, blue), 2-thiouracil (green) and 4-thiouracil (red). **A:** Empty vector carrying bacteria (negative control). **B:** TudS_A producing bacteria (positive control). **C:** TudS_PP producing bacteria. **D:** TudS_PU producing bacteria. **E:** TudS_KT producing bacteria. The dotted lines represent the standard deviation, number of biological replicates $n \geq 3$.

Growth of all recombinant TudS expressing *E. coli* strains was observed in the presence of both 2-thiouracil and 4-thiouracil, indicating that they could desulfurize these compounds (Figure 21). Such results indicate that all investigated TudS proteins share the same thiouracil utilization phenotype in vivo. Interestingly, bacteria expressing all three investigated TudS enzymes, along with TudS_A, demonstrated a prolonged exponential phase when growing on 2-thiouracil (green trace). Given that the bacterial growth rate during the exponential phase on 4-thiouracil (red trace) was in all cases similar to the positive control (blue trace), a substrate preference towards 4-thiolated compounds is implied.

3.1.2. Uracil auxotrophic *Pseudomonas putida* KT2440 utilize exogenous 4-thiouracil(uridine)

To gain insight into its possible physiological function, bacteria with endogenously encoded *tudS* gene were further investigated. *Pseudomonas putida* KT2440 was chosen for these studies because it is a well-established, genetically traceable laboratory strain with available molecular biology tools for manipulation. Moreover, in addition to the TudS encoding gene, the *P. putida* KT2440 genome also encodes TudS-DUF1722, a protein also within the scope of this work.

The fact that overexpression of recombinant TudS proteins restores the growth phenotype of uracil auxotrophic *E. coli* prompted the question of whether the endogenous TudS in *P. putida* KT2440 could, on its own, restore the growth of uracil auxotrophs on thiouracils and thiouridines. Several *P. putida* KT2440 strains with markerless deletions were generated including the $\Delta pyrF$ (gene necessary for de novo synthesis of uridine) and the double $\Delta pyrF \Delta tudS$ deletion strains. Additional strains were also generated for use in subsequent experiments. The generation of these markerless mutant strains was carried out by adapting the method of Oh et al. (163) using the pUC19_ *sacB* suicide vector (164). All *P. putida* KT2440 strains generated in this study, along with their specific features, are listed in Table 2.

Table 2. *Pseudomonas putida* KT2440 markerless mutant strains generated in this study.

Strain	Features
<i>P. putida</i> KT2440 $\Delta thil$	Strain deficient in tRNA s4U synthesis
<i>P. putida</i> KT2440 $\Delta tudS$	Strain lacking endogenous TudS
<i>P. putida</i> KT2440 $\Delta tudS$ -DUF1722	Strain lacking endogenous TudS-DUF1722
<i>P. putida</i> KT2440 $\Delta tudS$ -DUF1722 $\Delta tudS$	Strain lacking endogenous TudS and TudS-DUF1722
<i>P. putida</i> KT2440 $\Delta pyrF$	Uracil auxotrophic strain
<i>P. putida</i> KT2440 $\Delta pyrF \Delta tudS$	Uracil auxotrophic strain lacking endogenous TudS

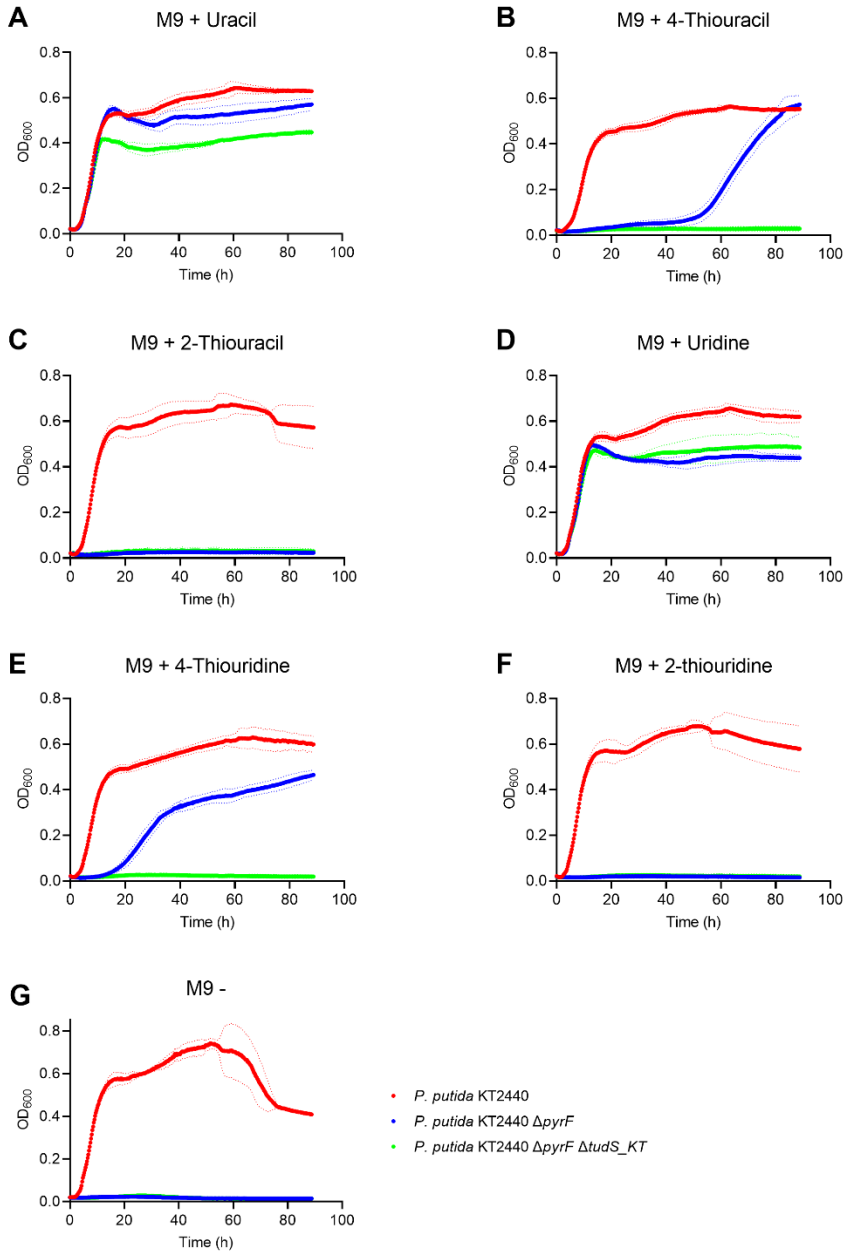


Figure 22. Growth curves of *P. putida* KT2440 wild-type (red trace), *P. putida* KT2440 Δ *pyrF* (blue trace), and *P. putida* KT2440 Δ *pyrF* Δ *tudS_KT* (green trace) in M9 minimal medium in the presence of: **A:** uracil (positive control); **B:** 4-thiouracil; **C:** 2-thiouracil; **D:** uridine; **E:** 4-thiouridine; **F:** 2-thiouridine; **G:** M9 with no supplement (negative control). Dotted lines represent standard deviation, number of biological replicates $n \geq 3$.

Uracil auxotroph knockout strains of *P. putida* KT2440 were grown in minimal medium containing 2- or 4-thiouracil containing compounds as sole sources of uracil (Figure 22). Growth of the single knockout $\Delta pyrF$ strain strictly depended on the presence of uracil (Figure 22A) or uridine (Figure 22D), and could also be recovered with 4-thiouracil (Figure 22B) and 4-thiouridine (Figure 22E). However, growth with the latter two was only observed after a significant lag phase, which may be explained by gene induction and de novo synthesis of TudS_KT and other enzymes (e.g., kinases for UTP synthesis). In contrast, no growth was observed with 2-thiouracil/2-thiouridine (Figure 22C/F), which is different to the *E. coli* HMS174 $\Delta pyrF$ overexpressing TudS homologs (Paragraph 3.1.1) that grew with 2-thiouracil.

This result indicates that the endogenous TudS_KT has a clear preference for 4-thiouracil over 2-thiouracil moiety-containing compounds, which is in line with the observation of prolonged exponential growth phase of *E. coli* uracil auxotrophs (Paragraph 3.1.1). As a control, the double knock-out $\Delta pyrF \Delta tudS_{KT}$ strain grew only in the presence of uracil/uridine (Figure 22A/D) but not in the presence of 4-thiouracil moiety-containing compounds (Figure 22B/E), confirming that TudS_KT enables the use of 4-thiouracil/4-thiouridine as exogenous uracil/uridine sources.

3.1.3. TudS-deficient cell growth is inhibited by 4-thiouracil(uridine)

Although not widely applied, the antibacterial effect of 4-thiouracil and 4-thiouridine on certain bacterial species has been known for a long time (190). It has been reported that the growth of *Bacillus subtilis* is inhibited by 4-thiouridine at a concentration of 96.2 μM , but not by 4-thiouracil, when both of these compounds are produced and excreted by *Streptomyces libani* into the medium (1). To test the effect of the *tudS* gene on bacterial growth, two *tudS* knockout strains, *Bacillus subtilis* 168 $\Delta tudS$ and *Pseudomonas putida* KT2440 $\Delta tudS$, were subjected to growth in rich LB medium supplemented with 4-thiouracil and 4-thiouridine.

The control wild-type *B. subtilis* 168 demonstrated growth in accordance with previous observations by Nishikiori et al. (1). While 4-thiouracil did not inhibit the growth, the growth of the wild-type bacteria was indeed slowed down by 4-thiouridine (Figure 23A, khaki trace). Despite experiencing an extended lag phase, the wild-type bacteria eventually continued to grow. Strikingly, the deletion of the *tudS* gene appeared to be lethal for *B. subtilis* 168 $\Delta tudS$ under experimental conditions mentioned above, as no growth was observed during the 20-hour incubation (Figure 23B, khaki trace).

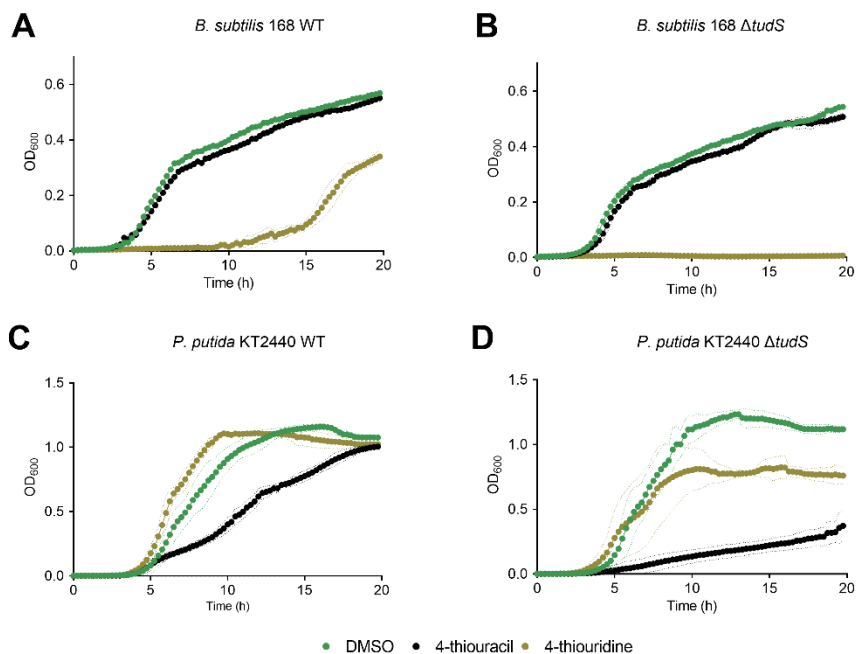


Figure 23. Growth curves of *Pseudomonas putida* KT2440 and *Bacillus subtilis* 168 bacteria in LB medium containing DMSO (vehicle, green trace), 100 μ M 4-thiouracil (black trace) or 100 μ M 4-thiouridine (khaki trace). **A:** Growth curve of wild type *B. subtilis* 168. **B:** Growth curve of *B. subtilis* $\Delta tudS$. **C:** Growth curve of wild type *P. putida* KT2440. **D:** Growth curve of *P. putida* KT2440 $\Delta tudS$. Dotted lines represent standard deviation, number of biological replicates $n \geq 3$.

The same experimental setup was applied to *P. putida* KT2440 $\Delta tudS$ mutant strain obtained in this study. Contrary to *B. subtilis*, wild-type *P. putida* KT2440 growth was marked by a growth rate decrease when growing on 4-thiouracil (Figure 23C, black trace), but not on 4-thiouridine (khaki trace). The deletion of *tudS* gene appeared not to be lethal contrary to *B. subtilis*, however resulted in more pronounced growth rate decrease when grown on 4-thiouracil (Figure 23D). The possible rationale of this effect is addressed in the discussion part (Paragraph 4) of this thesis.

3.1.4. TudS enzymes are monomeric 4-thio-UMP desulfidases

The results presented in this section were obtained in collaboration with J. Fuchs from Prof. Dr. M. Boll's group at the University of Freiburg, Freiburg im Breisgau, Germany, between January 5, 2022, and May 13, 2022. The molar mass of TudS_PP and its activity with 4-Thio-UTP were determined by J. Fuchs. Initial studies of TudS_A activity with 2-thiouracil, 2,4-dithiouracil, and 4-thiouracil were performed by Dr. A. Aučynaitė and J. Fuchs. Catalytic

constants of TudS_A represented in Table 3 were determined by Dr. A. Aučynaitė and J. Fuchs.

Despite the observed growth restoration of uracil auxotrophic bacteria through the utilization of thiomodified nucleobases, the substrate specificity and cellular function of TudS enzymes remained unknown, necessitating further in vitro exploration. Preliminary tests have indicated that among three newly investigated TudS proteins, TudS_PP was the most suitable candidate for further in vitro characterization. Due to the FeS cluster of TudS proteins being vulnerable to oxygen exposure, protein purification and all subsequent in vitro procedures were conducted under strictly anaerobic conditions.

To produce the recombinant TudS_PP with C-terminal 6xHis-tag heterologously, the gene was cloned into the pLATE31 vector. Overexpression of the recombinant gene was carried out in *E. coli* BL21(DE3) Δ iscR strain, which is optimized for the production of heterologous FeS proteins (see section 1.3.3). The protein was then purified using cobalt affinity chromatography.

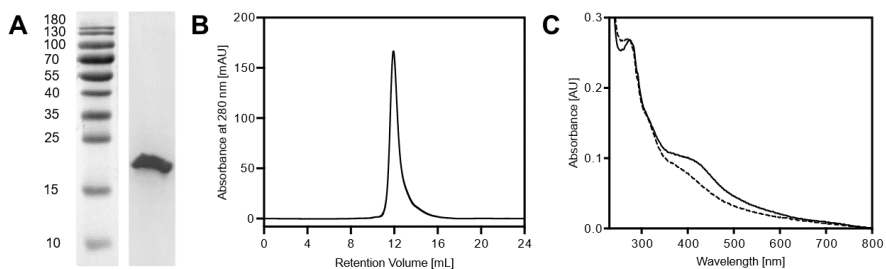


Figure 24. Analysis of TudS_PP after heterologous production and anaerobic purification. **A:** SDS-PAGE analysis of the elution fraction of TudS_PP after Co-NTA chromatography (~8 μ g). **B:** Analysis of purified TudS_PP after Superdex 75 10/300 GL gel filtration chromatography. **C:** UV-visible spectra of TudS_PP (bold line) and after $[4\text{Fe-4S}]^{2+}$ cluster reduction with 10 mM sodium dithionite at pH 7.3 (dotted line).

The purity of the anaerobically purified recombinant TudS_PP protein was analyzed using SDS-PAGE (Figure 24A), which showed that the purification yielded homogeneous TudS_PP. Size exclusion chromatography of recombinant TudS_PP (Figure 24B) resulted in a single elution peak at 19.6 ± 0.1 kDa, consistent with a monomeric protein architecture (theoretical TudS_PP molecular mass ≈ 18.5 kDa). Ultraviolet-visible (UV-vis) spectroscopy analysis of TudS_PP exhibited a broad shoulder between 370 and 470 nm, which was partially bleached upon the addition of sodium dithionite, with a difference maximum at 429 nm (Figure 24C). This spectral change is characteristic of a $[4\text{Fe-4S}]^{2+}$ cluster (191). Iron content determination using ferene assay indicated the presence of 2.99 ± 0.23 Fe per

protein monomer. In agreement with previous observations (146), TudS_PP desulfurized 2-thiouracil and 4-thiouracil, with the latter being converted at an approximately 100-fold higher rate at 0.5 mM substrate concentrations.

Initial studies by colleagues on TudS_A indicated that, when the substrate concentration was varied, only the data obtained with 4-thiouracil fit a Michaelis-Menten curve, whereas a rather linear regression curve was obtained with 2-thiouracil (Appendix 3). This finding strongly indicates that TudS enzymes specifically bind only 4-thiouracil but not 2-thiouracil, which is in agreement with the growth results observed in Paragraph 3.1.1. When 2,4-dithiouracil was used as a TudS_A substrate, the sulfur atom was abstracted first at the 4-position, forming 2-thiouracil as an intermediate, which upon prolonged incubation was further desulfurized to uracil (Appendix 4).

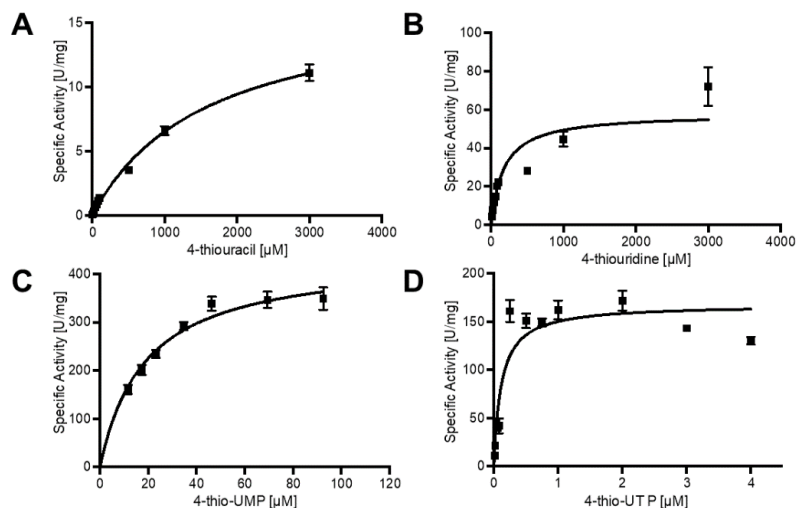
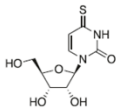
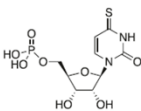
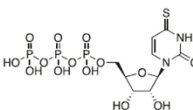


Figure 25. The fit of data obtained for the conversion of 4-thiouracil, 4-thiouridine, 4-thiouridine monophosphate, and 4-thiouridine triphosphate by TudS_PP to Michaelis-Menten curves. **A:** TudS_PP + 4-thiouracil. **B:** TudS_PP, 4-thiouridine. **C:** TudS_PP + 4-thio-UMP. **D:** TudS_PP + 4-thio-UTP. Error bars represent standard error, $n \geq 3$.

Given that 4-thiouracil is the preferred substrate over 2-thiouracil for TudS_PP, three other nucleobase derivatives containing a 4-thiouracil moiety were tested. TudS_PP was tested for its desulfurization activity with 4-thiouridine, 4-thiouridine-5'-monophosphate (4-thio-UMP), and 4-thiouridine-5'-triphosphate (4-thio-UTP). The specific activity of TudS_PP with various substrate concentrations and the Michaelis-Menten curves fitted to the corresponding data are presented in Figure 25.

Table 3. Catalytic parameters for desulfurization of 4-thiouracil, 4-thiouridine, 4-thio-UMP, and 4-thio-UTP by anaerobically purified TudS proteins and the structures of corresponding substrates. All values are normalized to 4 Fe per protein.

Enzyme	Substrate	k_{cat} (s ⁻¹)	K_m (mM)	k_{cat}/K_m (M ⁻¹ s ⁻¹)	V_{max} (U mg ⁻¹)
TudS_A	4-thiouracil 	0.70 ± 0.05	0.24 ± 0.03	2.90 × 10 ³	2.4 ± 0.2
TudS_P		4.93 ± 0.43	1.49 ± 0.27	3.27 × 10 ³	15.9 ± 1.4
TudS_A	4-thiouridine 	8.8 ± 0.9	3.1 ± 0.6	2.88 × 10 ³	30.1 ± 3.1
TudS_P		19.9 ± 4.7	0.2 ± 0.09	1.03 × 10 ⁵	64.3 ± 15.3
TudS_A	4-thiouridine monophosphate 	293 ± 44	0.038 ± 0.013	7.77 × 10 ⁶	1000 ± 149
TudS_P		138 ± 16	0.020 ± 0.007	7.63 × 10 ⁶	447 ± 51
TudS_A	4-thiouridine triphosphate 	68.6 ± 3.4	0.100 ± 0.023	6.85 × 10 ⁵	234 ± 12
TudS_P		52.3 ± 2.4	0.117 ± 0.026	4.48 × 10 ⁵	168 ± 8

The k_{cat}/K_m for 4-thiouridine as a substrate was over 300-fold higher than for 4-thiouracil. Strikingly, TudS_PP exhibited the highest k_{cat}/K_m values with 4-thio-UMP (2230-fold higher than with 4-thiouracil), whereas for 4-thio-UTP, k_{cat}/K_m values were approximately 10-fold lower than for 4-thio-UMP. Similar results were observed by colleagues with TudS_A, where the k_{cat}/K_m values for TudS_A were 2650-fold higher than with 4-thiouracil, however, the increased k_{cat} for 4-thiouridine, unlike TudS_PP, was accompanied by the increase of K_m . The catalytic parameters of both TudS proteins for 4-thiouracil derivative desulfurization and the molecular structures of the substrates are represented in Table 3.

For the structural comparisons of TudS_PP to TudS_A, a three-dimensional model of TudS_PP was generated using AlphaFold (178). A model of TudS_PP, which shares 54% amino acid sequence identity with TudS_A was superimposed onto the TudS_A crystal structure obtained at 1.8 Å resolution (PDB ID: 6Z96) using ChimeraX (Figure 26A) (192). Superimposition of the model of TudS_PP showed that the protein is compliant with the TudS_A crystal structure. In particular, the positions of the residues essential for catalysis are conserved in both TudS enzymes (Figure 26B): the cysteines that ligate the [4Fe-4S]²⁺ cluster in TudS_A (Cys10, Cys43, Cys104) are equivalent to Cys9, Cys41, Cys112 in TudS_PP, and the conserved glutamic acid and serine residues that were proposed to participate in catalysis TudS_A (Glu45, Ser101, Ser103) are equivalent to Glu43, Ser109, Ser111 in TudS_PP.

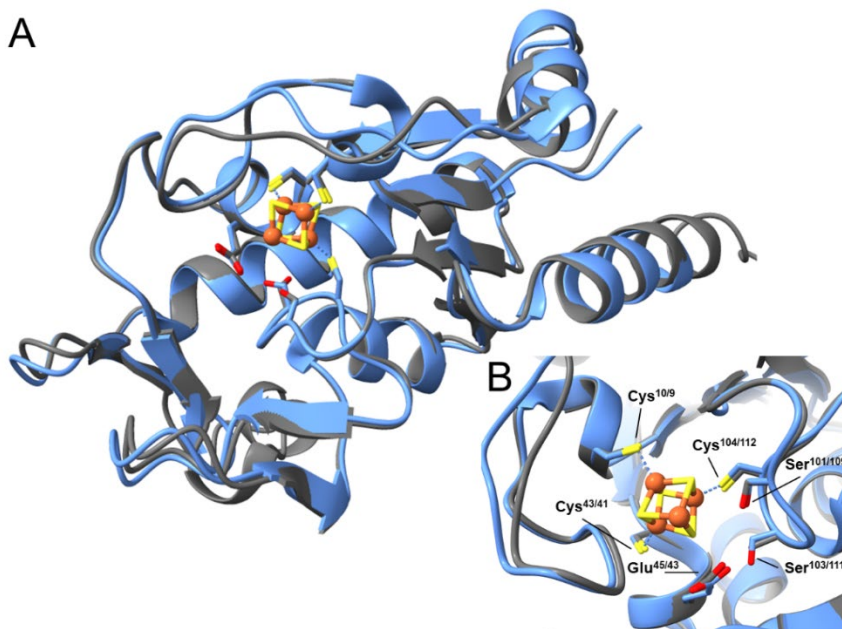


Figure 26. **A:** Superposition of the TudS_PP AlphaFold model (blue) onto the TudS_A crystal structure (gray) (PDB ID: 6Z96). **B:** Close-up view of the active sites of the superposed models showing that the three cysteine residues (Cys10(TudS_A)/9(TudS_PP), Cys43/41 and Cys104/112) that ligate the [4Fe-4S] cluster, as well as the conserved residues (Ser101/109, Ser103/111, and Glu45/43), which were proposed to assist in catalysis, occupy similar positions in the two proteins. The RMSD is 0.669 Å over 142 well-aligned atom pairs and 1.019 Å across all 150 aligned pairs.

Results in this section indicate that TudS_PP and TudS_A, originating from two different bacterial classes, share a pronounced preference for 4-thio-UMP as a substrate. Moreover, they demonstrate a high catalytic efficiency for 4-thio-UTP, a compound that might be synthesized *in vivo* from 4-thio-UMP and erroneously inserted into bacterial RNA (84).

3.1.5. TudS does not affect 4-thiouridine content in tRNA

Given that 4-thiouridine (s4U), to the best of our knowledge, is conserved in tRNA, the next objective was to examine whether the absence or presence of TudS affects tRNA s4U content. The impact of the absence of TudS-containing genes on tRNA s4U content was tested in *Pseudomonas putida* KT2440 mutant strains obtained in paragraph 3.1.2.

Bulk tRNA was isolated from the wild type *P. putida* KT2440, the $\Delta tudS_{KT}$, $\Delta tudS-DUF1722_{KT}$ single knockout, and $\Delta tudS_{KT} \Delta tudS-DUF1722_{KT}$ double knockout strains. Additionally, tRNA was

isolated from a $\Delta thiI$ knockout strain, in which the gene encoding the tRNA sulfur transferase involved in s4U formation is knocked out.

The isolated bulk tRNA was hydrolyzed, dephosphorilated, and analyzed by HPLC-MS/MS. In agreement with observations in other bacterial species (193), s4U was absent in bulk $\Delta thiI$ knockout strain tRNA serving as a negative control. However, no statistically significant difference in s4U content was observed between the wild-type strain and the other knockout strains (Figure 27A).

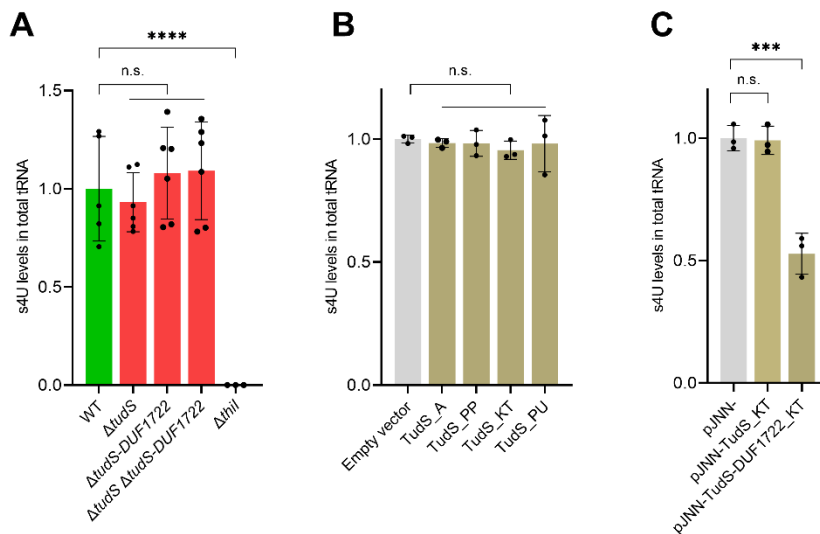


Figure 27. **A:** 4-thiouridine levels in tRNA of *P. putida* KT2440 wild-type and knockout strains. WT – wild type strain, $\Delta thiI$ – tRNA sulfurtransferase knockout strain, $\Delta tudS$ – single knockout strain, $\Delta tudS$ -DUF1722 – single knockout strain, $\Delta tudS$ $\Delta tudS$ -DUF1722 – double knockout strain. **B:** 4-thiouridine levels in tRNA of *E. coli* heterologously expressing investigated TudS proteins, empty vector – negative control. **C:** 4-thiouridine levels in tRNA of *P. putida* KT2440 homologously overexpressing TudS_KT and TudS-DUF1722. pJNN-empty vector – negative control. n.s.: $p \geq 0.05$; ***: $p < 0.001$; ****: $p < 0.0001$, compared to negative control (empty vector), one-way ANOVA with Dunnet’s post hoc test. Error bars represent the standard deviation, black dots represent individual measurements from biological replicates.

The possibility of TudS domain-containing protein production downregulation in wild-type *P. putida* KT2440 under standard growth conditions may be assumed. In this case it would result in no difference in tRNA s4U content upon knocking out the TudS domain-containing protein genes. To assure the presence of TudS in the cell, all the investigated TudS (Table 1) were heterologously overexpressed in *E. coli* BL21(DE3). However, overexpression of TudS and the analysis of subsequently isolated tRNA

resulted in no statistically significant difference between the control and tested samples (Figure 27B).

Although the different TudS proteins demonstrate uniform *in vivo* catalytical activity on individual nucleobases, they might demonstrate certain specificity for tRNA. The origin of investigated TudS genes is different from *E. coli*, where they were heterologously overexpressed, and its tRNA pool might not contain the suitable substrate. To overcome this issue, both *P. putida* KT2440 TudS-domain containing protein encoding genes were cloned into pJNN *Pseudomonas* expression vector, suitable for overexpression in latter strain. Both TudS and TudS-DUF1722 encoding genes were homologously overexpressed and subsequently the tRNA s4U content was investigated.

The homologous overexpression of native TudS_{KT} did not affect the s4U content of tRNA; however, approximately twofold decrease in the s4U content of isolated tRNAs was observed when TudS-DUF1722 was overexpressed homologously, suggesting that this protein is possibly involved in tRNA demodification (Figure 27C). In the upcoming sections, the role and mechanisms of the TudS-DUF1722² fusion protein will be explored in detail to better understand its potential involvement in tRNA s4U demodification.

² In the following sections the TudS-DUF1722 fusion proteins will be referred to as RudS, which stands for tRNA 4-thiouracil desulfidases.

3.2. Function of RudS (TudS-DUF1722) proteins

3.2.1 TudS and RudS do not share phenotypes in vivo

As mentioned in the previous section, the presence of the *tudS* gene in *Pseudomonas putida* KT2440 enabled the growth of the uracil auxotrophic strain using 4-thiouracil or 4-thiouridine as the sole source of uracil. This ability was lost when the *tudS* gene was knocked out. In addition to *tudS*, the strain also contains the *rudS* gene (GenBank locus ID: PP_0741) which encodes the TudS-DUF1772 fusion protein RudS. However, no growth of *P. putida* KT2440 Δ *pyrF Δ *tudS*_KT was observed during the same experiment, indicating that RudS, unlike TudS, could not rescue the uracil auxotrophic strain. Although the *rudS* gene is present, its potential downregulation during the experiment cannot be ruled out.*

To verify whether RudS is truly incapable of restoring the growth phenotype, its gene was cloned into pLATE11 vector and overexpressed in uracil auxotrophic *E. coli* HMS 174 Δ *pyrF* strain, replicating the experimental conditions described in section 3.1.1.

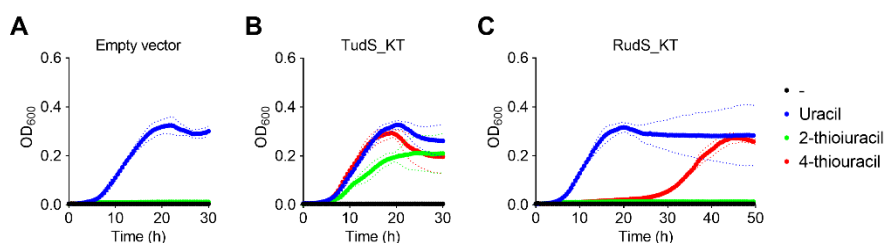


Figure 28. Growth curves of uracil auxotrophic *E. coli* HMS 174 Δ *pyrF* producing *P. putida* KT2440 TudS domain containing proteins. **A:** Empty vector carrying bacteria (negative control). **B:** TudS_KT producing bacteria. **C:** RudS_KT producing bacteria. Dotted lines represent standard deviation, number of biological replicates $n \geq 3$.

While TudS_KT producing cells were showing the usual TudS-like phenotype and grew on 2-thiouracil and 4-thiouracil as sole sources of uracil (Figure 28B), RudS_KT producing cells demonstrated a different growth pattern and showed no growth on 2-thiouracil. Additionally, these cells demonstrated an approximately threefold prolonged lag phase when supplemented with 4-thiouracil (Figure 28C). This suggests that RudS_KT exhibits only residual activity towards 4-thiouracil as a substrate.

To find out whether this is a common feature of RudS proteins, four additional RudS-coding genes were cloned from common laboratory strains and soil bacteria. The vast majority of RudS sequences, over 99%, come from

prokaryotic organisms (4718 bacterial and 175 archaeal sequences, according to the UniProt database (172)). However, 10 viral RudS sequences were also identified, all belonging to the *Siphoviridae* family of viruses. From these, the RudS_vir sequence from the *Escherichia* phage 1H12 was selected for further study. All investigated RudS encoding genes are listed in Table 4.

Table 4. RudS encoding genes used in this study.

Insert	Origin	GeneBank accession ID (189)	Gene locus tag
RudS_KT	<i>Pseudomonas putida</i> KT2440	AE015451	PP_0741
RudS_TT	<i>Thermus thermophilus</i> HB8	AP008227	TTHB112
RudS_ST	<i>Salmonella enterica</i> subsp. <i>enterica</i> LT2	AE006468	STM1389
RudS_PU	<i>Pseudomonas</i> sp. MIL9	JAFEHE010000014	JQF37_16640
RudS_PP	<i>Pseudomonas</i> sp. MIL19	JAPPVG010000016	N1078_12140
RudS_vir	<i>Escherichia</i> phage 1H12	NC_049947	H3V29_gp66

To compare the different RudS orthologs to RudS_KT, the experiment in uracil auxotrophic *E. coli* was replicated using selected candidates. The overexpression of RudS orthologs from other species showed different phenotypes in comparison to RudS_KT (Figure 29A). RudS from *Thermus thermophilus* (Figure 29B) and *Salmonella enterica* (Figure 29C) did not complement the uracil auxotrophic cells, demonstrating no thiouracil desulfidation activity in vivo and acting in the same manner as does the

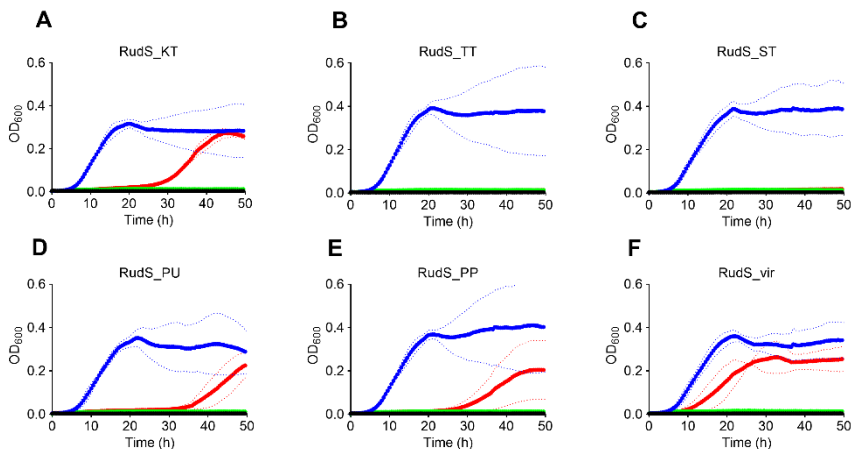


Figure 29. Growth curves of uracil auxotrophic *E. coli* HMS 174 $\Delta pyrF$ producing RudS orthologs from different species. **A:** RudS_KT producing bacteria **B:** RudS_TT producing bacteria. **C:** RudS_ST producing bacteria. **D:** RudS_PU producing bacteria **E:** RudS_PP producing bacteria. **F:** RudS_vir producing bacteria. Dotted lines represent standard deviation, number of biological replicates $n \geq 3$.

negative control (Figure 28A). RudS from *Pseudomonas* sp. (Figure 29D and Figure 29E) acted similarly to RudS_KT. Bacteria expressing RudS from *Escherichia* phage demonstrated the quickest growth restoration response on 4-thiouracil (Figure 29F) and could not restore the growth phenotype using 2-thiouracil, exactly alike its bacterial counterparts.

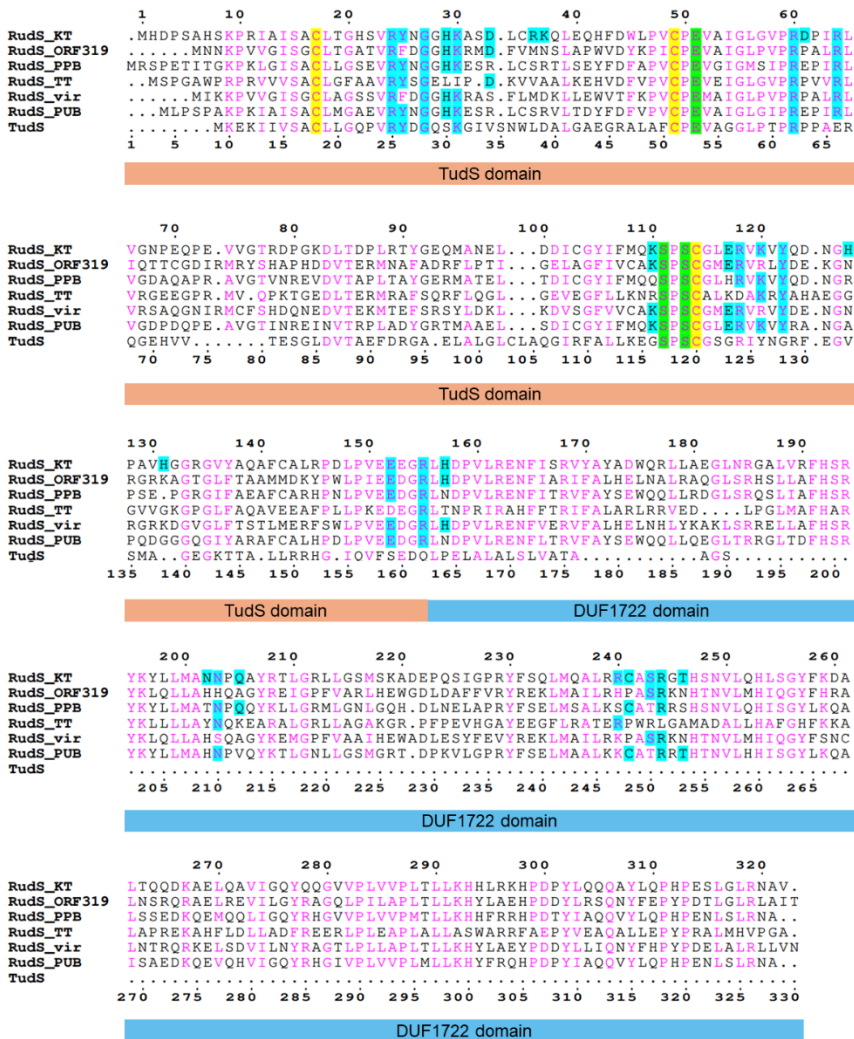


Figure 30. Sequence alignment of investigated RudS orthologs and TudS. Conserved cysteine residues involved in iron-sulfur cluster formation are highlighted in yellow. Conserved glutamic acid and serine residues catalyzing the 4-thiouridine desulfidation reaction are highlighted in green. Amino acids bioinformatically predicted in tRNA binding and/or catalysis are highlighted in cyan. Residues depicted in pink indicate high conservation (>70% identity or similarity).

Contrary to the TudS proteins (Figure 21), which are capable of quickly restoring the growth phenotype using both the 2- and 4-thiouracil, the investigated RudS proteins (Figure 29) are either not effective at all with these substrates, or demonstrate a preference for 4-thiouracil, albeit after an extended lag phase (with the exception of the viral-origin protein).

The RudS phenotype differences in uracil auxotrophic bacteria suggest that desulfidation of individual molecules indeed is not the primary function of this protein family, and some of the members do not show this activity at all. However, the amino acid sequence analysis (Figure 30) shows that all of these proteins contain all the previously established amino acids (146) within the TudS domain required for both the iron-sulfur cluster formation and the catalysis of thiouridine moiety desulfidation.

3.2.2 Phylogenetic analysis indicates a link between ThiI and RudS

Observation of either promiscuous or absent TudS-like activity in RudS suggested that TudS and RudS likely have distinct functions in vivo. However, the presence of the TudS domain within RudS implies a potential role related to 4-thiouridine desulfidation. This assumption is supported by the fact that genes encoding the DUF1722 domains are conserved in prokaryotes, as well as are the genes encoding ThiI, the enzyme responsible for s4U synthesis. PhyloCorrelate analysis (194) of bacterial and archaeal genes revealed a notable pattern: most prokaryotic species with the DUF1722 domain (n=4246) gene also encode the ThiI gene (n=3993, or 94% of DUF1722 encoding species). To further investigate this potential connection, a phylogenetic analysis was performed by dr. Audrius Laurynėnas, and the results are shown in Figure 31.

RudS homologous proteins (857) were identified among 884 reference genomes (843 Bacteria and 41 Archaea). ThiI homologous proteins were found among 1866 genomes. In 637 genomes, both full RudS and ThiI proteins are present. Although there are sporadic instances where ThiI is not present in the same genome, there are also two distinct groups of organisms that lack the ThiI homologue used in this analysis (Figure 31, Groups A and B). Group B mostly consists of thermophilic sulfate-reducing bacteria. Group A is very diverse, encompassing different morphologies and metabolic processes. The organisms in these groups might possess ThiI homologues that differ in architecture from the *E. coli* homologue used to generate this tree, as indicated in section 1.2.6. Additionally, it is possible that they may not have the s4U modification altogether, but still retain the RudS enzyme.

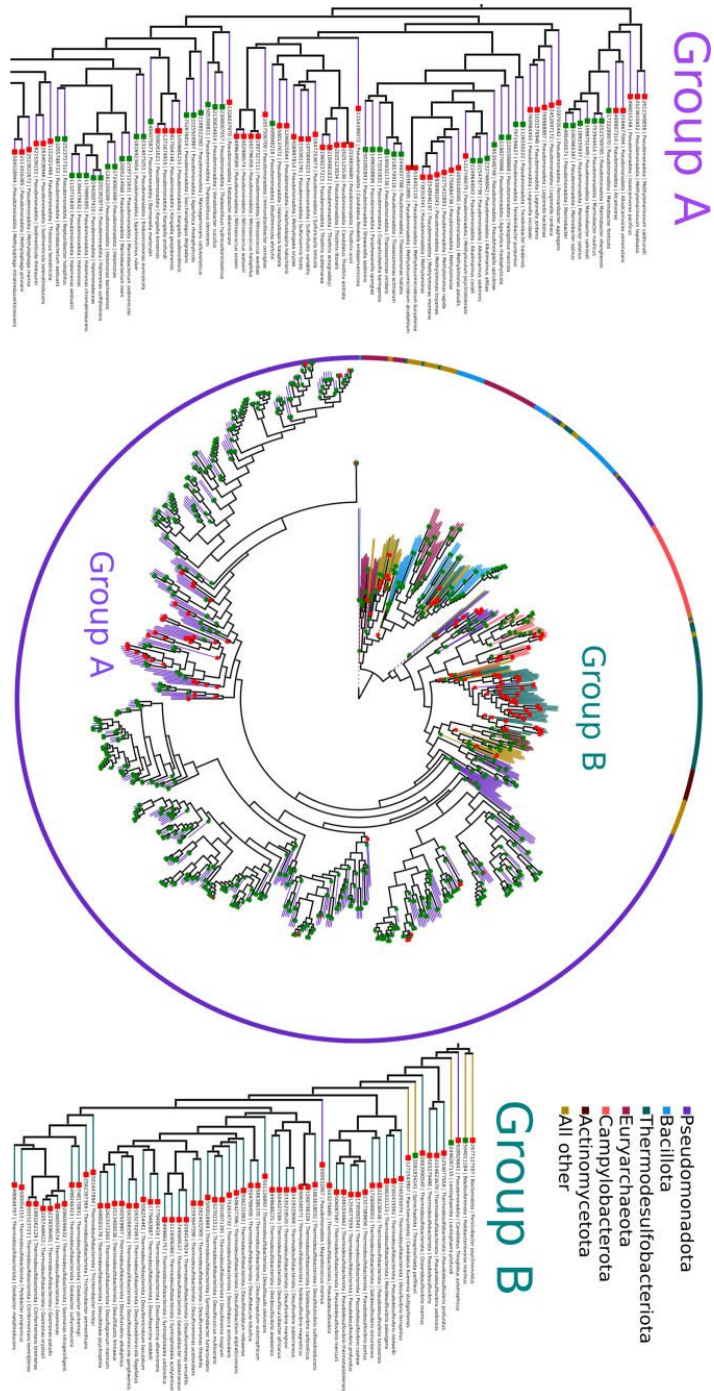


Figure 31. Phylogenetic tree of 884 RudS homologues identified among complete reference genomes of 332 Archaea, 5042 Bacteria, and 47 viruses. The presence (green square) or absence of ThiI (red square) in the same genome is indicated. Group A and Group B mark organism groups that lack the *E. coli* ThiI homologue.

In conclusion, the phylogenetic analysis of RudS homologues from bacteria and archaea with known complete genomes confirmed that most organisms with a RudS gene also encode ThiI, reinforcing the link between these two enzymes.

3.2.3 tRNA desulfidation activity of RudS in vivo

The experiments with the uracil auxotrophic bacteria have shown that although RudS proteins have a TudS domain and the same conservative amino acid residues, they demonstrate either promiscuous or no TudS-like activity. In addition, the presence of both the gene encoding a stand-alone TudS and the gene encoding a fusion RudS protein in some bacterial genomes suggests that TudS and RudS should have distinct functions in vivo. The domain architecture of RudS implies its potential role in 4-thiouracil moiety desulfidation and to the best of knowledge the only source of 4-thiouracil containing nucleotides in vivo is the prokaryotic tRNA.

Although the experiments with *P. putida* KT2440 *rudS* knockout strains described in section 3.1.5 showed no significant differences in tRNA s4U content compared to the wild type, the homologous overexpression of RudS resulted in twofold decrease of tRNA s4U content (Figure 27). To determine whether this is a common phenotype of RudS proteins, the next step was to overexpress all investigated RudS orthologs in *E. coli*, isolate bulk tRNA, and examine its s4U content.

RudS genes listed in Table 4 were overexpressed in *E. coli* BL21(DE3) followed by bulk tRNA extraction, digestion to single nucleosides, and quantification of s4U content using HPLC-MS/MS. The analysis revealed a substantial decrease in s4U content in tRNA samples extracted from RudS overexpressing cells in comparison to negative control carrying an empty vector (Figure 32).

Although all six overexpressed RudS orthologs led to a significant decrease in s4U content, the level of decrease differed among samples. The highest decrease of s4U content was observed in samples overexpressing RudS_KT from *Pseudomonas putida* KT2440 (26-fold in comparison to negative control) followed by RudS_ST from *Salmonella enterica* (18.3-fold), while overexpression of viral RudS and RudS_PU from *Pseudomonas* sp. MIL9 resulted in smallest decreases (5.9- and 4.7-fold respectively).

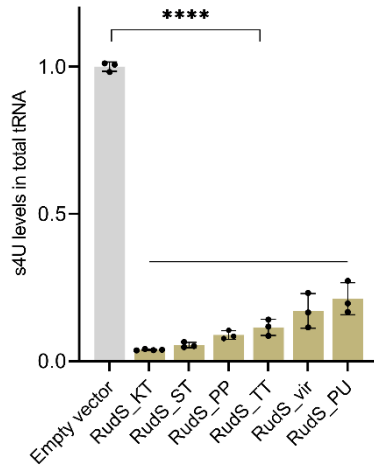


Figure 32. s4U content in *E. coli* BL21(DE3). s4U levels in *E. coli* total tRNA upon expression of RudS encoding genes. ****: $p < 0.0001$, compared to negative control (empty vector), one-way ANOVA with Dunnet's post hoc test. Error bars represent the standard deviation, black dots represent individual measurements from biological replicates.

The variation in s4U content reduction among different RudS proteins raises a question of whether this is due to differences in heterologous expression levels or the specificity of RudS. To find this out, His-tags were introduced to the N-termini of RudS proteins for detection with anti-His-Tag antibodies using Western blot. The western blot analysis revealed that RudS_KT while causing the most significant reduction in tRNA s4U content did not show the highest soluble protein levels in bacterial cytosol (Figure 33). In contrast, the amount RudS from *Thermus thermophilus* in bacterial cytosol was the highest (~1.7-fold higher than RudS_KT), although the tRNA s4U desulfidation caused by this protein was lower (8.7-fold, Figure 32).

Such a phenomenon could be explained by suboptimal temperature conditions for a protein originating from a thermophilic organism. It might also be due to inefficient substrate recognition, as tRNAs in thermophilic microorganisms often possess unique body (non-anticodon) modifications not found in their mesophilic counterparts (195). The soluble fractions of RudS_ST and RudS_PP detected by Western blot were lower in comparison to RudS_KT, aligning with the observed reduction of s4U content (Figure 32). Interestingly, despite 4.7-fold reduction of s4U, no soluble fraction of RudS_PU was detected in 2 μg of bacterial lysate indicating that even undetectable amounts of this protein are sufficient to desulfidize tRNAs significantly. On the other hand, RudS_vir stood out with relatively high

protein levels, comparable to those of RudS_ST, yet its tRNA desulfidation activity appeared to be lower.

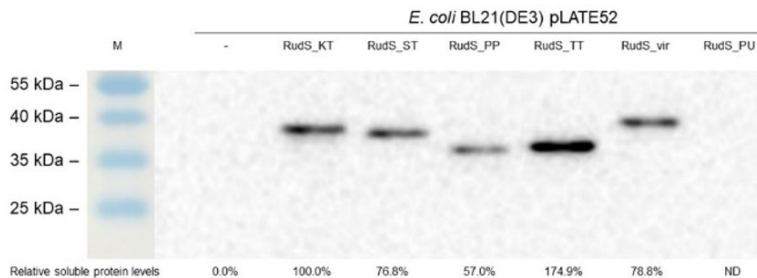


Figure 33. Western blot analysis of soluble protein fractions in bacterial lysates (2 μ g per lane). M-protein ladder, His-tagged RudS were detected using anti-His primary antibodies, empty pLATE11 vector (-) was used as a negative control. Relative protein levels were calculated in comparison to RudS_KT (100%) fraction.

All tested RudS variants exhibited activity towards tRNA, indicating that RudS enzymes function as tRNA de-modifying erasers, targeting the 4-thiouridine modification in tRNA molecules. The growth restoration of uracil auxotrophic cells (Figure 28, Figure 29) and characteristics of the TudS domain (140) suggest that RudS converts the s4U modification to uridine *in vivo*. To confirm this, total tRNA extracted from control and RudS_KT overexpressing cells were sequenced using nanopore-based nano-tRNAseq (169). Although this method could not distinguish the modified s4U residue in control samples, the sequencing results of RudS_KT-affected samples indicated the presence of uridine at the 8(9)th position. Combination of these data with previous findings concludes that RudS catalyzes the conversion of tRNA s4U to uridine.

3.2.4 The [4Fe-4S] cluster is necessary for RudS function

Previous work suggested a reaction mechanism by which the TudS enzymes desulfidate the 4-thiouracil containing molecules (146): the key element of this enzymatic reaction is the [4Fe-4S] cluster coordinated by three cysteine residues within the active centre of the TudS enzyme, with the fourth iron engaging in substrate binding. As indicated in Figure 30, all the investigated RudS sequences possess the same three conservative cysteines within the TudS domain which are most likely involved in iron-sulfur cluster formation. To validate the hypothesis that RudS enzymes employ the same mechanism of action because of their TudS domain, vectors encoding all investigated RudS homologues bearing a single amino acid substitutions for

all the conservative cysteines were generated. These vectors were used for in vivo RudS activity measurements replicating the conditions described in paragraph 3.2.3.

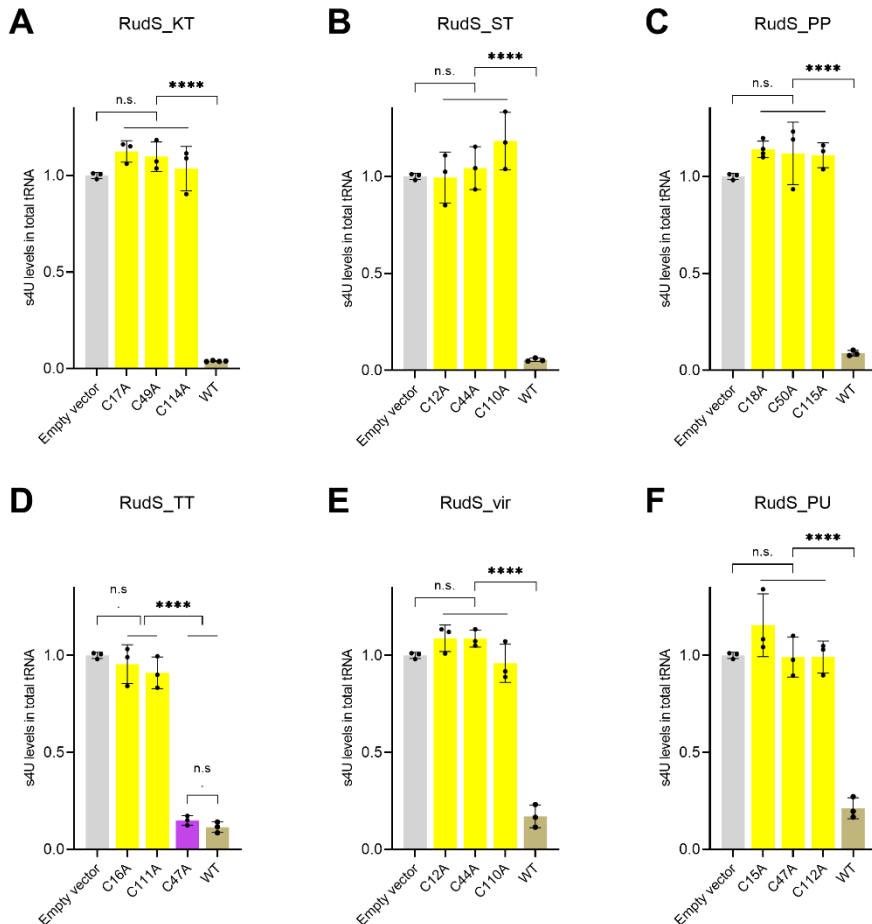


Figure 34. s4U levels in *E. coli* total tRNA upon expression of RudS with conserved cysteine substitutions. **A:** RudS_KT. **B:** RudS_ST. **C:** RudS_PP. **D:** RudS_TT. **E:** RudS_vir. **F:** RudS_PU. ****: $p < 0.0001$, n.s.: $p \geq 0.05$ compared to WT or negative control, one way ANOVA with Bonferroni's post hoc test. Error bars represent the standard deviation, black dots represent individual measurements from biological replicates.

The overexpression of the majority of cysteine-substituted RudS mutants resulted in the absence of tRNA s4U desulfidation activity (Figure 34) with the single outlier being the RudS_TT C47A protein variant which reduced the tRNA s4U content to levels comparable with those of the wild type (Figure 34D, purple). Such a phenomenon was previously reported in *Bacteroides thetaiotaomicron* fumarase: this protein still forms an active iron-sulfur cluster

using only two cysteine ligands despite lacking the third and remains active, but is more prone to oxidative stress (196).

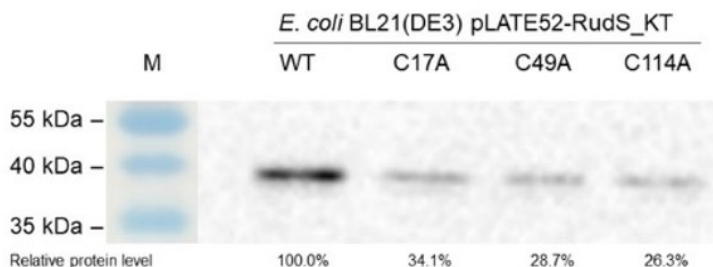


Figure 35. Western blot analysis of soluble protein fractions in bacterial lysates (2 μ g per lane). RudS_KT mutants with substituted cysteines involved in iron-sulfur cluster formation.

After analyzing the *in vivo* activity of all the RudS orthologs, RudS_KT, which had the highest activity and good solubility, was selected for further detailed study. To ensure that the observed effects of the mutants were not due to a lack of soluble protein, a Western blot was performed to detect RudS_KT cysteine substitutes, confirming the presence of soluble protein in the bacterial cytosol (Figure 35). The protein levels determined by Western blot indicate that mutant proteins are present in the cell, although their amounts are ~4-fold lower than those of the wild-type. This phenomenon can be attributed to the destabilization of the recombinant protein, likely resulting from disrupted FeS cluster assembly. This disruption may impair proper folding and/or trigger subsequent degradation, as has been reported for other recombinant FeS cluster-containing proteins (197). However, the results described in section 3.2.3 indicate that such an amount of active RudS should be sufficient to observe its activity *in vivo*.

3.2.5 Recombinant RudS_KT is active *in vitro*

Previous studies showed that the iron-sulfur cluster in TudS is highly labile when exposed to oxygen, leading to an inactive enzyme when purified aerobically (145). Nevertheless, N-terminally His-tagged RudS_KT was produced in *E. coli* and purified (Figure 36A) under aerobic conditions with minimal oxygen exposure, as detailed in the methods section.

On a molecular size exclusion chromatography column, RudS_KT eluted as a 37.1 ± 0.7 kDa protein (theoretical molar mass of ≈ 39 kDa), indicating a monomeric architecture (Figure 36B). The recombinant protein exhibited a brown color typical for Fe-S cluster-containing proteins. Iron content determination using ferene assay indicated the presence of 1.01 ± 0.13 Fe per

protein monomer, suggesting the major population of protein having damaged Fe–S cluster, assumably caused by the exposure to oxygen. Despite the poor iron content, UV spectrum of purified protein demonstrated spectrum characteristic for $[4\text{Fe-4S}]^{2+}$ clusters (191), which was partially bleached upon treatment with dithionite (Figure 36C). Despite indications of a damaged $[4\text{Fe-4S}]$ cluster, purified RudS_KT remained soluble over extended periods of time.

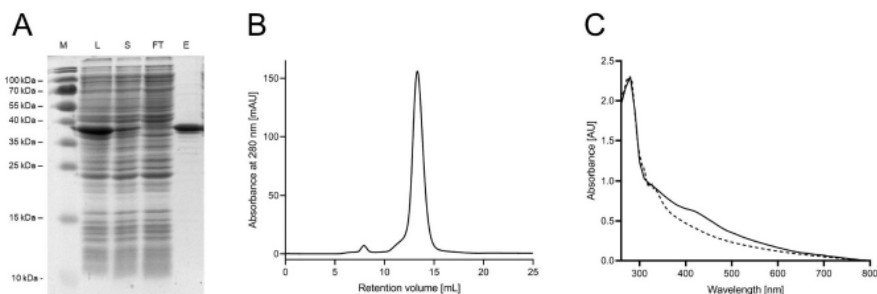


Figure 36. **A:** Recombinant N-6xHis tagged RudS_KT purification using affinity chromatography (M – molecular marker, L – bacterial lysate, S – soluble fraction, FT – flow through, E – eluted protein (theoretical mass 39.21 kDa). **B:** Elution peak of purified RudS_KT after Superose 12 10/300 GL gel filtration chromatography (mass 37.1 ± 0.7 kDa). **C:** bold graph – UV-vis spectra of RudS_KT as purified (35 μM); dotted graph – RudS_KT after $[4\text{Fe-4S}]^{2+}$ cluster reduction with 10 mM sodium dithionite at pH 8.

To test direct tRNA binding, as is typical for tRNA modifying enzymes, an electromobility shift assay (EMSA) was conducted with *E. coli* total tRNA. C-terminally his-tagged *E. coli* pseudouridine synthase (TruB) was cloned from *E. coli* BL21(DE3) and purified to serve as a positive shift control (198).

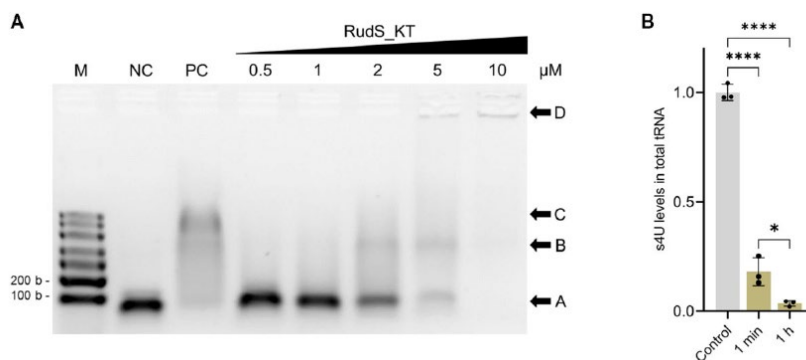


Figure 37. Purified recombinant RudS_KT interacts with tRNA in vitro. **A:** Electrophoretic mobility shift assay. M – molecular marker, NC – tRNA control, PC – positive shift control (1:6 molar ratio, using *E. coli* TruB pseudouridine synthase); 0.5–10 μM of RudS_KT was added to binding mixture resulting in 1:1–1:20 tRNA–RudS_KT molar ratios. Arrowhead A indicates unbound tRNA, B – tRNA–RudS_KT complex, C – tRNA–TruB complex, D – gel wells. **B:** Recombinant RudS_KT desulfidation activity in vitro using *E. coli* total tRNA. **** $p < 0.0001$, * $p < 0.05$, one-way ANOVA with Bonferroni’s post hoc test. Error bars represent the standard deviation, black dots represent individual measurements from replicates.

EMSA revealed a concentration-dependent protein band shift, confirming the RudS_KT-tRNA complex (Figure 37A).

To ensure that RudS_KT is directly responsible for the observed decrease in tRNA s4U content, the in vitro tRNA desulfidation reaction was performed using commercially available total *E. coli* tRNA. Contrary to previous observations with TudS, the aerobically purified and desalted RudS_KT protein retained activity. An approximately 13-fold molar excess of aerobically purified RudS_KT reduced the 4-thiouridine content in tRNA by ~80% over 1 min and by ~95% over 1 h (Figure 37B). The desulfidation of the substrate was incomplete, likely due to the degradation of the remaining iron-sulfur clusters, although the inaccessibility of s4U due to non-physiological conditions or incorrect tRNA folding cannot be ruled out.

As the 4-thiouridine content in tRNA is reported to vary under UV stress, which is causing a production of bacterial alarmones (82), the impact of alarmones to RudS_KT activity was tested in vitro. Alarmones guanosine pentaphosphate (pppGpp) and tetraphosphate (ppGpp) were supplemented to tRNA s4U desulfidation reaction in vitro. However, no statistically significant changes in the RudS enzymatic activity when using a 1:10 concentration ratio of RudS to (p)ppGpp were observed (Figure 38).

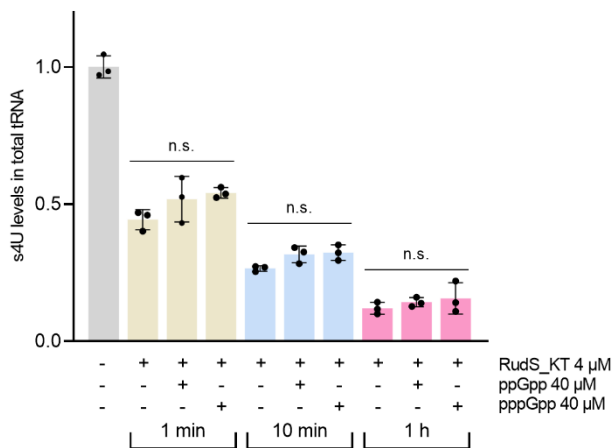


Figure 38. Effect of guanosine tetraphosphate and pentaphosphate (ppGpp and pppGpp respectively) on RudS_KT in vitro activity. Three samples obtained within a single time point were compared to each other using one way ANOVA with Bonferroni's post hoc test (n.s.: $p \geq 0.05$). Error bars represent the standard deviation, black dots represent individual measurements from replicates.

3.2.6 RudS_KT-tRNA interaction mechanism

Molecular modeling, docking and molecular dynamic simulations represented in this section were performed by Dr. Audrius Laurynėnas.

Analysis by HHpred (199) using RudS_KT models generated by AlphaFold2 (178) and trRosetta (179) (Figure 39A) indicated the previously reported crystallographically established TudS_A structure (PDBID:6z96) (146) to be the closest identified homologue of RudS_KT sharing the similarity in the organization of the TudS domain (Figure 39B). The active center with the iron-sulfur cluster transferred from PDBID:6z96 had identical amino acids, except Lys98 in TudS is replaced by Met108 in RudS_KT, suggesting a similar catalytic mechanism for desulfidation (146). However, the DUF1722 of RudS_KT, which is consisting of two compact groups of four alpha helices (Figure 39A, cyan) had no structural matches when analyzed by Dali structural homology search (200).

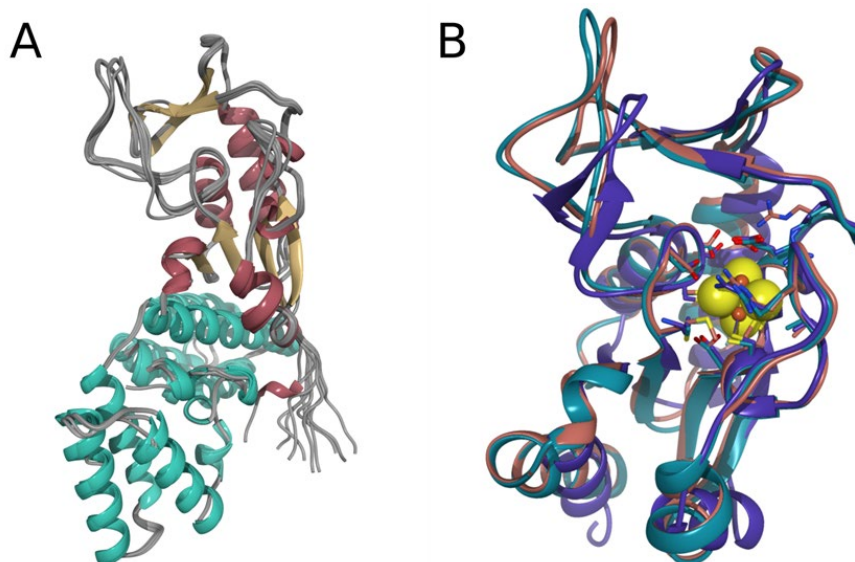


Figure 39. A: a superposition of AlphaFold2 and RosettaFold models colored by secondary structure (alpha helices of DUF1722 domain are cyan). B: structural comparison of best AlphaFold2 (teal) and trRosetta (salmon) models with closest homologue (PDBID:6z96) with structure identified with HHpred (purple). Iron-sulfur cluster is represented with spheres.

Molecular dynamics simulations showed, that DUF1722 domain was mobile relative to the catalytical domain. However, the TudS domain structure remained consistent throughout the simulations. The key differences of

RudS_KT from TudS_A included an extended loop (amino acids 116-135) and a mobile loop (amino acids 18-33). The mobility of these loops may make the enzyme's active center more open, allowing it to accommodate large substrates like tRNAs, at the expense of smaller substrates like thiouracil.

Series of molecular dynamics simulations were performed on a selected tRNA structure as well. A phenylalanine tRNA from *E. coli* with a thiouridine modification at the 8th position was chosen as the model substrate (PDBID:6y3g) (71). The thiouridine moiety was initially buried and inaccessible for enzymatic attack. Since it was unlikely to flip out spontaneously during the molecular dynamics simulation, this residue was flipped out manually and molecular dynamics simulation was performed using the same methodology as for the holoenzyme. The ribose and phosphate backbone remained stable throughout the simulation and the last frames of these simulations were used to model the RudS-tRNA complexes.

The structures from previous MD simulations of the RudS_KT holoenzyme and the tRNA with the exposed thiouridine were used for docking studies with HDOCK (188). However, none of the docked complexes had iron-sulfur distances relevant for catalysis (Top 15 complexes are depicted in Figure 40).

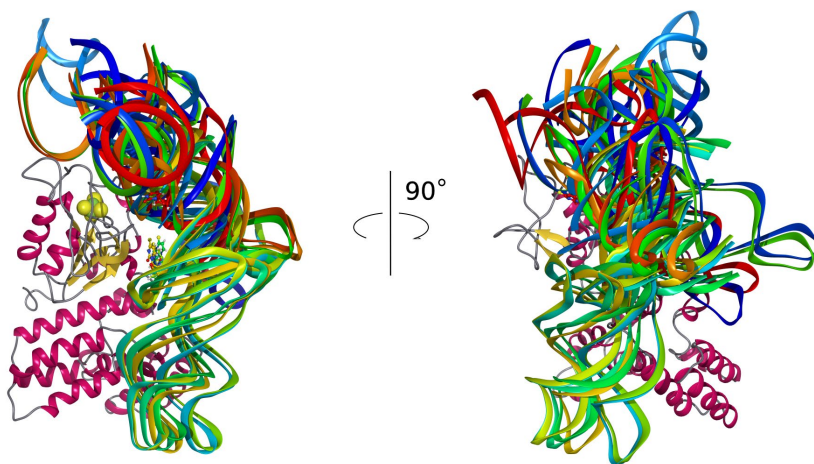


Figure 40. Top 15 complexes produced by docking *E. coli* phenylalanine tRNA with thiouridine flipped out to the RudS_KT holoenzyme with HDOCK.

Nevertheless, these structures provided a preliminary hypothesis on how tRNA might bind to the holoenzyme. Structures identified seven groups of amino acids (six groups G1-G6 for amino acids in each loop interacting with tRNA and a separate group CAT for catalytic amino acids) near the tRNA that might play a role in catalysis or substrate binding (Table 5).

Table 5. Groups of amino acids that are close to tRNA and might play a role in enzymatic catalysis and/or substrate binding.

G1	G2	G3	G4	G5	G6	CAT
Arg24	Arg60	Lys110	Glu152	Asn202	Arg240	Glu51
Tyr25	Asp61	Glu117	Arg155	Asn203	Cys241	Ser111
Asn26	Arg64	Arg118	His157	Gln205	Ser243	Ser113
Gly27		Lys120			Arg244	
His29		Tyr122			Thr246	
Lys30		His127				
Asp33		His131				
Arg36						
Lys37						

The hypothesized amino acids listed in Table 5 were mutated into methionines and investigated experimentally *in vivo* under the conditions used in paragraph 3.2.3. Mutations of proposed catalytic amino acids (Table 5, CAT) essentially abolished desulfidase activities, while other mutations had varying effects (Figure 41). Each group (G1–G6) contained at least one amino acid affecting enzymatic activity. The presence of soluble mutant proteins was confirmed by introduction of N-terminal His-Tag and Western blot analysis (Figure 42).

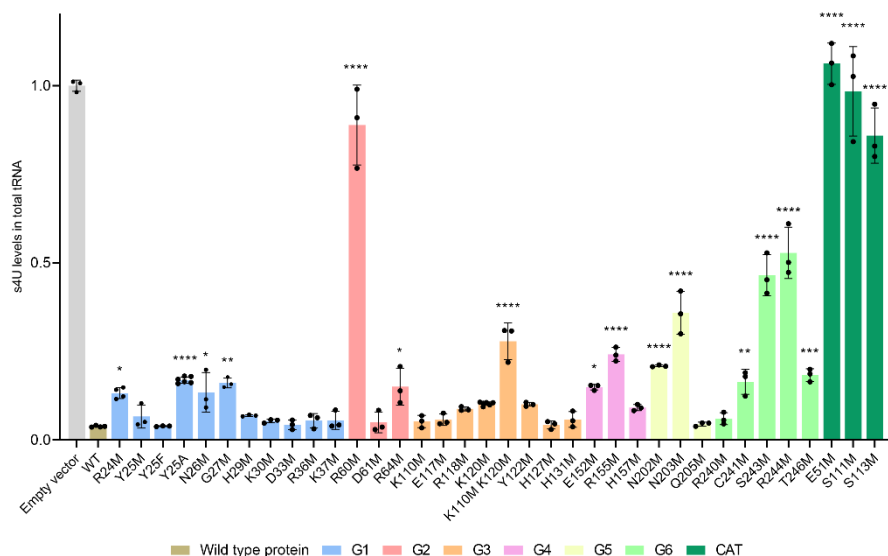


Figure 41. s4U levels in *E. coli* total tRNA upon expression of RudS_KT with single amino acid substitutions. ****: $p < 0.0001$, ***: $p < 0.001$, **: $p < 0.01$, *: $p < 0.05$, n.s.: $p \geq 0.05$ compared to WT, one way ANOVA with Dunnet's post hoc test. Error bars represent the standard deviation, black dots represent individual measurements from biological replicates.

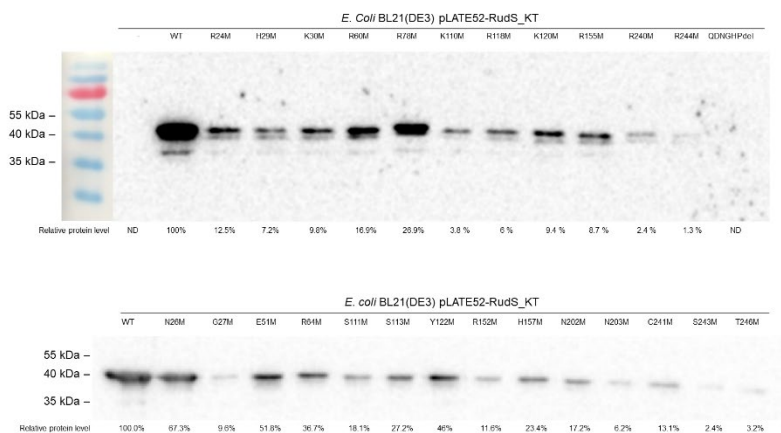


Figure 42. Western blot analysis of soluble protein fractions in bacterial lysates (2 μ g per lane) expressing RudS_KT mutants having affected *in vivo* activity and predicted to participate in catalysis and/or substrate binding. Relative protein levels are normalized to wild type RudS_KT.

Furthermore, the best HDOCK RudS_KT structure was subjected to constrained molecular dynamics simulations generating two models. **Model 1:** with thiouridine sulfur atom 2 \AA away from the iron ion in the iron-sulfur cluster (S/Fe restraint). Additionally, restraints were applied to other catalytic distances of key atoms or groups within the catalytic site. **Model 2:** only the S/Fe restraint was applied, allowing the rest of the complex to relax more freely, potentially revealing induced fit changes, for protein and tRNA to adjust their structures upon binding to better accommodate each other. Then the experimental results were compared to MD simulations of two RudS_KT holoenzyme-tRNA complex models described in the Appendix 5.

The superposition of the catalytic domains (amino acids 11-168) from the models and the holoenzyme, showed high similarity except for the previously discussed mobile loops, which are less mobile in the enzyme-substrate complex (Figure 43).

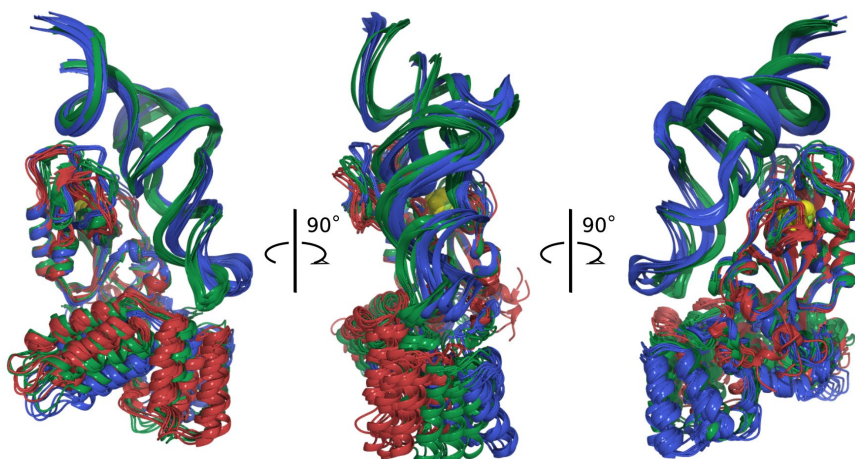


Figure 43. Superposition of RudS_KT model 1 (blue), model 2 (green), and holoenzyme (red) final models.

Both RudS_KT models suggest that the DUF1722 domain interacts with the anticodon arm and anticodon of the tRNA, while the catalytic TudS domain interacts with the variable loop, acceptor stem, and D arm of the tRNA. The DUF1722 domain's mobility relative to the catalytic TudS domain was evident in both models, likely accommodating various tRNA substrates with thiouridine modifications. In model 2 (with only S/Fe restraint) the catalytic domain remained stable at the end of molecular dynamic simulation and its structure did not undergo significant changes, indicating that it had likely reached a stable conformation. The structure revisited catalytically relevant conformation, where the Ser113 hydroxyl hydrogen and Glu51 sidechain carboxy oxygen distances reach ~ 2 Å. Notably, the amino acids Glu51, Ser111, and Ser113, previously identified as catalytic based on RudS_KT homology with TudS, produced inactive enzymes when mutated to methionines (Figure 41).

Strikingly, an additional catalytic amino acid has been identified, Arg60, which functions to orient Glu51 and provide a positive charge that could stabilize transitional states during proton removal from water and the nucleophilic attack of thiouridine by the produced hydroxide ion (the catalytic center is depicted in Figure 44). This arginine is fully conserved in the entire family of homologous RudS proteins. Retrospective analysis revealed a homologous arginine serving the same purpose in the experimentally determined structure of TudS_A (60).

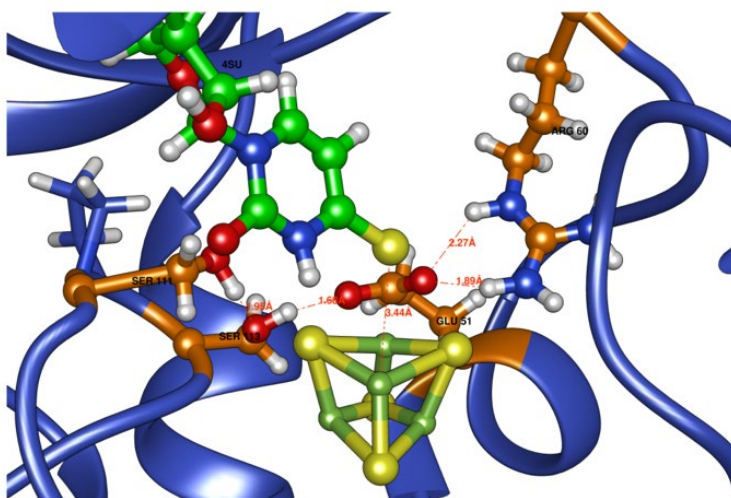


Figure 44. RudS_KT catalytic center with relevant distances indicated.

Comparison of randomly selected frames from model 2 and model 1 molecular dynamics shows that the orientations of catalytic amino acids relative to the thioridine moiety are very similar in both RudS_KT models (Figure 45).

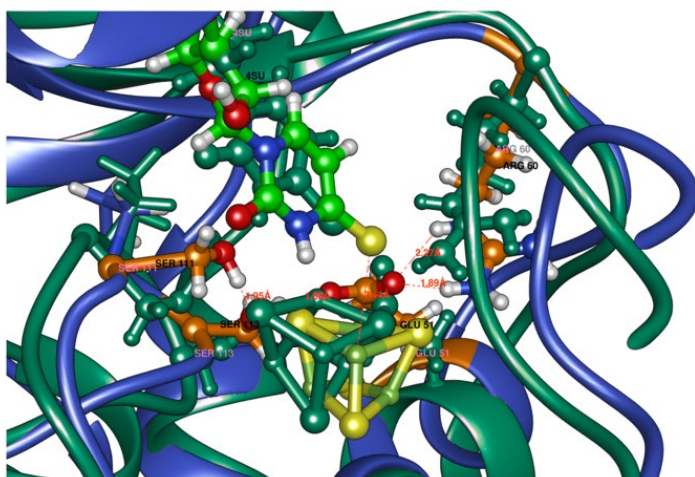


Figure 45. Superposition of RudS_KT catalytic centers of model 1 and model 2.

Both RudS_KT models feature an additional base involved in tRNA-enzyme active site binding (Figure 46). In the experimental tRNA structure, the base U45 (PDBID: 6y3g) is unpaired and was initially dangling outside during tRNA simulations, whether the thioridine side chain was paired inside or manually flipped outside.

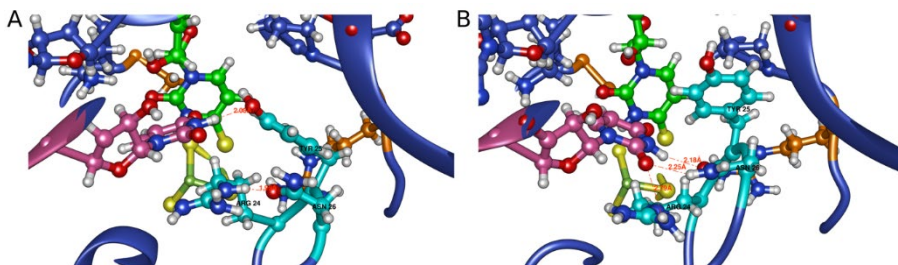


Figure 46. A and B: U45 (pink) interactions with Arg24, Tyr25, Asn26 (cyan), and thiouridine (green).

A similar flipped uridine is present in at least three other known *E. coli* tRNA structures: valine tRNA (PDBID: 7eqj), initiator formylmethionine tRNA (PDBID: 5l4o), and aspartate tRNA (PDBID: 6ugg). This uridine participates in an extensive network, forming a double hydrogen bond with Asn26. The nearby Arg24 suggests the possibility of a cation- π stabilizing interaction, being oriented by a hydrogen bond with the backbone carbonyl oxygen atom of Gly27. These structural observations are consistent in both models. Mutating these amino acids to methionine results in diminished RudS_KT enzymatic desulfidase activity (Figure 41).

The lower-than-expected variation in enzymatic activity can be explained by methionine's ability to form hydrogen bonds. Additionally, mutating Tyr25 to methionine resulted in a mutant protein functionally identical to the wild type, so two additional mutants of Tyr25 were generated, one to alanine, which had decreased activity, and one to phenylalanine, which had the same activity as the wild type RudS_KT (Figure 41).

The DUF1722 domain in RudS_KT interacts with both the anticodon stem and the anticodon of tRNAs (Figure 47A). While the molecular dynamics simulations may not depict the final binding state accurately, specific frames identified highlight the significance of Ser243 and Arg244. These amino acids, could potentially along with other unidentified residues, interact with the anticodon bases and the anticodon phosphate backbone (Figure 47 B, C, and D). These interactions are mostly opportunistic, except for Arg244, which predominantly interacts with tRNA backbone phosphates.

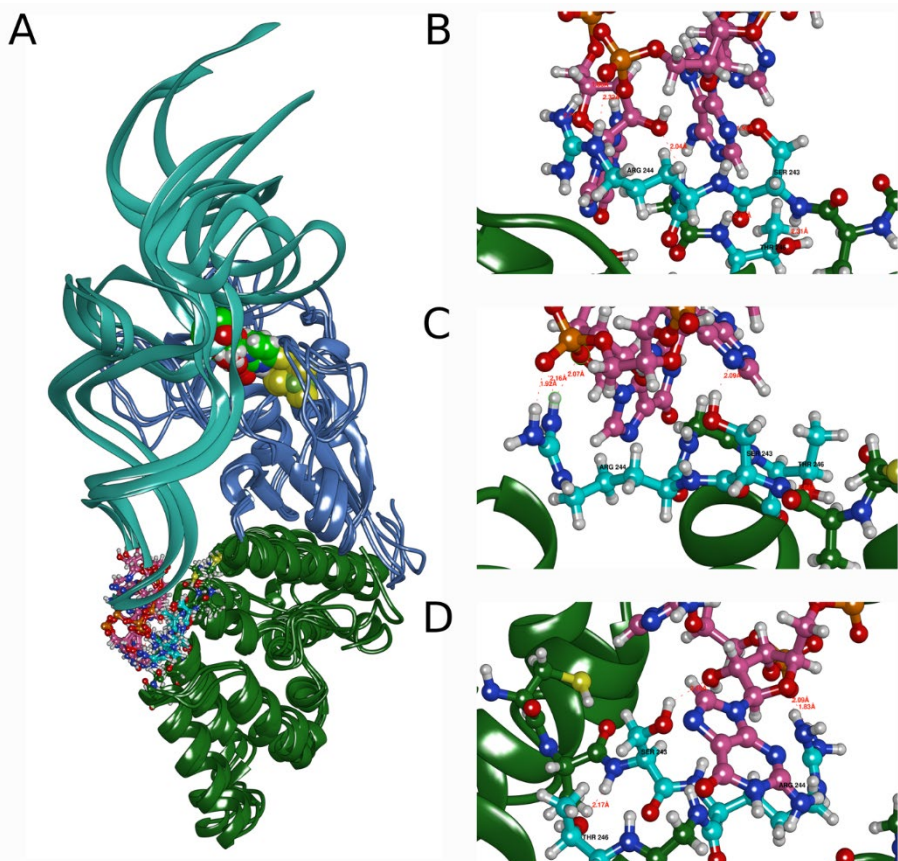


Figure 47. A: Overall structure of the RudS_KT-tRNA complex. Spheres represent 4-thiouridine and the iron-sulfur cluster. The DUF1722 domain is shown in dark green. The anticodon part of the tRNA is depicted with explicit pink ball-and-stick atom representations. B, C, and D: Various conformations of Ser243 and Arg244 interacting with tRNA and Thr246 (amino acids in cyan).

A summary of the rationale behind the enzymatic activities of mutants is outlined in Table 6.

Table 6. Effect of mutagenesis of predicted RudS_KT amino acids involved in enzymatic catalysis and/or substrate binding for s4U content in total *E. coli* tRNA. AVG – relative s4U content, stdev – standard deviation. Statistical significance was calculated by applying one-way ANOVA with Dunnet’s post-hoc test. ****: $p < 0.0001$, ***: $p < 0.001$, **: $p < 0.01$, *: $p < 0.05$, n.s.: $p \geq 0.05$ compared to WT.

Mutant	AVG	stdev	p-value	Group	Remarks
WT	0.04	0	-	-	Wild type RudS_KT
E51M	1.06	0.06	****	CAT	Catalytic amino acid; conserved; removes proton from water molecule
S111M	0.98	0.13	****	CAT	Catalytic amino acid; conserved; stabilizes Glu51
S113M	0.86	0.08	****	CAT	Catalytic amino acid; stabilizes Glu51

R24M	0.14	0.02	*	G1	Interacts with Gly27 backbone carbonyl, Asn26 side chain carbonyl and nearby ribose ring oxygen. Pi-stacking interaction with U45
Y25M	0.07	0.03	n.s.	G1	Shields active center from the tRNAs phosphates. Opportunistically forms hydrogen bond with ribose OH group
Y25A	0.17	0.01	****	G1	
Y25F	0.04	0	n.s.	G1	
N26M	0.14	0.06	*	G1	Interacts with U45 forming hydrogen bond
G27M	0.16	0.01	**	G1	Part of flexible loop, forms hydrogen bond with Arg24 via backbone carbonyl
H29M	0.07	0	n.s.	G1	No important interactions observed
K30M	0.05	0.01	n.s.	G1	Occasionally interacts with tRNA phosphates and Asp33
D33M	0.04	0.01	n.s.	G1	No important interactions observed (salt bridge with Arg36)
R36M	0.05	0.02	n.s.	G1	No important interactions observed (salt bridge with Asp33)
K37M	0.06	0.03	n.s.	G1	No important interactions observed
R60M	0.89	0.11	****	G2	Catalytic amino acid; stabilizes Glu51
D61M	0.05	0.03	n.s.	G2	Occasionally interacts with bases in the tRNA
R64M	0.15	0.05	*	G2	Occasionally interacts with riboses in the tRNA
K110M	0.05	0.02	n.s.	G3	Interacts with thiouridine base ribose and phosphate in tRNA
E117M	0.06	0.02	n.s.	G3	Salt bridge with Arg155
R118M	0.09	0.01	n.s.	G3	Interaction with tRNAs riboses
K120M	0.1	0.01	n.s.	G3	Interaction with tRNAs phosphates
Y122M	0.1	0.01	n.s.	G3	Orientation of Lys120 and Arg64
H127M	0.04	0.01	n.s.	G3	No interaction
H131M	0.06	0.02	n.s.	G3	No interaction
K110M, K120M	0.28	0.05	****	G3	Synergistic effect, Lys110 partial compensation by Lys120
E152M	0.15	0.01	*	G4	Salt bridge with Arg155
R155M	0.24	0.02	****	G4	Salt bridge with Glu152, Van der Waals interaction with tRNA ribose
H157M	0.09	0	n.s.	G4	Hydrogen bond with ribose ring oxygen
N202M	0.21	0	****	G5	Backbone stabilization via side chain in turn
N203M	0.36	0.06	****	G5	Backbone stabilization via side chain in turn
Q205M	0.04	0.01	n.s.	G5	No interaction
R240M	0.06	0.02	n.s.	G6	No interaction
C241M	0.16	0.04	**	G6	No interaction
S243M	0.47	0.06	****	G6	Interaction with anticodon base
R244M	0.53	0.07	****	G6	Interaction with phosphate in anticodon region
T246M	0.18	0.02	***	G6	Backbone interaction via side chain; interaction with Ser243

3.2.7 Overexpression of RudS_KT in *E. coli* diminishes UVA-triggered growth delay

To gain insight into the potential role of RudS proteins in bacterial physiology, we overexpressed RudS_KT in *E. coli* and subjected the cells to UVA. Since 4-thiouridine is a known effector of bacterial UVA response, causing a growth delay and stringent response (73), we expected that the overexpression of RudS_KT could help overcome the previously reported UVA-induced growth delay in *E. coli* (76). The bacteria were exposed to approximately 100 kJ/m² UVA, and their growth was subsequently monitored. Control samples were kept in darkness. Both RudS_KT overexpressing and control samples kept in the dark (Figure 48, open symbols) did not show any notable difference at the initial growth stage, indicating that recombinant protein did not have a significant impact initially. However, differences began to appear after 3 h, with the growth of RudS_KT overexpressing bacteria (blue symbols) slowing down in comparison to empty vector-carrying bacteria (black symbols). UVA irradiation indeed slowed the growth of *E. coli* (Figure 48, solid symbols), causing a ~105 min growth delay compared to non-irradiated empty vector-carrying cells. Remarkably, the overexpression of RudS_KT reduced this delay to approximately 60 minutes, indicating a positive effect on bacterial growth under these experimental conditions. The difference in the growth lag between irradiated RudS_KT overexpressing cells (blue symbols) and empty vector-carrying cells (black symbols) was approximately 45 min.

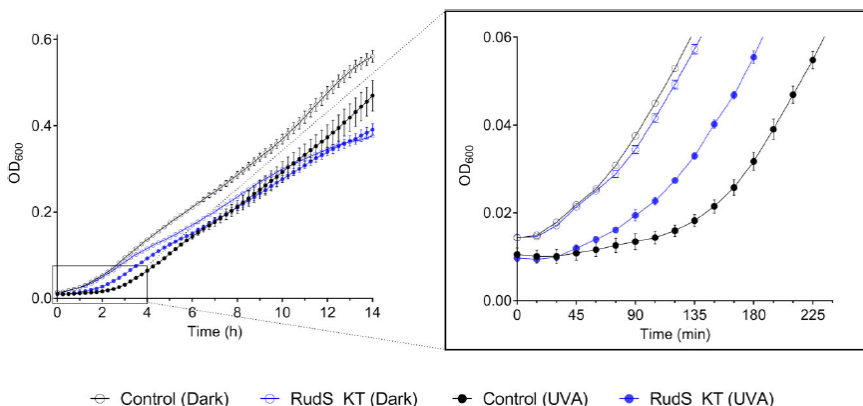


Figure 48. UVA-triggered growth delay reduction in *E. coli* BL21(DE3) overexpressing RudS_KT. Solid symbols represent the growth curves of UVA-irradiated bacteria overexpressing RudS_KT (blue symbols) and carrying empty vector (black symbols). Open symbols represent the growth curves of RudS_KT overexpressing bacteria (blue symbols) and bacteria carrying the empty vector (black symbols) maintained in the dark within the same period.

4. DISCUSSION

Insights into the physiological functions of TudS

The stand-alone TudS is the predominant architecture among TudS domain-containing proteins, representing 58.5% of all reported sequences (148). The results of this study indicate that these enzymes catalyze the desulfidation of individual molecules of 4-thiouracil derivatives. To the best of our knowledge, s4U is conserved in tRNA, where it is abundantly present: in *E. coli* approximately 70% of total tRNAs contain this modification (53).

Most of the RNA content by mass in bacteria is made up of rRNA. During exponential growth, *E. coli* possesses approximately 50,000 ribosomes. However, the copy number of highly modified tRNAs during the same conditions is 7.5-fold higher (~375,000), while mRNA has, at most, ten copies for each of the ~2000 mRNAs species (201). Although being stable during exponential growth, environmental stress, e.g. oxidative stress, leads to the rapid degradation of tRNAs (202). The mechanisms of tRNA degradation in bacteria are understudied. However, one can assume that such a process should release a plethora of modified nucleotides, which can either remain within the cell or be released into the environment upon cell lysis.

In addition to endogenous nucleotide salvage, bacteria can efficiently scavenge exogenous nucleosides and nucleobases, and use them as carbon and nitrogen sources, as well as for nucleic acid synthesis (203). This is achieved by utilizing multiple nucleoside transporters, with the major ones in *E. coli* being NupC and NupG (204). The utilization of exogenously supplied 4-thiouridine for RNA synthesis is evident for *E. coli* (84), indicating that s4U can be successfully converted to 4-thio-UMP and then to 4-thio-UTP in vivo. The desulfidation of 4-thio-UMP and 4-thio-UTP by TudS is therefore critical not only for recycling tRNA-derived modified monophosphate nucleosides but also for preventing erroneous incorporation of resulting 4-thiouridine triphosphates into RNA during transcription.

The hypothesis emphasizing the toxicity of erroneously incorporated 4-thio-UTP is supported by the observations of 4-thiouracil-caused growth rate reduction of *Pseudomonas putida* KT2440 cells (Figure 23). Notably, the growth delay was drastically increased in *tudS* gene knockouts, while 4-thiouridine only marginally affected the growth of both strains. In contrast, the growth of *Bacillus subtilis* was not affected by 4-thiouracil at all for both *tudS*-possessing and knockout strains. However, a pronounced delay was caused by s4U in *B. subtilis*, and growth was totally abolished by the knockout of *tudS* gene.

The differences between the effects of 4-thiouracil and 4-thiouridine could be explained by examining the genome of both bacteria. *P. putida* KT2440 encodes uracil phosphoribosyltransferase (AAN66371, EC: 2.4.2.9) which could be responsible for the formation of 4-thio-UTP from 4-thiouracil, but it does not encode uridine kinase (EC: 2.7.1.48), which could form the same compound from 4-thiouridine. In contrast, the genome of *B. subtilis* encodes uridine kinase (NP_390611), potentially capable of forming 4-thio-UTP from 4-thiouridine. Notably, it has been reported previously that the growth of *B. subtilis* is inhibited by 4-thiouridine, but not by 4-thiouracil, when both of these compounds are produced and excreted by *Streptomyces libani* into the growth medium (1).

Taking all kinetic data together, TudS enzymes preferentially act as 4-thio-UMP desulfidases but also display a catalytic activity with 4-thiouridine (1-2 orders of magnitude lower) and 4-thiouracil (2-3 orders of magnitude lower). This finding strongly suggests that the function of TudS is to recycle 4-thio-UMP, which directly derives from hydrolytic cleavage of tRNAs by cellular RNAses. However, in addition to the most likely function of TudS in tRNA-derived 4-thio-UMP recycling to evade its erroneous incorporations into RNA, TudS allows bacteria to scavenge exogenous modified nucleobases and nucleosides and reuse them for RNA synthesis while also detoxifying their environment.

Insights into the structure and catalysis by RudS_KT

Structural examination of RudS_KT from *Pseudomonas putida* KT2440 was conducted using molecular docking and molecular dynamics simulations, with subsequent experimental investigation connecting the proposed models and experimentally observed desulfidase activities of mutants. The investigation of the hypothesized catalytic amino acids (Glu51, Ser111, Ser113 and Arg60) and cysteines holding iron-sulfur cluster (Cys17, Cys49, and Cys114) by mutational analysis essentially abolished the RudS desulfidase activity, confirming their critical role in catalysis. Additionally, the models identified other important residues (Asn26, Arg24, Tyr25, Ser243, Arg244) for tRNA binding and catalysis, and their mutations resulted in diminished RudS_KT enzymatic activities. The effects of single amino acid substitutions to methionine (158) were all in line with the models we propose, except in the case of Tyr25, where two additional mutants were employed. The Tyr25 mutation to methionine was functionally identical to the WT enzyme, which is at odds with its position in the modeled complex—Tyr25 provides shielding of the active center from tRNA's phosphates and their negative charge, which would destabilize the transitional state and disrupt

catalysis. The RudS_KT Tyr25 to alanine mutant displayed decreased enzymatic activity, while the Tyr25 to phenylalanine mutant retained the same activity as WT. That might be explained by methionine being large enough to provide substantial electrostatic shielding; therefore, only the Tyr25 to alanine variant function was significantly affected by the substitution.

The proposed models of the RudS enzyme–tRNA substrate complex suggest that the DUF1722 domain primarily interacts with the anticodon arm and anticodon of the tRNA substrate, while the catalytic TudS domain interacts with the variable loop, acceptor stem, and D arm of the tRNA.

Insights into physiological function of RudS proteins

The DUF1722 genes are predominantly reported in bacteria (94.2% of all sequences) with archaeal DUF1722 making up only 5.1%. 74.4% of DUF1722s are fused with the TudS gene and only 21.4% of known DUF1722 genes encode a stand-alone protein (148). Genes encoding RudS are often found in light-responsive operons (Figure 49), which are responsible for UV-induced DNA damage repair (i.e., DNA-photolyases) or light-induced oxidative stress response (i.e., carotenoid biosynthesis gene clusters) (154). Recent studies in the genus *Pseudomonas* have revealed the role of light-inducible transcriptional regulators in controlling the expression of light-responsive genes. These regulators belong to the MerR family and are adenosyl B12-dependent, making them sensitive to light (class II LitR regulators). In the dark, LitR regulators function as negative regulators, suppressing the transcription of light-inducible genes. However, when exposed to 450 nm blue light, LitRs become deactivated. One of the operons controlled by this mechanism encodes PhrB DNA photolyase, LitR, and RudS (153, 205).

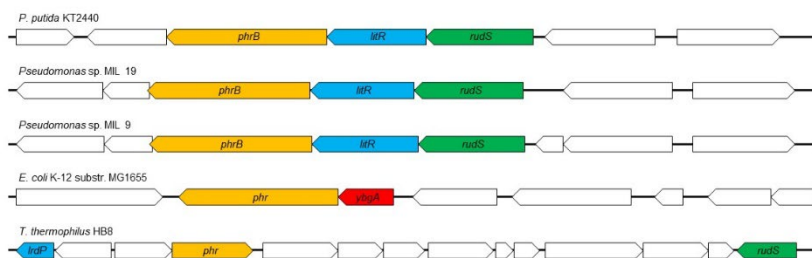


Figure 49. Organization of RudS and YbgA encoding genome loci. Genes highlighted in green – RudS encoding gene; red – DUF1722 encoding gene; orange – DNA photolyase encoding genes; blue – light-inducible transcription regulator encoding genes.

At the same time, the tRNA s4U modification is known to act as a photosensitive residue in tRNA, crosslinking with neighboring cytidine in the 13th position upon exposure to near-UV radiation. Near-UV light triggers a bacterial growth delay effect causing some tRNA species to become poor substrates for aminoacylation resulting in accumulation of uncharged tRNA and transient cessation of protein synthesis (206, 207). The accumulation of ribosomes stalled with non-aminoacylated tRNA is known to initiate a stringent response (208), which is the most likely mechanism causing alarmone guanosine tetraphosphate (ppGpp) accumulation after cell irradiation by UVA (75, 76).

Paradoxically, *E. coli* Δ *thiI* mutants, incapable of s4U tRNA modification biosynthesis, are less susceptible to the combination of short wavelength UV and UVA, as s4U is the primary target of the latter irradiation. Subsequently, this eliminates a damaging synergistic effect of UVA and UVB or UVC irradiation observed in *E. coli* (81, 209). The presence of RudS gene in such cases could help overcome UVA-induced deceleration of protein synthesis, thereby ensuring the functionality of DNA damage repair machinery. On the other hand, studies with *Salmonella typhimurium* revealed that 4-thiouridine plays a crucial role in resistance to near-UV irradiation, with mutants lacking 4-thiouridine and those deficient in ppGpp synthesis being sensitive to near-UV-induced killing; it further suggested a model wherein ppGpp and ApppGpp induce the synthesis of a set of then unidentified proteins essential for resistance to near-UV irradiation in response to the crosslinking of 4-thiouridine in tRNA (75). It is worth noting that *Salmonella typhimurium* possesses a RudS encoding gene (RudS_ST in this study, ORF319 previously) under the control of a transcription regulator of MerR family (152, 210), while *E. coli* does not.

The prevalence of DUF1722 genes in bacteria, often fused with TudS, and their association with light-responsive genes, suggest a light-induced mechanism for prokaryotic tRNA s4U de-modification. Although it is most likely, that this mechanism only supports the protein translation during UV-stress, it may also play a role in regulating alarmone levels during UV-induced tRNA cross-linking and the stringent response, serving as a bacterial survival strategy under UV stress. Although in vitro experiments showed no changes in the enzymatic activity of RudS_KT in the presence of the (p)ppGpp molecules, this does not rule out the possibility that the alarmones and RudS are part of the same regulatory mechanism within the cell, interacting through currently unknown intermediary factors or pathways.

This speculation could be supported by the case of *Enterobacter cloacae*, which demonstrated that pre-treating bacteria with sub-lethal doses of UVA

that during evolution, in certain species, the gene encoding RudS may have undergone a split, resulting in separate stand-alone TudS and stand-alone DUF1722 encoding genes.

Moreover, nano-tRNAseq analysis of tRNA extracted from RudS_KT overexpressing *E. coli* cells revealed a significant decrease (~2-fold) in the abundance of tRNA Ser(GTC) and tRNA Tyr(GTA) compared to control samples (Figure 50). These findings parallel previous observations (24) that the lack of s4U modification causes a degradosome-mediated degradation of tRNA Ser(TGA) and tRNA Tyr(GTA) in *Vibrio cholerae* during the stationary growth phase. Although the reduction we observed in *E. coli* is not as dramatic as in *Vibrio cholerae*, this co-occurrence suggests an underlying physiological mechanism that responds to s4U levels in tRNA.

CONCLUSIONS

1. Stand-alone TudS proteins catalyze the desulfidation of 4-thiouracil derivatives, with the highest activity towards 4-thio-UMP.
2. The *tudS* gene enables uracil auxotrophic bacteria to utilize exogenous 4-thiouracil and 4-thiouridine as uracil sources.
3. The *tudS* gene in *P. putida* and *B. subtilis* is responsible for detoxifying the environment and overcoming growth inhibition caused by 4-thiouracil-containing compounds.
4. RudS (a TudS-DUF1722 fusion protein) functions as a tRNA 4-thiouridine de-modification enzyme.
5. RudS activity depends on [4Fe-4S] cluster, sharing the catalytic mechanism with TudS. RudS_KT residues Glu51, Ser111, Ser113 and the newly identified Arg60 are the residues responsible for catalysis.
6. The DUF1722 domain of RudS mediates tRNA-binding, by interacting with the anticodon arm and anticodon, while the catalytic TudS domain interacts with the variable loop, acceptor stem, and D arm of the tRNA.
7. RudS allows *E. coli* to reduce UVA-caused growth delay.

REFERENCES

1. Nishikiori,T., Hiruma,S., Kurokawa,T., Saito,S. and Shimada,N. (1992) MICROBIAL PRODUCTION OF 4-THIOURIDINE. *J. Antibiot. (Tokyo)*, **45**, 1376–1377.
2. Probst-Rüd,S., Nyangaresi,P.O., Adeyeye,A.A., Ackermann,M., Beck,S.E. and McNeill,K. (2024) Synergistic effect of UV-A and UV-C light is traced to UV-induced damage of the transfer RNA. *Water Res.*, **252**.
3. Berg,J.M., Tymoczko,J.L. and Strye,L. (2002) Biochemistry, Fifth Edition.
4. Shepherd,J. and Ibba,M. (2015) Bacterial transfer RNAs. *FEMS Microbiol. Rev.*, **39**, 280.
5. Gegenheimert,P. and Apirion,D. (1981) Processing of procaryotic ribonucleic acid. *Microbiol. Rev.*, **45**, 502.
6. Apirion,D. and Miczak,A. (1993) RNA processing in prokaryotic cells. *Bioessays*, **15**, 113–120.
7. Ayan,G.B., Park,H.J. and Gallie,J. (2020) The birth of a bacterial trna gene by large-scale, tandem duplication events. *Elife*, **9**, 1–43.
8. Giegé,R., Jühling,F., Pütz,J., Stadler,P., Sauter,C. and Florentz,C. (2012) Structure of transfer RNAs: similarity and variability. *Wiley Interdiscip. Rev. RNA*, **3**, 37–61.
9. de Crécy-Lagard,V. and Jaroch,M. (2021) Functions of Bacterial tRNA Modifications: From Ubiquity to Diversity. *Trends Microbiol.*, **29**, 41–53.
10. Cappannini,A., Ray,A., Purta,E., Mukherjee,S., Boccaletto,P., Moafinejad,S.N., Lechner,A., Barchet,C., Klaholz,B.P., Stefaniak,F., *et al.* (2023) MODOMICS: a database of RNA modifications and related information. 2023 update. *Nucleic Acids Res.*, 10.1093/nar/gkad1083.
11. Zhang,W., Foo,M., Eren,A.M. and Pan,T. (2022) tRNA modification dynamics from individual organisms to metaepitranscriptomics of microbiomes. *Mol. Cell*, **82**, 891–906.
12. El Yacoubi,B., Bailly,M. and De Crécy-Lagard,V. (2012) Biosynthesis and function of posttranscriptional modifications of transfer RNAs. *Annu. Rev. Genet.*, **46**, 69–95.
13. Smith,T.J., Giles,R.N. and Koutmou,K.S. (2024) Anticodon stem-loop tRNA modifications influence codon decoding and frame maintenance during translation. *Semin. Cell Dev. Biol.*, **154**, 105–113.
14. de Crécy-Lagard,V., Ross,R.L., Jaroch,M., Marchand,V., Eisenhart,C., Brégeon,D., Motorin,Y. and Limbach,P.A. (2020) Survey and Validation of tRNA Modifications and Their Corresponding Genes in *Bacillus subtilis* sp *Subtilis* Strain 168. *Biomolecules*, **10**, 1–23.
15. Lei,L. and Burton,Z.F. (2022) ‘Superwobbling’ and tRNA-34 Wobble and tRNA-37 Anticodon Loop Modifications in Evolution and Devolution of the Genetic Code. *Life (Basel, Switzerland)*, **12**.
16. Urbonavičius,J., Qian,Q., Durand,J.M.B., Hagervall,T.G. and Björk,G.R. (2001) Improvement of reading frame maintenance is a common

- function for several tRNA modifications. *EMBO J.*, **20**, 4863–4873.
17. Mbiu, G. Henri Grosjean DNA and RNA Modification Enzymes: Structure, Mechanism, Function and Evolution DNA and RNA Modification Enzymes: Structure, Mechanism, Function and Evolution.
 18. Motorin, Y. and Helm, M. (2011) RNA nucleotide methylation. *Wiley Interdiscip. Rev. RNA*, **2**, 611–631.
 19. Charette, M. and Gray, M.W. (2000) Pseudouridine in RNA: What, Where, How, and Why. *IUBMB Life*, **49**, 341–351.
 20. Dalluge, J.J., Hashizume, T., Sopchik, A.E., McCloskey, J.A. and Davis, D.R. (1996) Conformational flexibility in RNA: the role of dihydrouridine. *Nucleic Acids Res.*, **24**, 1073–1079.
 21. Herschlag, D. (1995) RNA chaperones and the RNA folding problem. *J. Biol. Chem.*, **270**, 20871–20874.
 22. Keffer-Wilkes, L.C., Veerareddygar, G.R., Kothe, U. and Feigon, J. (2016) RNA modification enzyme TruB is a tRNA chaperone. *Proc. Natl. Acad. Sci. U. S. A.*, **113**, 14306–14311.
 23. Keffer-Wilkes, L.C., Soon, E.F. and Kothe, U. (2020) The methyltransferase TrmA facilitates tRNA folding through interaction with its RNA-binding domain. *Nucleic Acids Res.*, **48**, 7981–7990.
 24. Kimura, S. and Waldor, M.K. (2019) The RNA degradosome promotes tRNA quality control through clearance of hypomodified tRNA. *Proc. Natl. Acad. Sci. U. S. A.*, **116**, 1394–1403.
 25. Chionh, Y.H., McBee, M., Babu, I.R., Hia, F., Lin, W., Zhao, W., Cao, J., Dziergowska, A., Malkiewicz, A., Begley, T.J., *et al.* (2016) tRNA-mediated codon-biased translation in mycobacterial hypoxic persistence. *Nat. Commun.*, **7**, 1–12.
 26. Vågbo, C.B., Svaasand, E.K., Aas, P.A. and Krokan, H.E. (2013) Methylation damage to RNA induced in vivo in *Escherichia coli* is repaired by endogenous AlkB as part of the adaptive response. *DNA Repair (Amst.)*, **12**, 188–195.
 27. Reichle, V.F., Petrov, D.P., Weber, V., Jung, K. and Kellner, S. (2019) NAIL-MS reveals the repair of 2-methylthiocytidine by AlkB in *E. coli*. *Nat. Commun.*, **10**, 1–11.
 28. Borek, C., Reichle, V.F. and Kellner, S. (2020) Synthesis and Metabolic Fate of 4-Methylthiouridine in Bacterial tRNA. *ChemBioChem*, **21**, 2768–2771.
 29. Dixit, S., Henderson, J.C. and Alfonzo, J.D. (2019) Multi-Substrate Specificity and the Evolutionary Basis for Interdependence in tRNA Editing and Methylation Enzymes. *Front. Genet.*, **10**.
 30. Randau, L., Stanley, B.J., Kohlway, A., Mehta, S., Xiong, Y. and Söll, D. (2009) A cytidine deaminase edits c to u in transfer RNAs in archaea. *Science (80-.)*, **324**, 657–659.
 31. Kimura, S., Srisuknimit, V., McCarty, K.L., Dedon, P.C., Kranzusch, P.J. and Waldor, M.K. (2022) Sequential action of a tRNA base editor in conversion of cytidine to pseudouridine. *Nat. Commun.*, **13**.

32. Prossliner,T., Agrawal,S., Heidemann,D.F., Sørensen,M.A. and Svenningsen,S.L. (2023) tRNAs Are Stable After All: Pitfalls in Quantification of tRNA from Starved Escherichia coli Cultures Exposed by Validation of RNA Purification Methods. *MBio*, **14**.
33. Yared,M.J., Marcelot,A. and Barraud,P. (2024) Beyond the Anticodon: tRNA Core Modifications and Their Impact on Structure, Translation and Stress Adaptation. *Genes* 2024, Vol. 15, Page 374, **15**, 374.
34. Phizicky,E.M. and Hopper,A.K. (2023) The life and times of a tRNA. *RNA*, **29**, 898–957.
35. Whipple,J.M., Lane,E.A., Chernyakov,I., D’Silva,S. and Phizicky,E.M. (2011) The yeast rapid tRNA decay pathway primarily monitors the structural integrity of the acceptor and T-stems of mature tRNA. *Genes Dev.*, **25**, 1173.
36. Li,Z., Reimers,S., Pandit,S. and Deutscher,M.P. (2002) RNA quality control: Degradation of defective transfer RNA. *EMBO J.*, **21**, 1132–1138.
37. Tomikawa,C., Yokogawa,T., Kanai,T. and Hori,H. (2010) N7-Methylguanine at position 46 (m7G46) in tRNA from *Thermus thermophilus* is required for cell viability at high temperatures through a tRNA modification network. *Nucleic Acids Res.*, **38**, 942.
38. Kimura,S. and Waldor,M.K. (2019) The RNA degradosome promotes tRNA quality control through clearance of hypomodified tRNA. *Proc. Natl. Acad. Sci. U. S. A.*, **116**, 1394–1403.
39. Deutscher,M.P. (2003) Degradation of Stable RNA in Bacteria. *J. Biol. Chem.*, **278**, 45041–45044.
40. Bernstein,J.A., Khodursky,A.B., Lin,P.H., Lin-Chao,S. and Cohen,S.N. (2002) Global analysis of mRNA decay and abundance in *Escherichia coli* at single-gene resolution using two-color fluorescent DNA microarrays. *Proc. Natl. Acad. Sci. U. S. A.*, **99**, 9697–9702.
41. Bechhofer,D.H. (2013) Nucleotide specificity in bacterial mRNA recycling. *Proc. Natl. Acad. Sci. U. S. A.*, **110**, 8765–8766.
42. Mohanty,B.K. and Kushner,S.R. Regulation of mRNA decay in *E. coli*. [10.1080/10409238.2021.1968784](https://doi.org/10.1080/10409238.2021.1968784).
43. Bechhofer,D.H. and Deutscher,M.P. (2019) Bacterial ribonucleases and their roles in RNA metabolism. *Crit. Rev. Biochem. Mol. Biol.*, **54**, 242.
44. Kanehisa,M. and Subramaniam (2002) The KEGG Database. *Novartis Found. Symp.*, **247**, 91–103.
45. Li,X., Li,K., Guo,W., Wen,Y., Meng,C. and Wu,B. (2022) Structure Characterization of *Escherichia coli* Pseudouridine Kinase *PsuK*. *Front. Microbiol.*, **13**.
46. Stanislauskienė,R., Lauryėnas,A., Rutkienė,R., Aučynaitė,A., Tauraitė,D., Meškienė,R., Urbelienė,N., Kaupinis,A., Valius,M., Kaliniene,L., *et al.* (2020) YqfB protein from *Escherichia coli*: an atypical amidohydrolase active towards N 4-acylcytosine derivatives. *Sci. Rep.*, **10**, 1–12.

47. Zhang,S., Liu,Y., Ma,X., Gao,X., Ru,Y., Hu,X. and Gu,X. (2024) Recent advances in the potential role of RNA N4-acetylcytidine in cancer progression. *Cell Commun. Signal.* 2024 221, **22**, 1–17.
48. Hitchcock,D.S., Fedorov,A.A., Fedorov,E. V., Almo,S.C. and Raushel,F.M. (2014) Discovery of a bacterial 5-methylcytosine deaminase. *Biochemistry*, **53**, 7426–7435.
49. Aučynaite,A., Rutkiene,R., Tauraite,D., Meškys,R. and Urbonavičius,J. (2018) Identification of a 2'-O-methyluridine nucleoside hydrolase using the metagenomic libraries. *Molecules*, **23**.
50. Ayadi,L., Galvanin,A., Pichot,F., Marchand,V. and Motorin,Y. (2019) RNA ribose methylation (2'-O-methylation): Occurrence, biosynthesis and biological functions. *Biochim. Biophys. Acta - Gene Regul. Mech.*, **1862**, 253–269.
51. Urbelienė,N., Meškienė,R., Tiškus,M., Stanislauskienė,R., Aučynaitė,A., Laurynėnas,A. and Meškys,R. (2020) A rapid method for the selection of amidohydrolases from metagenomic libraries by applying synthetic nucleosides and a uridine auxotrophic host. *Catalysts*, **10**, 445.
52. Lipsett,M.N. (1966) Disulfide Bonds in sRNA. *Cold Spring Harb. Symp. Quant. Biol.*, **31**, 449–455.
53. THOMAS,G. and FAVRE,A. (1980) 4-Thiouridine Triggers Both Growth Delay Induced by Near-Ultraviolet Light and Photoprotection. *Eur. J. Biochem.*, **113**, 67–74.
54. Emilsson,V., Näslund,A.K. and Kurlad,C.G. (1992) Thiolation of transfer RNA in Escherichia coli varies with growth rate. *Nucleic Acids Res.*, **20**, 4499.
55. Shigi,N. (2021) Biosynthesis and degradation of sulfur modifications in tRNAs. *Int. J. Mol. Sci.*, **22**.
56. Tomikawa,C., Ohira,T., Inoue,Y., Kawamura,T., Yamagishi,A., Suzuki,T. and Hori,H. (2013) Distinct tRNA modifications in the thermoacidophilic archaeon, Thermoplasma acidophilum. *FEBS Lett.*, **587**, 3575–3580.
57. Kimura,S. and Waldor,M.K. (2019) The RNA degradosome promotes tRNA quality control through clearance of hypomodified tRNA. *Proc. Natl. Acad. Sci. U. S. A.*, **116**, 1394–1403.
58. Griffey,R.H., Davis,D.R. and Yamaizumi,Z. (1986) 15N-labeled tRNA. Identification of 4-thiouridine in Escherichia coli tRNA1(Ser) and tRNA2(Tyr) by 1H-15N two-dimensional NMR spectroscopy. *J. Biol. Chem.*, **261**, 12074–12078.
59. Kompatscher,M., Bartosik,K., Erharter,K., Plangger,R., Juen,F.S., Kreutz,C., Micura,R., Westhof,E. and Erlacher,M.D. (2024) Contribution of tRNA sequence and modifications to the decoding preferences of E. coli and M. mycoides tRNAGlyUCC for synonymous glycine codons. *Nucleic Acids Res.*, **52**, 1374–1386.
60. Kumar,R.K. and Davis,D.R. (1997) Synthesis and Studies on the Effect of 2-Thiouridine and 4-Thiouridine on Sugar Conformation and RNA

- Duplex Stability. *Nucleic Acids Res.*, **25**, 1272–1280.
61. Nomura, Y., Ohno, S., Nishikawa, K. and Yokogawa, T. (2016) Correlation between the stability of tRNA tertiary structure and the catalytic efficiency of a tRNA-modifying enzyme, archaeal tRNA-guanine transglycosylase. *Genes to Cells*, **21**, 41–52.
 62. Hoffmann, A., Lorenz, C., Fallmann, J., Wolff, P., Lechner, A., Betat, H., Mörl, M. and Stadler, P.F. (2024) Temperature-Dependent tRNA Modifications in Bacillales. *Int. J. Mol. Sci.* 2024, Vol. 25, Page 8823, **25**, 8823.
 63. Hori, H., Saneyoshi, M., Kumagai, I., Miura, K.I. and Watanabe, K. (1989) Effects of modification of 4-thiouridine in E. coli tRNA^r on its methyl acceptor activity by thermostable Gm-methylases. *J. Biochem.*, **106**, 798–802.
 64. Pritchard, J.R., Chao, M.C., Abel, S., Davis, B.M., Baranowski, C., Zhang, Y.J., Rubin, E.J. and Waldor, M.K. (2014) ARTIST: High-Resolution Genome-Wide Assessment of Fitness Using Transposon-Insertion Sequencing. *PLoS Genet.*, **10**.
 65. Tejada-Arranz, A., de Crécy-Lagard, V. and de Reuse, H. (2020) Bacterial RNA degradosomes: molecular machines under tight control. *Trends Biochem. Sci.*, **45**, 42.
 66. Ashwood, B., Pollum, M. and Crespo-Hernández, C.E. (2019) Photochemical and Photodynamical Properties of Sulfur-Substituted Nucleic Acid Bases. *Photochem. Photobiol.*, **95**, 33–58.
 67. Favre, A., Saintomé, C., Fourrey, J.L., Clivio, P. and Laugâa, P. (1998) Thionucleobases as intrinsic photoaffinity probes of nucleic acid structure and nucleic acid-protein interactions. *J. Photochem. Photobiol. B Biol.*, **42**, 109–124.
 68. Favre, A., Yaniv, M. and Michels, A.M. (1969) The photochemistry of 4-thiouridine in Escherichia coli t-RNA^{Val}. *Biochem. Biophys. Res. Commun.*, **37**, 266–271.
 69. Favre, A., Roques, B. and Fourrey, J.L. (1972) Chemical structures of the TU-C and TU-Cred products derived from E. coli tRNA. *FEBS Lett.*, **24**, 209–214.
 70. Yaniv, M., Chestier, A., Gros, F. and Favre, A. (1971) Biological activity of irradiated tRNA^{Val} containing a 4-thiouridine-cytosine dimer. *J. Mol. Biol.*, **58**, 381–388.
 71. Bourgeois, G., Seguin, J., Babin, M., Gondry, M., Mechulam, Y. and Schmitt, E. (2020) Structural basis of the interaction between cyclodipeptide synthases and aminoacylated tRNA substrates. *Rna*, **26**, 1589–1602.
 72. Soszynska-Jozwiak, M., Pszczola, M., Piasecka, J., Peterson, J.M., Moss, W.N., Taras-Goslinska, K., Kierzek, R. and Kierzek, E. (2021) Universal and strain specific structure features of segment 8 genomic RNA of influenza A virus—application of 4-thiouridine photocrosslinking. *J. Biol. Chem.*, **297**, 101245.

73. Favre,A., Hajnsdorf,E., Thiam,K. and Caldeira de Araujo,A. (1985) Mutagenesis and growth delay induced in Escherichia coli by near-ultraviolet radiations. *Biochimie*, **67**, 335–342.
74. Dantur,K.I. and Pizarro,R.A. (2004) Effect of growth phase on the Escherichia coli response to ultraviolet-A radiation: Influence of conditioned media, hydrogen peroxide and acetate. *J. Photochem. Photobiol. B Biol.*, **75**, 33–39.
75. Kramer,G.F., Baker,J.C. and Ames,B.N. (1988) Near-UV stress in Salmonella typhimurium: 4-Thiouridine in tRNA, ppGpp, and ApppGpp as components of an adaptive response. *J. Bacteriol.*, **170**, 2344–2351.
76. Oppezzo,O.J. and Pizarro,R.A. (2001) Sublethal effects of ultraviolet A radiation on Enterobacter cloacae. *J. Photochem. Photobiol. B Biol.*, **62**, 158–165.
77. Ramabhadran,T. V. and Jagger,J. (1976) Mechanism of growth delay induced in Escherichia coli by near ultraviolet radiation. *Proc. Natl. Acad. Sci. U. S. A.*, **73**, 59–63.
78. Winther,K.S., Roghanian,M. and Gerdes,K. (2018) Activation of the Stringent Response by Loading of RelA-tRNA Complexes at the Ribosomal A-Site. *Mol. Cell*, **70**, 95-105.e4.
79. Traxler,M.F., Summers,S.M., Nguyen,H.T., Zacharia,V.M., Hightower,G.A., Smith,J.T. and Conway,T. (2008) The global, ppGpp-mediated stringent response to amino acid starvation in Escherichia coli. *Mol. Microbiol.*, **68**, 1128.
80. de Jager,T.L., Cockrell,A.E. and Du Plessis,S.S. (2017) Ultraviolet Light Induced Generation of Reactive Oxygen Species. *Adv. Exp. Med. Biol.*, **996**, 15–23.
81. Probst-Rüd,S., McNeill,K. and Ackermann,M. (2017) Thiouridine residues in tRNAs are responsible for a synergistic effect of UVA and UVB light in photoinactivation of Escherichia coli. *Environ. Microbiol.*, **19**, 434–442.
82. Oppezzo,O.J. and Pizarro,R.A. (2002) Transient reduction in the tRNA 4-thiouridine content induced by ultraviolet A during post-irradiation growth in Enterobacter cloacae. *J. Photochem. Photobiol. B Biol.*, **66**, 207–212.
83. Oppezzo,O.J. and Pizarro,R.A. (2003) Inhibition of sulfur incorporation to transfer RNA by ultraviolet-A radiation in Escherichia coli. *J. Photochem. Photobiol. B Biol.*, **71**, 69–75.
84. Bezerra,R. and Favre,A. (1990) In vivo incorporation of the intrinsic photolabel 4-thiouridine into Escherichia coli RNAs. *Biochem. Biophys. Res. Commun.*, **166**, 29–37.
85. Woodford,T.A., Schlegel,R. and Pardee,A.B. (1988) Selective isolation of newly synthesized mammalian mRNA after in vivo labeling with 4-thiouridine or 6-thioguanosine. *Anal. Biochem.*, **171**, 166–172.
86. Ascano,M., Hafner,M., Cekan,P., Gerstberger,S. and Tuschl,T. (2012) Identification of RNA-protein interaction networks using PAR-CLIP.

- Wiley Interdiscip. Rev. RNA*, **3**, 159–177.
87. Russo, J., Heck, A.M., Wilusz, J. and Wilusz, C.J. (2017) Metabolic labeling and recovery of nascent RNA to accurately quantify mRNA stability. *Methods*, **120**, 39–48.
 88. Ohashi, S., Nakamura, M., Acharyya, S., Inagaki, M., Abe, N., Kimura, Y., Hashiya, F. and Abe, H. (2024) Development and Comparison of 4-Thiouridine to Cytidine Base Conversion Reaction. *ACS Omega*, **9**, 9300–9308.
 89. Favre, A., Moreno, G., Blondel, M.O., Kliber, J., Vinzens, F. and Salet, C. (1986) 4-thiouridine photosensitized RNA-protein crosslinking in mammalian cells. *Biochem. Biophys. Res. Commun.*, **141**, 847–854.
 90. Mishima, Y. and Steitz, J.A. (1995) Site-specific crosslinking of 4-thiouridine-modified human tRNA(3Lys) to reverse transcriptase from human immunodeficiency virus type I. *EMBO J.*, **14**, 2679.
 91. Garibaldi, A., Carranza, F. and Hertel, K.J. (2017) Isolation of Newly Transcribed RNA Using the Metabolic Label 4-thiouridine. *Methods Mol. Biol.*, **1648**, 169.
 92. Miller, C., Schwab, B., Maier, K., Schulz, D., Dümcke, S., Zacher, B., Mayer, A., Sydow, J., Marcinowski, L., Dölken, L., *et al.* (2011) Dynamic transcriptome analysis measures rates of mRNA synthesis and decay in yeast. *Mol. Syst. Biol.*, **7**, 458.
 93. Sugio, Y., Yamagami, R., Shigi, N. and Hori, H. (2023) A selective and sensitive detection system for 4-thiouridine modification in RNA. *RNA*, **29**, 241–251.
 94. Riml, C., Amort, T., Rieder, D., Gasser, C., Lusser, A. and Micura, R. (2017) Osmium-Mediated Transformation of 4-Thiouridine to Cytidine as Key To Study RNA Dynamics by Sequencing. *Angew. Chem. Int. Ed. Engl.*, **56**, 13479–13483.
 95. Herzog, V.A., Reicholf, B., Neumann, T., Rescheneder, P., Bhat, P., Burkard, T.R., Wlotzka, W., Von Haeseler, A., Zuber, J. and Ameres, S.L. (2017) Thiol-linked alkylation of RNA to assess expression dynamics. *Nat. Methods* **2017** *1412*, **14**, 1198–1204.
 96. Schofield, J.A., Duffy, E.E., Kiefer, L., Sullivan, M.C. and Simon, M.D. (2018) TimeLapse-seq: adding a temporal dimension to RNA sequencing through nucleoside recoding. *Nat. Methods*, **15**, 221–225.
 97. Taylor, S. V., Kelleher, N.L., Kinsland, C., Chiu, H.J., Costello, C.A., Backstrom, A.D., McLafferty, F.W. and Begley, T.P. (1998) Thiamin Biosynthesis in *Escherichia coli*: IDENTIFICATION OF ThiS THIOCARBOXYLATE AS THE IMMEDIATE SULFUR DONOR IN THE THIAZOLE FORMATION. *J. Biol. Chem.*, **273**, 16555–16560.
 98. Webb, E., Claas, K. and Downs, D.M. (1997) Characterization of thiI, a new gene involved in thiazole biosynthesis in *Salmonella typhimurium*. *J. Bacteriol.*, **179**, 4399.
 99. Mueller, E.G., Buck, C.J., Palenchar, P.M., Barnhart, L.E. and Paulson, J.L. (1998) Identification of a gene involved in the generation of 4-

- thiouridine in tRNA. *Nucleic Acids Res.*, **26**, 2606–2610.
100. Bender, R.A. (2011) The Danger of Annotation by Analogy: Most “thiI” Genes Play No Role in Thiamine Biosynthesis. *J. Bacteriol.*, **193**, 4574–4575.
 101. Martinez-Gomez, N.C., Palmer, L.D., Vivas, E., Roach, P.L. and Downs, D.M. (2011) The rhodanese domain of ThiI is both necessary and sufficient for synthesis of the Thiazole moiety of thiamine in *Salmonella enterica*. *J. Bacteriol.*, **193**, 4582–4587.
 102. He, N., Zhou, J., Bimai, O., Oltmanns, J., Ravanat, J.L., Velours, C., Schünemann, V., Fontecave, M. and Golinelli-Pimpaneau, B. (2022) A subclass of archaeal U8-tRNA sulfurases requires a [4Fe-4S] cluster for catalysis. *Nucleic Acids Res.*, **50**, 12969–12978.
 103. Waterman, D.G., Ortiz-Lombardía, M., Fogg, M.J., Koonin, E. V. and Antson, A.A. (2006) Crystal Structure of *Bacillus anthracis* ThiI, a tRNA-modifying Enzyme Containing the Predicted RNA-binding THUMP Domain. *J. Mol. Biol.*, **356**, 97–110.
 104. Rodriguez-Monge, L., Ouzounis, C.A. and Kyrpides, N.C. (1998) A ferredoxin-like domain in RNA polymerase 30/40-kDa subunits. *Trends Biochem. Sci.*, **23**, 169–170.
 105. Fislage, M., Roovers, M., Tuszyńska, I., Bujnicki, J.M., Droogmans, L. and Versées, W. (2012) Crystal structures of the tRNA:m2G6 methyltransferase Trm14/TrmN from two domains of life. *Nucleic Acids Res.*, **40**, 5149.
 106. Roovers, M., Oudjama, Y., Fislage, M., Bujnicki, J.M., Versées, W. and Droogmans, L. (2012) The open reading frame TTC1157 of *Thermus thermophilus* HB27 encodes the methyltransferase forming N2-methylguanosine at position 6 in tRNA. *RNA*, **18**, 815–824.
 107. Armengaud, J., Urbonavičius, J., Fernandez, B., Chaussin, G., Bujnicki, J.M. and Grosjean, H. (2004) N2-methylation of guanosine at position 10 in tRNA is catalyzed by a THUMP domain-containing, S-adenosylmethionine-dependent methyltransferase, conserved in archaea and eukaryota. *J. Biol. Chem.*, **279**, 37142–37152.
 108. Gurha, P. and Gupta, R. (2008) Archaeal Pus10 proteins can produce both pseudouridine 54 and 55 in tRNA. *RNA*, **14**, 2521–2527.
 109. Hori, H. (2023) Transfer RNA Modification Enzymes with a Thiouridine Synthetase, Methyltransferase and Pseudouridine Synthase (THUMP) Domain and the Nucleosides They Produce in tRNA. *Genes (Basel)*, **14**.
 110. You, D., Xu, T., Yao, F., Zhou, X. and Deng, Z. (2008) Direct evidence that ThiI is an ATP pyrophosphatase for the adenylation of uridine in 4-thiouridine biosynthesis. *Chembiochem*, **9**, 1879–1882.
 111. Bork, P. and Koonin, E. V. (1994) A P-loop-like motif in a widespread ATP pyrophosphatase domain: Implications for the evolution of sequence motifs and enzyme activity. *Proteins Struct. Funct. Bioinforma.*, **20**, 347–355.
 112. Ogunkola, M., Wolff, L., Fenteng, E.A., Duffus, B.R. and Leimkühler, S.

- (2024) *E. coli* MnmA Is an Fe-S Cluster-Independent 2-Thiouridylase. *Inorganics* 2024, Vol. 12, Page 67, **12**, 67.
113. Bimai,O., Legrand,P., Ravanat,J.L., Touati,N., Zhou,J., He,N., Lénon,M., Barras,F., Fontecave,M. and Golinelli-Pimpaneau,B. (2023) The thiolation of uridine 34 in tRNA, which controls protein translation, depends on a [4Fe-4S] cluster in the archaeum *Methanococcus maripaludis*. *Sci. Rep.*, **13**.
 114. Chen,M., Asai,S.I., Narai,S., Nambu,S., Omura,N., Sakaguchi,Y., Suzuki,T., Ikeda-Saito,M., Watanabe,K., Yao,M., *et al.* (2017) Biochemical and structural characterization of oxygen-sensitive 2-thiouridine synthesis catalyzed by an iron-sulfur protein TtuA. *Proc. Natl. Acad. Sci. U. S. A.*, **114**, 4954–4959.
 115. Palenchar,P.M., Buck,C.J., Cheng,H., Larson,T.J. and Mueller,E.G. (2000) Evidence that ThiI, an enzyme shared between thiamin and 4-thiouridine biosynthesis, may be a sulfurtransferase that proceeds through a persulfide intermediate. *J. Biol. Chem.*, **275**, 8283–8286.
 116. Mueller,E.G., Palenchar,P.M. and Buck,C.J. (2001) The role of the cysteine residues of ThiI in the generation of 4-thiouridine in tRNA. *J. Biol. Chem.*, **276**, 33588–33595.
 117. Cipollone,R., Ascenzi,P., Tomao,P., Imperi,F. and Visca,P. (2008) Enzymatic Detoxification of Cyanide: Clues from *Pseudomonas aeruginosa* Rhodanese. *J. Mol. Microbiol. Biotechnol.*, **15**, 199–211.
 118. Kambampati,R. and Lauhon,C.T. (2000) Evidence for the transfer of sulfane sulfur from IscS to ThiI during the in vitro biosynthesis of 4-thiouridine in *Escherichia coli* tRNA. *J. Biol. Chem.*, **275**, 10727–10730.
 119. Flint,D.H. (1996) *Escherichia coli* Contains a Protein That Is Homologous in Function and N-terminal Sequence to the Protein Encoded by the *nifS* Gene of *Azotobacter vinelandii* and That Can Participate in the Synthesis of the Fe-S Cluster of Dihydroxy-acid Dehydratase. *J. Biol. Chem.*, **271**, 16068–16074.
 120. Veerareddygarri,G.R., Klusman,T.C. and Mueller,E.G. (2016) Characterization of the catalytic disulfide bond in *E. coli* 4-thiouridine synthetase to elucidate its functional quaternary structure. *Protein Sci.*, **25**, 1737–1743.
 121. Neumann,P., Lakomek,K., Naumann,P.T., Erwin,W.M., Lauhon,C.T. and Ficner,R. (2014) Crystal structure of a 4-thiouridine synthetase-RNA complex reveals specificity of tRNA U8 modification. *Nucleic Acids Res.*, **42**, 6673–6685.
 122. Liu,Y., Vinyard,D.J., Reesbeck,M.E., Suzuki,T., Manakongtreecheep,K., Holland,P.L., Brudvig,G.W. and Söll,D. (2016) A [3Fe-4S] cluster is required for tRNA thiolation in archaea and eukaryotes. *Proc. Natl. Acad. Sci. U. S. A.*, **113**, 12703–12708.
 123. Chen,M., Ishizaka,M., Narai,S., Horitani,M., Shigi,N., Yao,M. and Tanaka,Y. (2020) The [4Fe-4S] cluster of sulfurtransferase TtuA desulfurizes TtuB during tRNA modification in *Thermus thermophilus*.

- Commun. Biol.*, **3**, 2–4.
124. Blanc,B., Gerez,C. and Ollagnier de Choudens,S. (2015) Assembly of Fe/S proteins in bacterial systems: Biochemistry of the bacterial ISC system. *Biochim. Biophys. Acta - Mol. Cell Res.*, **1853**, 1436–1447.
 125. Kiley,P.J. and Beinert,H. (2003) The role of Fe-S proteins in sensing and regulation in bacteria. *Curr. Opin. Microbiol.*, **6**, 181–185.
 126. Vallières,C., Benoit,O., Guittet,O., Huang,M.-E., Lepoivre,M., Golinelli-Cohen,M.-P. and Vernis,L. (2024) Iron-sulfur protein odyssey: exploring their cluster functional versatility and challenging identification. *Metallomics*, **16**, 25.
 127. Volbeda,A., Martinez,M.T.P., Crack,J.C., Amara,P., Gigarel,O., Munnoch,J.T., Hutchings,M.I., Darnault,C., Le Brun,N.E. and Fontecilla-Camps,J.C. (2019) Crystal Structure of the Transcription Regulator RsrR Reveals a {2Fe-2S} Cluster Coordinated by Cys, Glu, and His Residues. *J. Am. Chem. Soc.*, **141**, 2367–2375.
 128. Blahut,M., Sanchez,E., Fisher,C.E. and Outten,F.W. (2020) Fe-S cluster biogenesis by the bacterial Suf pathway. *Biochim. Biophys. Acta - Mol. Cell Res.*, **1867**, 118829.
 129. Blanc,B., Gerez,C. and Ollagnier de Choudens,S. (2015) Assembly of Fe/S proteins in bacterial systems: Biochemistry of the bacterial ISC system. *Biochim. Biophys. Acta*, **1853**, 1436–1447.
 130. Lill,R. (2009) Function and biogenesis of iron–sulphur proteins. *Nat. 2009 4607257*, **460**, 831–838.
 131. Pastore,A. and Puccio,H. (2013) Frataxin: a protein in search for a function. *J. Neurochem.*, **126**, 43–52.
 132. Lange,H., Kaut,A., Kispal,G. and Lill,R. (2000) A mitochondrial ferredoxin is essential for biogenesis of cellular iron-sulfur proteins. *Proc. Natl. Acad. Sci. U. S. A.*, **97**, 1050–1055.
 133. Giel,J.L., Rodionov,D., Liu,M., Blattner,F.R. and Kiley,P.J. (2006) IscR-dependent gene expression links iron-sulphur cluster assembly to the control of O₂-regulated genes in Escherichia coli. *Mol. Microbiol.*, **60**, 1058–1075.
 134. Fleischhacker,A.S., Stubna,A., Hsueh,K.L., Guo,Y., Teter,S.J., Rose,J.C., Brunold,T.C., Markley,J.L., Münck,E. and Kiley,P.J. (2012) Characterization of the [2Fe-2S] cluster of Escherichia coli transcription factor IscR. *Biochemistry*, **51**, 4453–4462.
 135. Vinella,D., Loiseau,L., de Choudens,S.O., Fontecave,M. and Barras,F. (2013) In vivo [Fe-S] cluster acquisition by IscR and NsrR, two stress regulators in Escherichia coli. *Mol. Microbiol.*, **87**, 493–508.
 136. Giel,J.L., Nesbit,A.D., Mettert,E.L., Fleischhacker,A.S., Wanta,B.T. and Kiley,P.J. (2013) Regulation of iron–sulphur cluster homeostasis through transcriptional control of the Isc pathway by [2Fe–2S]–IscR in Escherichia coli. *Mol. Microbiol.*, **87**, 478–492.
 137. Akhtar,M.K. and Jones,P.R. (2008) Deletion of iscR stimulates recombinant clostridial Fe-Fe hydrogenase activity and H₂-

- accumulation in *Escherichia coli* BL21(DE3). *Appl. Microbiol. Biotechnol.*, **78**, 853–862.
138. Wang, X. Bin, Niu, S., Yang, X., Ibrahim, S.K., Pickett, C.J., Ichiye, T. and Wang, L.S. (2003) Probing the Intrinsic Electronic Structure of the Cubane [4Fe-4S] Cluster: Nature's Favorite Cluster for Electron Transfer and Storage. *J. Am. Chem. Soc.*, **125**, 14072–14081.
 139. Khoroshilova, N., Popescu, C., Münck, E., Beinert, H. and Kiley, P.J. (1997) Iron-sulfur cluster disassembly in the FNR protein of *Escherichia coli* by O₂: [4Fe-4S] to [2Fe-2S] conversion with loss of biological activity. *Proc. Natl. Acad. Sci. U. S. A.*, **94**, 6087.
 140. Zhou, J., Bimai, O., Arragain, S., Pecqueur, L. and Golinelli-Pimpaneau, B. (2022) TtuA and TudS, Two [4Fe-4S]-Dependent Enzymes Catalyzing Nonredox Sulfuration or Desulfuration Reactions. *Encycl. Inorg. Bioinorg. Chem.*, 10.1002/9781119951438.EIBC2811.
 141. Flint, D.H. and Allen, R.M. (1996) Iron-sulfur proteins with nonredox functions. *Chem. Rev.*, **96**, 2315–2334.
 142. Bennett, B., Gruer, M.J., Guest, J.R. and Thomson, A.J. (1995) Spectroscopic Characterisation of an Aconitase (AcnA) of *Escherichia coli*. *Eur. J. Biochem.*, **233**, 317–326.
 143. Castro, L., Tórtora, V., Mansilla, S. and Radi, R. (2019) Aconitases: Non-redox Iron-Sulfur Proteins Sensitive to Reactive Species. *Acc. Chem. Res.*, **52**, 2609–2619.
 144. Broderick, J.B. (2003) Iron–Sulfur Clusters in Enzyme Catalysis. *Compr. Coord. Chem. II*, **8**, 739–757.
 145. Aučynaitė, A., Rutkienė, R., Gasparavičiūtė, R., Meškys, R. and Urbonavičius, J. (2018) A gene encoding a DUF523 domain protein is involved in the conversion of 2-thiouracil into uracil. *Environ. Microbiol. Rep.*, **10**, 49–56.
 146. Zhou, J., Pecqueur, L., Aučynaitė, A., Fuchs, J., Rutkienė, R., Vaitekūnas, J., Meškys, R., Boll, M., Fontecave, M., Urbonavičius, J., *et al.* (2021) Structural Evidence for a [4Fe-5S] Intermediate in the Non-Redox Desulfuration of Thiouracil. *Angew. Chemie - Int. Ed.*, **60**, 424–431.
 147. Arragain, S., Bimai, O., Legrand, P., Caillat, S., Ravanat, J.L., Touati, N., Binet, L., Atta, M., Fontecave, M., Golinelli-Pimpaneau, B., *et al.* (2017) Nonredox thiolation in tRNA occurring via sulfur activation by a [4Fe-4S] cluster. *Proc. Natl. Acad. Sci. U. S. A.*, **114**, 7355–7360.
 148. Paysan-Lafosse, T., Blum, M., Chuguransky, S., Grego, T., Pinto, B.L., Salazar, G.A., Bileschi, M.L., Bork, P., Bridge, A., Colwell, L., *et al.* (2023) InterPro in 2022. *Nucleic Acids Res.*, **51**, D418–D427.
 149. Ma, C. and Rupert, C.S. (1995) Promoters of the *phr* gene in *Escherichia coli* K-12. *MGG Mol. Gen. Genet.*, **248**, 52–58.
 150. Traxler, M.F., Zacharia, V.M., Marquardt, S., Summers, S.M., Nguyen, H.T., Stark, S.E. and Conway, T. (2011) Discretely calibrated regulatory loops controlled by ppGpp partition gene induction across the

- ‘feast to famine’ gradient in *Escherichia coli*. *Mol. Microbiol.*, **79**, 830.
151. Hansen-Wester, I. and Hensel, M. (2001) Salmonella pathogenicity islands encoding type III secretion systems. *Microbes Infect.*, **3**, 549–559.
 152. Echarren, M.L., Figueroa, N.R., Vitor-Horen, L., Pucciarelli, M.G., García-del Portillo, F. and Soncini, F.C. (2021) Balance between bacterial extracellular matrix production and intramacrophage proliferation by a Salmonella-specific SPI-2-encoded transcription factor. *Mol. Microbiol.*, **116**, 1022–1032.
 153. Sumi, S., Mutaguchi, N., Ebuchi, T., Tsuchida, H., Yamamoto, T., Suzuki, M., Natsuka, C., Shiratori-Takano, H., Shintani, M., Nojiri, H., *et al.* (2020) Light response of *Pseudomonas putida* KT2440 mediated by class II LitR, a photosensor homolog. *J. Bacteriol.*, **202**, 1–19.
 154. Takano, H., Agari, Y., Hagiwara, K., Watanabe, R., Yamazaki, R., Beppu, T., Shinkai, A. and Ueda, K. (2014) LdrP, a cAMP receptor protein/FNR family transcriptional regulator, serves as a positive regulator for the light-inducible gene cluster in the megaplasmid of *Thermus thermophilus*. *Microbiol. (United Kingdom)*, **160**, 2650–2660.
 155. Petkevičius, V., Vaitekūnas, J., Gasparavičiūtė, R., Tauraitė, D. and Meškys, R. (2021) An efficient and regioselective biocatalytic synthesis of aromatic N-oxides by using a soluble di-iron monooxygenase PmlABCDEF produced in the *Pseudomonas* species. *Microb. Biotechnol.*, **14**, 1771–1783.
 156. Sambrook, J. and Russell, D.W. (2001) Molecular Cloning: a laboratory manual. *New York Cold Spring Harb. Lab. Press*.
 157. Huang, Y. and Zhang, L. (2017) An in vitro single-primer site-directed mutagenesis method for use in biotechnology. In *Methods in Molecular Biology*. Humana Press Inc., Vol. 1498, pp. 375–383.
 158. Gray, V.E., Hause, R.J. and Fowler, D.M. (2017) Analysis of large-scale mutagenesis data to assess the impact of single amino acid substitutions. *Genetics*, **207**, 53–61.
 159. Askitosari, T.D., Boto, S.T., Blank, L.M. and Rosenbaum, M.A. (2019) Boosting heterologous phenazine production in *pseudomonas putida* KT2440 through the exploration of the natural sequence space. *Front. Microbiol.*, **10**, 479675.
 160. Pfennig, N. (1978) *Rhodocyclus purpureus* gen. nov. and sp. nov., a ring shaped, vitamin B12 requiring member of the family Rhodospirillaceae. *Int. J. Syst. Bacteriol.*, **28**, 283–288.
 161. Tschsch, A. and Pfennig, N. (1984) Growth yield increase linked to caffeate reduction in *Acetobacterium woodii*. *Arch. Microbiol.*, **137**, 163–167.
 162. Studier, F.W. (2005) Protein production by auto-induction in high density shaking cultures. *Protein Expr. Purif.*, **41**, 207–234.
 163. Oh, M.H., Lee, J.C., Kim, J., Choi, C.H. and Han, K. (2015) Simple method for markerless gene deletion in multidrug-resistant *Acinetobacter*

- baumannii. *Appl. Environ. Microbiol.*, **81**, 3357–3368.
164. Krasauskas,R., Skerniškytė,J., Armalytė,J. and Sužiedėlienė,E. (2019) The role of *Acinetobacter baumannii* response regulator BfmR in pellicle formation and competitiveness via contact-dependent inhibition system. *BMC Microbiol.*, **19**, 1–12.
165. Choi,K.H., Kumar,A. and Schweizer,H.P. (2006) A 10-min method for preparation of highly electrocompetent *Pseudomonas aeruginosa* cells: Application for DNA fragment transfer between chromosomes and plasmid transformation. *J. Microbiol. Methods*, **64**, 391–397.
166. Bradford,M.M. (1976) A rapid and sensitive method for the quantitation of microgram quantities of protein utilizing the principle of protein-dye binding. *Anal. Biochem.*, **72**, 248–254.
167. Hennessy,D.J., Reid,G.R., Smith,F.E. and Thompson,S.L. (1984) Ferene — a new spectrophotometric reagent for iron. *Can. J. Chem.*, **62**, 721–724.
168. Catala,M., Gato,A., Tisné,C. and Barraud,P. (2020) Preparation of Yeast tRNA Sample for NMR Spectroscopy. *Bio-protocol*, **10**, 1–16.
169. Lucas,M.C., Prysycz,L.P., Medina,R., Milenkovic,I., Camacho,N., Marchand,V., Motorin,Y., Ribas de Pouplana,L. and Novoa,E.M. (2024) Quantitative analysis of tRNA abundance and modifications by nanopore RNA sequencing. *Nat. Biotechnol.*, **42**, 72–86.
170. Edwards,A.M., Addo,M.A. and Dos Santos,P.C. (2021) tRNA Modifications as a Readout of S and Fe-S Metabolism. *Methods Mol. Biol.*, **2353**, 137–154.
171. Fernández,F.J., Gómez,S., Navas-Yuste,S., López-Esteba,M. and Vega,M.C. (2017) Protein-tRNA agarose gel retardation assays for the analysis of the N6-threonylcarbamoyladenine TcdA function. *J. Vis. Exp.*, **2017**, 1–6.
172. The UniProt Consortium (2023) UniProt: the Universal Protein Knowledgebase in 2023. *Nucleic Acids Res.* 51:D523–D531 (2023). **51**, 523–531.
173. Finn,R.D., Clements,J. and Eddy,S.R. HMMER web server: interactive sequence similarity searching. 10.1093/nar/gkr367.
174. Zimmermann,L., Stephens,A., Nam,S.Z., Rau,D., Kübler,J., Lozajic,M., Gabler,F., Söding,J., Lupas,A.N. and Alva,V. (2018) A Completely Reimplemented MPI Bioinformatics Toolkit with a New HHpred Server at its Core. *J. Mol. Biol.*, **430**, 2237–2243.
175. Cock,P.J.A., Antao,T., Chang,J.T., Chapman,B.A., Cox,C.J., Dalke,A., Friedberg,I., Hamelryck,T., Kauff,F., Wilczynski,B., *et al.* (2009) Biopython: freely available Python tools for computational molecular biology and bioinformatics. *Bioinformatics*, **25**, 1422–1423.
176. Sokal,R.R. and Michener,C.D. (1958) A statistical method for evaluating systematic relationships. **38**, 1409–1438.
177. Huerta-Cepas,J., Serra,F. and Bork,P. (2016) ETE 3: Reconstruction, Analysis, and Visualization of Phylogenomic Data. *Mol. Biol. Evol.*, **33**,

- 1635–1638.
178. Bryant,P., Pozzati,G. and Elofsson,A. (2022) Improved prediction of protein-protein interactions using AlphaFold2. *Nat. Commun.*, **13**, 1–11.
179. Du,Z., Su,H., Wang,W., Ye,L., Wei,H., Peng,Z., Anishchenko,I., Baker,D. and Yang,J. (2021) The trRosetta server for fast and accurate protein structure prediction. *Nat. Protoc.*, **16**, 5634–5651.
180. Steinegger,M. and Söding,J. (2017) MMseqs2 enables sensitive protein sequence searching for the analysis of massive data sets. *Nat. Biotechnol.*, **35**, 1026–1028.
181. Remmert,M., Biegert,A., Hauser,A. and Söding,J. (2012) HHblits: Lightning-fast iterative protein sequence searching by HMM-HMM alignment. *Nat. Methods*, **9**, 173–175.
182. Lee,T.S., Allen,B.K., Giese,T.J., Guo,Z., Li,P., Lin,C., Dwight McGee,T., Pearlman,D.A., Radak,B.K., Tao,Y., *et al.* (2020) Alchemical binding free energy calculations in AMBER20: Advances and best practices for drug discovery. *J. Chem. Inf. Model.*, **60**, 5595–5623.
183. Maier,J.A., Martinez,C., Kasavajhala,K., Wickstrom,L., Hauser,K.E. and Simmerling,C. (2015) ff14SB: Improving the Accuracy of Protein Side Chain and Backbone Parameters from ff99SB. *J. Chem. Theory Comput.*, **11**.
184. Tendwa,M.B., Chebon-bore,L., Lobb,K., Musyoka,T.M. and Tastan Bishop,Ö. (2021) Force field parameters for Fe^{2+} 4s²-4 clusters of dihydropyrimidine dehydrogenase, the 5-fluorouracil cancer drug deactivation protein: A step towards in silico pharmacogenomics studies. *Molecules*, **26**.
185. Zgarbová,M., Otyepka,M., Šponer,J., Mládek,A., Banáš,P., Cheatham,T.E. and Jurečka,P. (2011) Refinement of the Cornell et al. Nucleic acids force field based on reference quantum chemical calculations of glycosidic torsion profiles. *J. Chem. Theory Comput.*, **7**, 2886–2902.
186. Pérez,A., Marchán,I., Svozil,D., Sponer,J., Cheatham,T.E., Loughton,C.A. and Orozco,M. (2007) Refinement of the AMBER force field for nucleic acids: Improving the description of α/γ conformers. *Biophys. J.*, **92**, 3817–3829.
187. Aduri,R., Psciuk,B.T., Saro,P., Taniga,H., Schlegel,H.B. and SantaLucia,J. (2007) AMBER force field parameters for the naturally occurring modified nucleosides in RNA. *J. Chem. Theory Comput.*, **3**, 1464–1475.
188. Yan,Y., Tao,H., He,J. and Huang,S.Y. (2020) The HDock server for integrated protein–protein docking. *Nat. Protoc.*, **15**, 1829–1852.
189. Benson,D.A., Cavanaugh,M., Clark,K., Karsch-Mizrachi,I., Lipman,D.J., Ostell,J. and Sayers,E.W. (2017) GenBank. *Nucleic Acids Res.*, **45**, D37–D42.
190. Isono,K. (1991) Current progress on nucleoside antibiotics. *Pharmacol.*

- Ther.*, **52**, 269–286.
191. Gibney,B.R., Mulholland,S.E., Rabanal,F. and Dutton,P.L. (1996) Ferredoxin and ferredoxin-heme maquettes. *Proc. Natl. Acad. Sci. U. S. A.*, **93**, 15041–15046.
 192. Pettersen,E.F., Goddard,T.D., Huang,C.C., Meng,E.C., Couch,G.S., Croll,T.I., Morris,J.H. and Ferrin,T.E. (2021) UCSF ChimeraX: Structure visualization for researchers, educators, and developers. *Protein Sci.*, **30**, 70–82.
 193. Bommiseti,P. and Bandarian,V. (2022) Site-Specific Profiling of 4-Thiouridine Across Transfer RNA Genes in Escherichia coli. *ACS Omega*, **7**, 4011–4025.
 194. Tremblay,B.J.M., Lobb,B. and Doxey,A.C. (2021) PhyloCorrelate: inferring bacterial gene-gene functional associations through large-scale phylogenetic profiling. *Bioinformatics*, **37**, 17–22.
 195. Hori,H., Kawamura,T., Awai,T., Ochi,A., Yamagami,R., Tomikawa,C. and Hirata,A. (2018) Transfer rna modification enzymes from thermophiles and their modified nucleosides in trna. *Microorganisms*, **6**, 1–46.
 196. Lu,Z. and Imlay,J.A. (2019) A conserved motif liganding the [4Fe–4S] cluster in [4Fe–4S] fumarases prevents irreversible inactivation of the enzyme during hydrogen peroxide stress. *Redox Biol.*, **26**.
 197. Liu,L. and Huang,M. (2015) Essential role of the iron-sulfur cluster binding domain of the primase regulatory subunit Pri2 in DNA replication initiation. *Protein Cell*, **6**, 194–210.
 198. Hoang,C. and Ferré-D’Amaré,A.R. (2001) Cocrystal structure of a tRNA Ψ55 pseudouridine synthase: Nucleotide flipping by an RNA-modifying enzyme. *Cell*, **107**, 929–939.
 199. Söding,J., Biegert,A. and Lupas,A.N. (2005) The HHpred interactive server for protein homology detection and structure prediction. *Nucleic Acids Res.*, **33**, 244–248.
 200. Holm,L., Kääriäinen,S., Rosenström,P. and Schenkel,A. (2008) Searching protein structure databases with DaliLite v.3. *Bioinformatics*, **24**, 2780–2781.
 201. Mackie,G.A. (2012) RNase E: at the interface of bacterial RNA processing and decay. *Nat. Rev. Microbiol.* 2013 *111*, **11**, 45–57.
 202. Zhong,J., Xiao,C., Gu,W., Du,G., Sun,X., He,Q.Y. and Zhang,G. (2015) Transfer RNAs Mediate the Rapid Adaptation of Escherichia coli to Oxidative Stress. *PLOS Genet.*, **11**, e1005302.
 203. BENZ,R., SCHMID,A., MAIER,C. and BREMER,E. (1988) Characterization of the nucleoside-binding site inside the Tsx channel of Escherichia coli outer membrane Reconstitution experiments with lipid bilayer membranes. *Eur. J. Biochem.*, **176**, 699–705.
 204. Patching,S.G., Baldwin,S.A., Baldwin,A.D., Young,J.D., Gallagher,M.P., Henderson,P.J.F. and Herbert,R.B. (2005) The nucleoside transport proteins, NupC and NupG, from Escherichia coli:

- specific structural motifs necessary for the binding of ligands. *Org. Biomol. Chem.*, **3**, 462–470.
205. Maruyama,T., Sumi,S., Kobayashi,M., Ebuchi,T., Kanasaki,Y., Yoshikawa,H., Ueda,K. and Takano,H. (2022) Class II LitR serves as an effector of “short” LOV-type blue-light photoreceptor in *Pseudomonas mendocina*. *Sci. Rep.*, **12**, 1–16.
 206. Carre,D.S., Thomas,G. and Favre,A. (1974) Conformation and functioning of tRNAs: cross-linked tRNAs as substrate for tRNA nucleotidyl-transferase and aminoacyl synthetases. *Biochimie*, **56**, 1089–1101.
 207. Blanchetot,A., Hajnsdorf,E. and Favre,A. (1984) Metabolism of tRNA in near-ultraviolet-illuminated *Escherichia coli* The tRNA repair hypothesis. *Eur. J. Biochem.*, **139**, 547–552.
 208. Brown,A., Fernández,I.S., Gordiyenko,Y. and Ramakrishnan,V. (2016) Ribosome-dependent activation of stringent control. *Nature*, **534**, 277–280.
 209. Probst-Rüd,S., Nyangaresi,P.O., Adeyeye,A.A., Ackermann,M., Beck,S.E. and McNeill,K. (2024) Synergistic effect of UV-A and UV-C light is traced to UV-induced damage of the transfer RNA. *Water Res.*, **252**, 121189.
 210. Tulin,G., Figueroa,N.R., Checa,S.K. and Soncini,F.C. (2024) The multifarious MerR family of transcriptional regulators. *Mol. Microbiol.*, **121**, 230–242.

APPENDICES

Appendix 1. Oligonucleotide primers used in this study.

Primer name	Sequence (>3')	Purpose
pLATE11_empty_FW	TGACTTCCCATCTCCGGTTT	Amplification of vector backbone for empty vector generation.
pLATE11_empty_RV	AGTTATATCTCCTCTCGATTAAATGTTA	
TudS_A_11_31_FW	AGAAGGAGATATAACTATGAAGGAAAAATCATAGTCAGCG	Amplification of tudS_A gene for cloning into pLATE11
TudS_A_11_52_RV	GGAGATGGGAAGTCATTATCAGGAGCCCGCTGC	
TudS_PP_11_31_FW	AGAAGGAGATATAACTATGCAGAAAATTCTGGTGAGTCGCTGC	Amplification of tudS_PP gene for cloning into pLATE11 and pLATE31 vectors
TudS_PP_11_52_RV	GGAGATGGGAAGTCATTAGCCCGCTCGATTGTCC	
TudS_PP_31_RV	GTGGTGGTGATGGTATGGCCGCCCTCGATTGTCC	
TudS_PU_11_31_FW	AGAAGGAGATATAACTATGCAGAAAATTCTGGTAAGCCGCTGTC	Amplification of tudS_PU gene for cloning into pLATE11
TudS_PU_11_52_RV	GGAGATGGGAAGTCATTAGCTCAGTTTTCCAGGGCTG	
TudS_KT_11_31_FW	AGAAGGAGATATAACTATGCACGACCCCTCCGCC	Amplification of tudS_KT gene for cloning into pLATE11
TudS_KT_11_52_RV	GGAGATGGGAAGTCATCAAGCAGATATTAGCCAAAGC	
KT2440_pyrF_1_FW	TGGCCTACCGGAGGCCAATGGGCC	Amplification of 5' flanking region of pyrF target gene in P. putida KT2440
KT2440_pyrF_2_RV	GGCATCGGTGGTTCGGCACAGGCCCGCAGGCGACATGGGCAGGGTCTC	
KT2440_pyrF_3_FW	GGGCGCTGTCGCAACCACCGATGCC	Amplification of 3' flanking region of pyrF target gene in P. putida KT2440
KT2440_pyrF_4_RV	GGCCGCCCTTTAGTGAGGGTTAATTCCTCGATGCCGTGCTGACGCGCATC	
KT2440_tudS_KT_1_FW	CGCACTTTCTGCCTGCCACCTGGT	Amplification of 5' flanking region of tudS_KT target gene in P. putida KT2440
KT2440_tudS_KT_2_RV	CACCCGCGAAAGGGCCGCACAGGTTCAATCAGAACGGGTTCATTGCCACG	
KT2440_tudS_KT_3_FW	ACCTGTGCCGGCCCTTTCGCGGGTG	Amplification of 3' flanking region of tudS_KT target gene in P. putida KT2440
KT2440_tudS_KT_RV	GGCCGCCCTTTAGTGAGGGTTAATTGAGCTGATCGACGAAATCGCCGACC	
KT2440_rudS_KT_1_FW	TACACCAATGCAAGGCTGCTTCGTG	Amplification of 5' flanking region of rudS_KT target gene in P. putida KT2440
KT2440_rudS_KT_2_RV	TGGGCAGCAAGTCCTCAGACCGCATGGCTGCCTCCGAAATAAACCTGTA	
KT2440_rudS_KT_3_FW	ATGCGGTCTGAGGACTTGCTGCCCA	Amplification of 3' flanking region of rudS_KT target gene in P. putida KT2440
KT2440_rudS_KT_4_RV	GGCCGCCCTTTAGTGAGGGTTAATTAGCTGTTGCTGTTACACGCGGG	
KT2440_thil_1_FW	CGCGACGCGATGGTCACGTGGTCT	Amplification of 5' flanking region of thil target gene in P. putida KT2440
KT2440_thil_2_RV	ACTGCCCCATACAGCCCCGGGTCTGGTTAACAGCGCGCAGGGCTG	
KT2440_thil_3_FW	GACGCCGGGCTGTATGGCGGCAGT	Amplification of 3' flanking region of thil target gene in P. putida KT2440
KT2440_thil_4_RV	GGCCGCCCTTTAGTGAGGGTTAATTAGCTGTTGCTGTTGCGGTGGCACCGGAGG	
FRT-PGK-gb2-neo-FRT_RV	TAATACGACTCACTATAGGGCTCGA	Amplification of kanamycin resistance cassette from FRT-PGK-gb2-neo-FRT PCR-template (Gene Bridges, Germany)
FRT-PGK-gb2-neo-FRT_FW	AATTAACCTCACTAAAGGGCGGCC	
pLATE_XbaI_FW	CCCCTCTAGAAATAATTTTG	Amplification of RBS, inserted gene and introduction of XbaI and NheI restriction sites using pLATE vectors as a template
pLATE_NheI_RV	AGTAGCTAGCCATGATTACGCTGCATG	
RudS_KT_52_FW	GGTTGGGAATTGCAACACGACCCTTCGCCCCAC	Amplification of rudS_KT gene for cloning into pLATE11 and pLATE52 vectors
RudS_KT_11_FW	AGAAGGAGATATAACTATGCACGACCCCTCCGCC	
RudS_KT_11_52_RV	GGAGATGGGAAGTCATCAGACCGCATTGCGCAAG	

RudS_ST_11_31_FW	AGAAGGAGATATAACTATGAATAACAAACCCGTAGTCGGC	Amplification of <i>rudS_ST</i> gene for cloning into pLATE11 and pLATE52 vectors
RudS_ST_11_52_RV	GGAGATGGGAAGTCATTAGGTGATGGCTAAGCGCAG	
RudS_ST_52_FW	GTTTGGGAATTGCAAAATAACAAACCCGTAGTCGGC	
RudS_PP_11_31_FW	AGAAGGAGATATAACTATGCGCTCACCAGAAACCATCACC	Amplification of <i>rudS_PP</i> gene for cloning into pLATE11 and pLATE52 vectors
RudS_PP_11_52_RV	GGAGATGGGAAGTCATTATAGGGCGTTACGCAAGCTG	
RudS_PP_52_FW	GTTTGGGAATTGCAACGCTCACCAGAAACCATCACC	
RudS_TT_11_31_FW	AGAAGGAGATATAACTATGAGCCAGGGGCGTGG	Amplification of <i>rudS_TT</i> gene for cloning into pLATE11 and pLATE52 vectors
RudS_TT_52_FW	GTTTGGGAATTGCAAAAGCCAGGGGCGTGG	
RudS_TT_11_52_RV	GGAGATGGGAAGTCATTAGGCCCGGGGACGTG	
RudS_PU_11_31_FW	AGAAGGAGATATAACTATGCTCCCTCCCTGCCAAAC	Amplification of <i>rudS_PU</i> gene for cloning into pLATE11 and pLATE52 vectors
RudS_PU_11_52_RV	GGAGATGGGAAGTCATTAGATGGCGTTTCGCAAGCTG	
RudS_PU_52_FW	GTTTGGGAATTGCAACTCCCTCCCTGCCAAAC	
RudS_vir_11_52_RV	GGAGATGGGAAGTCATTAGTTCACCAAGAGTCTTAGAGCCAGTTCATC	Amplification of <i>rudS_vir</i> gene for cloning into pLATE11 and pLATE52 vectors
RudS_vir_11_31_FW	AGAAGGAGATATAACTATGATAAAAAACCTGCTGTTGGGATCAGTGG	
RudS_vir_52_FW	GTTTGGGAATTGCAAAATAAAAAACCTGCTGTTGGGATCAGTGG	
RudS_ST_C12A	AGTCGGCATTAGCGGAGCTGACTGGCGCC	Site directed mutagenesis of conservative cysteines using pLATE11 or pLATE52 vectors with insert as a template.
RudS_ST_C44A	CCTACAAACCGATCGCCCCGGAGGTGGCGA	
RudS_ST_C110A	TGTGTGTGCAAAATCGCCAGTCCCGAATGGAGCG	
RudS_TT_C16A	TGTGTTGAGCGCCCGCCTGGGGTTCGCC	
RudS_TT_C47A	CTTCGTCCCGTCGCCCGGAGGTGGAG	
RudS_TT_C111A	CCGCTCCCTCCCGCCCTGAAGGAC	
RudS_KT_C17A	CGCCATCAGCGCCCGCTGACCGGGCAC	
RudS_KT_C49A	GACTGGCTACCCGTGGCTCCGGAAGTGGCAAT	
RudS_KT_C114A	TCTTCATGCAGAAGTCACCTTCAGCGGCCCTGGAACG	
RudS_PP_C18A	TGGGCATCAGTGGCGCTTACTGGGTCCG	
RudS_PP_C50A	TTTCGCCCCGTGGCCCCGAAGTAGGG	
RudS_PP_C115A	CAGTCCCCGTCCGCGCCTGCACCG	
RudS_PU_C15A	CGCCATCAGCGCCCGCTGATGGGCGCA	
RudS_PU_C47A	TTTCGTGCCGTGCCCCGGAAGTCGCG	
RudS_PU_C112A	GAAATCGCGTCCGCGGACTGGAGCGG	
RudS_vir_C12A	TCGTTGGGATCAGTGGTCTTGGCCGGTCTTCTG	
RudS_vir_C44A	TGGAATGGGTAACATTCAAACAGTAGCTCCGGAATGGCTA	
RudS_vir_C110A	GTGCAAATCTCCTAGCGCTGGTATGGAACGCGTGC	
RudS_KT_R24M	ACCGGGCACAGCGTGATGACAACGCGGCCAC	
RudS_KT_Y25A	GTGGCCCGCTTGGCGCGCACGCTGTGC	
RudS_KT_Y25F	GGCCGCGCTTGAAGCGCACGCTG	
RudS_KT_Y25M	CTTGTGGCCGCGTTCATGCGCACGCTGTGCC	
RudS_KT_N26M	GTGGCCGCCATGTAGCGCACGCTGTGC	
RudS_KT_G27M	GGAGGCCTTGTGGCCATGTTGTAGCGCACGCT	
RudS_KT_H29M	CAGGTGCGAGGCCTTCATGCCGCGTGTAGCG	
RudS_KT_K30M	CGGAGGCCATGTGGCCGCGTGT	
RudS_KT_D33M	GCTGTTTACGGCACAGCATGGAGGCCTTGTGGCCG	
RudS_KT_R36M	AAGGCCTCGACCTGTGCATGAAACAGCTGGAACAGCAC	
RudS_KT_K37M	GTGCTGTTCCAGTGCATACGGCACAGTTCGGAG	
RudS_KT_E51M	CCAAGCCGATTGCCACCATCGGACACACGGGTAGC	
RudS_KT_R60M	GGCTTGGGTGTCCCGATGGACCCGATTCCGCTG	
RudS_KT_D61M	GACCAGGCGAATCGGCATGCGCGGGACACCCAA	
RudS_KT_R64M	CCCGCGCACCCGATTATGCTGGTGGCAACCC	
RudS_KT_K110M	GGCCGATGAAGGTGACATGTCATGAAGATGTAG	
RudS_KT_S111M	CGTTCAGGCGCATGAAGGCATCTTCGATGAAGATGTAGC	
RudS_KT_S113M	CGTTCAGGCGCACATAGGTGACTTCTGCATGAAGATGTAGCC	
RudS_KT_E117M	CCTGATAAACCTTTACCCGCATCAGGCCGATGAAGGTGAC	
RudS_KT_R118M	CCTGATAAACCTTTACCATTTCCAGGCGCATGAAGGTGAC	
RudS_KT_K120M	TCCTGATAAACCATACCCGTTCCAGGCCG	
RudS_KT_Y122M	GGCCGTTGCTCTGCATAACCTTTACCCGTTCCAGGCCG	
RudS_KT_H127M	TTATCAGGACAACGGCATGCCGCGCTGCATGGTG	
RudS_KT_H131M	CCACCCGCGCTGATGGGTGGCCGTGGG	
RudS_KT_E152M	GCAGGCGGCCCTTCCATTTCTACTGGCAGTCCGGG	
RudS_KT_R155M	CCAGTAGAAGAAGAAGGCATGCTGCATGACCCGTGCTG	
RudS_KT_H157M	GAAGAAGGCGCCTGATGGACCTGTGCTGCGC	
RudS_KT_N202M	CGATAGGCCTGGGGATTCATGGCCATCAGCAAATAC	
RudS_KT_N203M	GATAGGCCTGGGGCATGTGGCCATCAGCAAATCTTGA	
RudS_KT_Q205M	GATGGCCAACAATCCCATGGCTATCGCACCCCTC	
RudS_KT_R240M	GCAGGCCCTGCGCATGTGCGCCAGCCGCG	

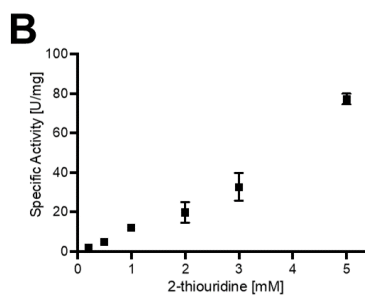
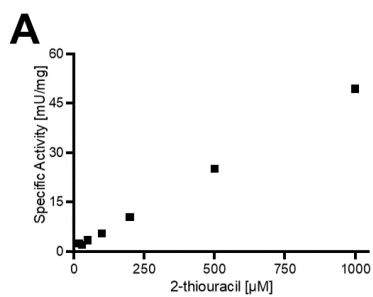
RudS_KT_C241M	GCCGCGGTGGCCATGCGGCGCAGGGC	
RudS_KT_S243M	GTGCCGCGCATGGCCGACGGCGCA	
RudS_KT_R244M	CGCGCTGCGCCAGCATGGGCACCCACAGTAAC	
RudS_KT_T246M	GCCAGCCGCGCATGCACAGTAACGTGC	

Appendix 2. Plasmid vectors used in this study.

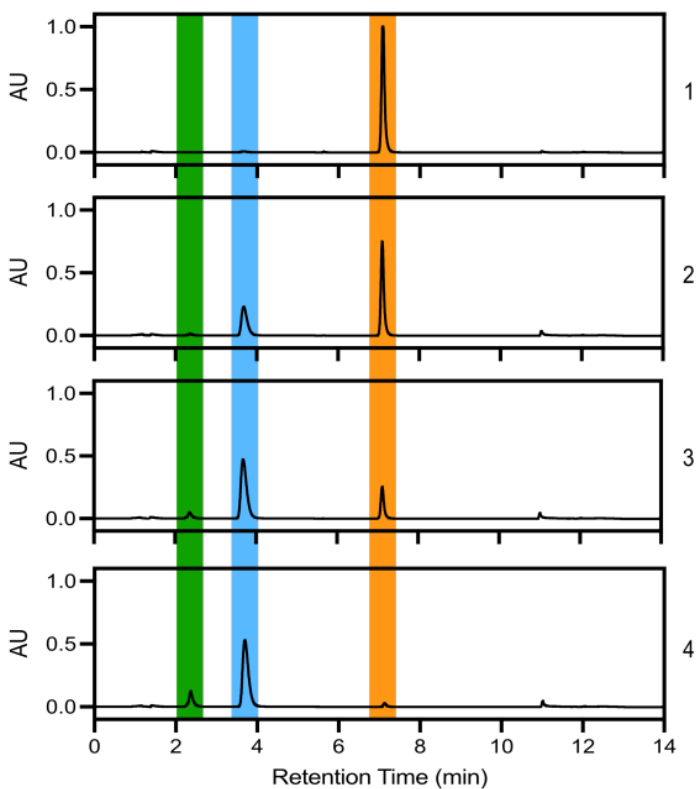
Plasmid vector	Comments	Source
pLATE11-	Empty vector constructed by amplification of backbone and blunt-end ligation.	This study
pET21b-DUF523Vcz	TudS_A encoding vector used as a template	(146)
pLATE11-TudS_A	TudS_A encoding expression vector	This study
pLATE11-TudS_PP	TudS_PP encoding expression vector	This study
pLATE11-TudS_PU	TudS_PU encoding expression vector	This study
pLATE11-TudS_KT	TudS_KT encoding expression vector	This study
pUC19_sacB	Suicide vector used for <i>P. putida</i> mutagenesis	(164)
pUC19_SacB_tudS_KT_mut	Suicide mutagenesis vector coding for tudS_KT flanking region and a kanamycin cassette. Upstream region was amplified using KT2440_tudS_KT_1_FW and KT2440_tudS_KT_2_RV primers, downstream region was amplified using KT2440_tudS_KT_3_FW and KT2440_tudS_KT_4_RV primers, kanamycin cassette was amplified using FRT-PGK-gb2-neo-FRT_RV and FRT-PGK-gb2-neo-FRT_FW primers.	This study
pUC19_SacB_pyrF_mut	Suicide mutagenesis vector coding for pyrF flanking region and a kanamycin cassette. Upstream region was amplified using KT2440_pyrF_1_FW and KT2440_pyrF_2_RV primers, downstream region was amplified using KT2440_pyrF_3_FW and KT2440_pyrF_4_RV primers, kanamycin cassette was amplified using FRT-PGK-gb2-neo-FRT_RV and FRT-PGK-gb2-neo-FRT_FW primers.	This study
pUC19_SacB_rudS_KT_mut	Suicide mutagenesis vector coding for rudS_KT flanking region and a kanamycin cassette. Upstream region was amplified using KT2440_rudS_KT_1_FW and KT2440_rudS_KT_2_RV primers, downstream region was amplified using KT2440_rudS_KT_3_FW and KT2440_rudS_KT_4_RV primers, kanamycin cassette was amplified using FRT-PGK-gb2-neo-FRT_RV and FRT-PGK-gb2-neo-FRT_FW primers.	This study
pUC19_SacB_thil_mut	Suicide mutagenesis vector coding for thil flanking region and a kanamycin cassette. Upstream region was amplified using KT2440_thil_1_FW and KT2440_thil_2_RV primers, downstream region was amplified using KT2440_thil_3_FW and KT2440_thil_4_RV primers, kanamycin cassette was amplified using FRT-PGK-gb2-neo-FRT_RV and FRT-PGK-gb2-neo-FRT_FW primers.	This study
pUC19	Cloning vector	Thermo Fisher Scientific, USA
pUC19_ΔtudS_KT_seq	Vector used for the sequencing of the tudS knockout site surrounding region. Insert was amplified using KT2440_tudS_KT_1_FW and KT2440_tudS_KT_4_RV primers.	This study
pUC19_ΔpyrF_seq	Vector used for the sequencing of the pyrF knockout site surrounding region. Insert was amplified using KT2440_pyrF_1_FW and KT2440_pyrF_4_RV primers.	This study
pUC19_ΔrudS_KT_seq	Vector used for the sequencing of the thil knockout site surrounding region. Insert was amplified using KT2440_rudS_KT_1_FW and KT2440_rudS_KT_4_RV primers.	This study
pUC19_Δthil_seq	Vector used for the sequencing of the thil knockout site surrounding region. Insert was amplified using KT2440_thil_1_FW and KT2440_thil_4_RV primers.	This study
pLATE31-TudS_PP	C-terminally his-tagged TudS_PP encoding expression vector	This study
pJNN	<i>P. putida</i> KT2440 expression vector	(159)
pJNN-tudS_KT	Gene and RBS site was amplified using pLATE_XbaI_FW and pLATE_NheI_RV primers using pLATE11-tudS_KT as a template and cloned through <i>XbaI</i> and <i>NheI</i> restriction sites.	This study
pJNN-rudS_KT	Gene and RBS site was amplified using pLATE_XbaI_FW and pLATE_NheI_RV primers using pLATE11-rudS_KT as a template and cloned through <i>XbaI</i> and <i>NheI</i> restriction sites.	This study
pBR322-RudS_vir	Synthetic vector encoding viral RudS	Synthesized by Thermo Fisher Scientific, USA
pLATE11-RudS_KT		
pLATE11-RudS_ST	RudS encoding expression vectors	This study

pLATE11-RudS_PP				
pLATE11-RudS_TT				
pLATE11-RudS_vir				
pLATE11-RudS_PU				
pLATE52-RudS_KT	RudS with N-terminal 6xHis-tag encoding expression vectors	This study		
pLATE52-RudS_ST				
pLATE52-RudS_PP				
pLATE52-RudS_TT				
pLATE52-RudS_vir				
pLATE52-RudS_PU				
pLATE11-RudS_KT_C114A				
pLATE11-RudS_KT_C49A				
pLATE11-RudS_KT_C17A	RudS with conservative cysteine substitution encoding expression vectors	This study		
pLATE11-RudS_ST_C12A				
pLATE11-RudS_ST_C44A				
pLATE11-RudS_ST_C110A				
pLATE11-RudS_PP_C18A				
pLATE11-RudS_PP_C50A				
pLATE11-RudS_PP_C115A				
pLATE11-RudS_TT_C16A				
pLATE11-RudS_TT_C47A				
pLATE11-RudS_TT_C111A				
pLATE11-RudS_vir_C12A				
pLATE11-RudS_vir_C44A				
pLATE11-RudS_vir_C110A				
pLATE11-RudS_PU_C15A				
pLATE11-RudS_PU_C47A				
pLATE11-RudS_PU_C112A				
pLATE52-RudS_KT_C114A			RudS_KT with conservative cysteine substitution and N-terminal 6xHis-tag encoding expression vectors	This study
pLATE52-RudS_KT_C49A				
pLATE52-RudS_KT_C17A				
pLATE11-RudS_KT_R24M	RudS_KT with amino acid predicted to participate in substrate binding and/or catalysis substitution and encoding expression vectors	This study		
pLATE11-RudS_KT_Y25M				
pLATE11-RudS_KT_Y25A				
pLATE11-RudS_KT_Y25F				
pLATE11-RudS_KT_N26M				
pLATE11-RudS_KT_G27M				
pLATE11-RudS_KT_H29M				
pLATE11-RudS_KT_K30M				
pLATE11-RudS_KT_D33M				
pLATE11-RudS_KT_R36M				
pLATE11-RudS_KT_K37M				
pLATE11-RudS_KT_E51M				
pLATE11-RudS_KT_R60M				
pLATE11-RudS_KT_D61M				
pLATE11-RudS_KT_R64M				
pLATE11-RudS_KT_K110M				
pLATE11-RudS_KT_S111M				
pLATE11-RudS_KT_S113M				
pLATE11-RudS_KT_E117M				
pLATE11-RudS_KT_R118M				
pLATE11-RudS_KT_K120M				
pLATE11-RudS_KT_Y122M				
pLATE11-RudS_KT_H127M				
pLATE11-RudS_KT_H131M				
pLATE11-RudS_KT_E152M				
pLATE11-RudS_KT_R155M				
pLATE11-RudS_KT_H157M				
pLATE11-RudS_KT_N202M				
pLATE11-RudS_KT_N203M				
pLATE11-RudS_KT_Q205M				
pLATE11-RudS_KT_R240M				
pLATE11-RudS_KT_C241M				
pLATE11-RudS_KT_S243M				
pLATE11-RudS_KT_R244M				
pLATE11-RudS_KT_T246M				
pLATE52-RudS_KT_R24M	This study			
pLATE52-RudS_KT_N26M				

pLATE52-RudS_KT_G27M	RudS with amino acid predicted to participate in substrate binding and/or catalysis substitution and N-terminal 6xHis-tag encoding expression vectors
pLATE52-RudS_KT_H29M	
pLATE52-RudS_KT_K30M	
pLATE52-RudS_KT_E51M	
pLATE52-RudS_KT_R60M	
pLATE52-RudS_KT_R64M	
pLATE52-RudS_KT_K110M	
pLATE52-RudS_KT_S111M	
pLATE52-RudS_KT_S113M	
pLATE52-RudS_KT_R118M	
pLATE52-RudS_KT_K120M	
pLATE52-RudS_KT_Y122M	
pLATE52-RudS_KT_E152M	
pLATE52-RudS_KT_R155M	
pLATE52-RudS_KT_H157M	
pLATE52-RudS_KT_N202M	
pLATE52-RudS_KT_N203M	
pLATE52-RudS_KT_R240M	
pLATE52-RudS_KT_C241M	
pLATE52-RudS_KT_S243M	
pLATE52-RudS_KT_R244M	
pLATE52-RudS_KT_T246M	



Appendix 3. Enzymatic activity data obtained for the conversion of 2-thiouracil and 2-thiouridine by TudS_A. **A:** TudS_A + 2-thiouracil (n=3, SE); **B:** TudS_A, 2-thiouridine (n=3, SE).



Appendix 4. UPLC elution diagrams for the conversion of 2,4-dithiouracil by TudS_A. TudS (50 μ M) was incubated with 500 μ M 2,4-dithiouracil for 0 min (lane 1), 1 min (lane 2), 5 min (lane 3), and 15 min (lane 4) at 30 $^{\circ}$ C anaerobically and the substrates/products were analyzed by UPLC. 2,4-thiouracil (orange) is first converted to 2-thiouracil (blue) and then to uracil (green) at a much lower rate. AU = arbitrary units for the diode array detection.

Appendix 5. Detailed description of molecular dynamics simulations.

The systems underwent minimization, heating to 300 K, and equilibration. Constant temperature and volume production runs (NTV) were conducted at 300 K using Langevin dynamics thermostat. For the initial simulations of the holoenzyme and complex, during heating and the first equilibration run of 200 ns, Cartesian positional restraints of 1 kcal/mol/ \AA^2 on backbone atoms of amino acids within ~ 7 \AA around the iron-sulfur cluster were applied. These restraints were relaxed during the next 200 ns, and subsequent molecular dynamics simulations involved only distance restraints as specified. The same conditions were used for tRNA simulations.

The top HADDOCK complex underwent a series of short molecular dynamics simulations, with 1 kcal/mol/ \AA^2 restraints on protein backbone atoms and 5 kcal/mol restraints on the distance between the sulfur atom in the

thiouridine moiety and the relevant iron atom. The distance restraint was incrementally reduced by one angstrom in each subsequent MD run until reaching a distance of 2 Å. The resultant complex then underwent 10 iterations of MD simulated annealing runs, each comprising 4 ns at temperatures ramping from 300 K to 400 K, 4 ns at 400 K, 4 ns cooling from 400 K to 250 K, 4 ns heating back to 350 K, 4 ns cooling back to 300 K, and finally 4 ns at 300 K, with restraints of 1 kcal/mol on protein backbone atoms and 5 kcal/mol/ Å² on the distance between the sulfur atom in the thiouridine moiety and the relevant iron atom. The final complex then underwent two different MD simulations, with the first one maintaining only 5 kcal/mol/ Å² restraint on the distance between the sulfur atom in the thiouridine moiety and the relevant iron atom, and the second one with an additional 4 distance restraints on specific Arg60, Glu51, Ser111, Ser113 atoms.

The best HDOCK model was used as a starting point in attempts to obtain a better model of the enzyme-substrate complex. Short molecular dynamics simulations with incrementally decreasing distance constraints for thiouridine sulfur and the relevant iron ion in the iron-sulfur cluster were conducted to bring the substrate and enzyme closer together. The obtained structures were then relaxed in 10 simulated annealing runs with previously described distance constraints and weak positional constraints on catalytic domain atoms within 7 angstroms around the iron-sulfur cluster. The resultant complex underwent initially restrained and restraint relaxation MD simulations as described in Methods and Materials, followed by a 640 ns simulation with the following 5 kcal/mol/ Å² distance constraints: Arg60 epsilon NH – Glu51 side chain carboxy O2; Glu51 side chain carboxy O1 – Ser113 side chain hydroxy group H; Ser113 side chain hydroxy group O – Ser111 side chain hydroxy group O, and thiouridine S – iron-sulfur cluster relevant iron ion. The last frame of this restrained simulation was used as an initial structure for two 260 ns simulations, where structure 1 retained the described above restraints, and structure 2 had only thiouridine S – iron-sulfur cluster restraint.

ACKNOWLEDGEMENTS

I would like to express my sincerest gratitude to my supervisors and scientific advisors, Prof. Dr. Rolandas Meškys, the head of the Department of Molecular Microbiology, and Dr. Agota Aučynaitė, who were always willing to help and guided me through this journey of doctoral studies.

My gratitude extends to my office colleagues, with whom I spent most of my time when not working in the lab. Dr. Agota Aučynaitė, a great supervisor and an incredible person, brought so much laughter into my days that I sometimes had to leave the office just to catch my breath. Viktorija Preitakaitė, a fantastic person and my office and lab partner, made every moment enjoyable. I'll let you pick the next song we will sing in the office in the morning until someone comes to shut us up. And Dr. Vytautas Petkevičius, who patiently and sincerely responded my countless spontaneous "Hey, can I ask you a question?" moments.

Additionally, I would like to thank Roberta Statkevičiūtė for our great and interesting discussions, whether work-related or existential and, of course, for the memorable table tennis matches. I'm also grateful to Justas Stonkus for helping generate ideas and solve problems, and to bachelor student Deimantė Povilaitytė, whose dedication and hard work significantly contributed to achieving great results. My gratitude also extends to all my fellow PhD students and every member of the Department of Molecular Microbiology and Biotechnology with whom I felt not alone throughout this journey.

I would also like to thank my collaborators from the University of Freiburg, Jonathan Fuchs and Prof. Dr. Matthias Boll, for allowing me to visit their lab and explore the fascinating world of anaerobic research. Special thanks to Dr. Audrius Laurynėnas for his invaluable contributions in bioinformatics, which helped me craft my thesis into a compelling story. I am also grateful to my thesis reviewers, Dr. Dukas Jurėnas and Dr. Patrick Pausch, whose insightful remarks allowed me to improve my thesis.

Finally, I want to express my heartfelt gratitude to my entire family especially my parents, who have always supported me and my choices; my sister, with whom I spent many hours in the library, sharing both study time and laughter; and my grandparents, who always encouraged me and made me feel proud of my achievements. And to all my friends who have been so supportive throughout this journey: Yes, I can finally answer that question I have been asked so many times, it should all be done by the February 6th, 2025.

LIST OF PUBLICATIONS

Fuchs, J.*, **Jamontas, R.***, Hoock, M. H., Oltmanns, J., Golinelli-Pimpaneau, B., Schünemann, V., Pierik, A. J., Meškys, R., Aučynaitė, A. and Boll, M. (2023) TudS desulfidases recycle 4-thiouridine-5'-monophosphate at a catalytic [4Fe-4S] cluster. *Commun. Biol.*, **6(1)**, 1092.

* These authors contributed equally

Jamontas, R., Laurynėnas, A., Povilaitytė, D., Meškys, R. and Aučynaitė, A. (2024) RudS: bacterial desulfidase responsible for tRNA 4-thiouridine demodification. *Nucleic Acids Res.*, **52(17)**, 10543-10562.

CONFERENCE PRESENTATIONS

Poster presentations:

Jamontas, R., Aučynaitė, A., Meškys, R. Endogenously expressed bacterial DUF523 proteins utilize 4-thiouracil and 4-thiouridine in vivo. 47th FEBS Congress – „Together in bioscience for a better future“, July 8-12, 2023, Tours, France.

Jamontas, R., Fuchs, J., Aučynaitė, A., Boll, M., Meškys, R. Bacteria recycle sulfur-modified nucleotides. 5th Congress of Baltic Microbiologists, October 11-13, 2023, Vilnius, Lithuania.

Jamontas, R., Povilaitytė, D., Meškys, R., Aučynaitė, A. TudS Domain-Containing Fusion Proteins Act as tRNA Demodifying Enzymes. 18th Microsymposium on RNA Biology, April 24-06, 2024, Vienna, Austria.

CURRICULUM VITAE

Name: Rapolas Jamontas

Date of birth: 1994 11 23

Work address: Department of Molecular Biology and Biotechnology, Institute of Biochemistry, Life Sciences Centre, Vilnius University, Saulėtekio av. 7, LT-10257, Vilnius, Lithuania

EDUCATION

- 2020 – 2024 **Vilnius University, PhD student in biochemistry**
PhD thesis: Demodification by TudS Proteins: From Individual Thionucleobases to Intact tRNA
Location: Department of Molecular Biology and Biotechnology, Institute of Biochemistry, Life Sciences Centre, Vilnius University.
Supervisors: Agota Aučynaitė, PhD, Prof. Rolandas Meškys, PhD
Consultants: Agota Aučynaitė, PhD, Prof. Rolandas Meškys, PhD
- 2017 – 2019 **Vilnius Gediminas Technical University, Master of Bioengineering**
Master thesis: Pathogenicity Assessment of Pendrin (SLC26A4) Variants
Supervisor: Priv.-Doz. Silvia Dossena, PhD
- 2013 – 2017 **Vilnius Gediminas Technical University, Bachelor of Bioengineering**
Bachelor thesis: Investigation of Enzymes Involved in the Catabolism of Modified Uridines
Supervisor: Agota Aučynaitė, PhD

RESEARCH EXPERIENCE

- 2020/10-present **Department of Molecular Biology and Biotechnology, Institute of Biochemistry, Life Sciences Centre, Vilnius University**
- 2018/06-2019/10 **Paracelsus Medical University of Salzburg, Institute of Pharmacology and Toxicology, Austria**
- 2017/10-2018/04 **Vilnius Gediminas Technical University, Faculty of Fundamental Sciences, Department of Chemistry and Bioengineering, Lithuania**
- 2016/04-2017/02 **Department of Molecular Biology and Biotechnology, Institute of Biochemistry, Life Sciences Centre, Vilnius University**

INDUSTRY EXPERIENCE

- 2020/01-2021/05 **Thermo Fisher Scientific Baltics, Lithuania,**
Junior scientist
MTEPC GSD, Microarray group

TEACHING EXPERIENCE

- 2021/10-present **Vilnius University, Lithuania**
Teaching assistant

Enzymology, laboratory course

2024/11-present

Vilnius University, Lithuania
Teaching assistant
Gene engineering, laboratory course

EMPLOYMENT IN PROJECTS

2021/06-2023/08

Research Council of Lithuania grant “Selective enzymatic system for prodrug activation”
Specialist

2022/11-2023/08

European Union funded project “Optimizing the network of higher education institutions and improving the quality of studies by merging Šiauliai University with Vilnius University”
Expert

TRAINEESHIPS

2018-2019

ERASMUS+, 8,5 months of traineeship in Austria (Paracelsus Medical University of Salzburg, Austria).

2022

ERASMUS+, 4 months of traineeship in Germany (Albert Ludwig University of Freiburg, Germany).

PUBLICATIONS

- Fuchs, J.*, **Jamontas, R.***, Hoock, M. H., Oltmanns, J., Golinelli-Pimpaneau, B., Schünemann, V., Pierik, A. J., Meškys, R., Aučynaitė, A. and Boll, M. (2023) TudS desulfidases recycle 4-thiouridine-5'-monophosphate at a catalytic [4Fe-4S] cluster. *Commun. Biol.*, **6(1)**, 1092.

*- These authors contributed equally

- **Jamontas, R.**, Laurynėnas, A., Povilaitytė, D., Meškys, R. and Aučynaitė, A. (2024) RudS: bacterial desulfidase responsible for tRNA 4-thiouridine de-modification. *Nucleic Acids Res.*, **52(17)**, 10543-10562.

POSTER PRESENTATIONS

- **Jamontas R***, Bernardinelli E, Matulevicius A, Rösch S, Patsch W, Rasp G, Sarikas A, Dossena S. „Assessment of functional and molecular features of pendrin (SLC26A4) variants found in the first Austrian cohort with hearing loss and enlarged vestibular aqueduct“. Abstract No. 105; Paracelsus Science Get Together Abstractband 2019, 28.06.2019. ISBN: 978-3-00-056506-9.
- **Bernardinelli E***, **Jamontas R**, Patsch W, Sarikas A, Dossena S. „Proteasomal inhibition results in augmented cellular expression and function of pendrin variants identified in patients with congenital hearing loss“. Abstract No. 94; Paracelsus Science Get Together Abstractband 2019, 28.06.2019. ISBN: 978-3-00-056506-9.

- **Dossena S***, Bernardinelli E, **Jamontas R**, Pan ZQ, Konrat R, Sarikas A. „Role of Cullin-RING E3 ubiquitin ligase CRL3Zbtb16 in the degradation of pathogenic pendrin variants“; Paracelsus Science Get Together "Virtual Science Summer" 17.8.2020.
- **Matulevičius A***, Bernardinelli E, **Jamontas R**, Avraham KB, Sarikas A, Dossena S. „Characterization of the human and murine pendrin (SLC26A4) variant p.L117F“; Paracelsus Science Get Together "Virtual Science Summer" 17.8.2020.
- **Jamontas R***, Aučynaitė A, Meškys R. „Endogenously expressed bacterial DUF523 proteins utilize 4-thiouracil and 4-thiouridine in vivo“; 47th FEBS Congress – „Together in bioscience for a better future“, 8-12.7.2023.
- **Jamontas R***, Fuchs J, Aučynaitė A, Boll M, Meškys R. „Bacteria recycle sulfur-modified nucleotides“; 5th Congress of Baltic Microbiologists, 11-13.10.2023
- **Jamontas, R***, Povilaitytė, D., Meškys, R., Aučynaitė, A. TudS Domain-Containing Fusion Proteins Act as tRNA Demodifying Enzymes. 18th Microsymposium on RNA Biology, 24-26.04.2024,

*Presenting author

ORGANIZATION OF SCIENTIFIC CONFERENCES

- 5th Congress of Baltic Microbiologists, 11-13.10.2023, Vilnius, Lithuania (Member of organizing comitee).

AWARDS

- Best Poster Award, Science Get Together (Paracelsus Medical University, Nuremberg, 28.06.2019), 500€ award.

SCIENTIFIC SUPERVISION

- Rokas Švelginas, bachelor student (molecular biology, Vilnius university, 2020-2021)
- Deimantė Povilaitytė, bachelor student (biochemistry, Vilnius university, 2022-2024)

LANGUAGE SKILLS

Language	Speaking	Understanding	Writing
English	C1	C1	C1
Russian	A2	B1	A2
German	B1	B1	A2
Lithuanian	Mother tongue		

SANTRAUKA

1. SANTRUMPOS

4-thio-UMP	4-tiouridino-5'-monofosfatas
4-thio-UTP	4-tiouridino-5'-trifosfatas
DUF1722	Nežinomos funkcijos domenas 1722
DUF523	Nežinomos funkcijos domenas 523
s4U	4-tiouridinas
UVA	320–400 nm UV bangos
UVB	280–320 nm UV bangos
UVC	100–280 nm UV bangos

2. ĮVADAS

Nukleorūgštys – funkciškai ir struktūriškai labai įvairios molekulės. Nenuostabu, kad vien įprastinių struktūrinių komponentų nepakanka tokiai gausybei funkcijų įgyvendinti. Ko gero tinkamiausias to pavyzdys yra transportinė RNR (tRNR). Šios molekulės yra neatsiejama baltymų sintezės dalis, ir nors tarpusavyje yra struktūriškai panašios, skirtingų rūšių tRNR turi unikalių savybių, leidžiančių joms dalyvauti itin specifinėse sąveikose. Be nukleotidų sekos, skirtingų tRNR unikalumą lemia jų potranskripcinės cheminės modifikacijos, kurių šiuo metu yra žinoma daugiau nei 100. Modifikacijos leidžia tRNR molekulėms įgauti tinkamą tretinę struktūrą, išlaikyti termodinaminį stabilumą, tiksliai dekoduoti informacinę RNR (iRNR) bei užtikrinti specifinę molekulių sąveiką.

Be įprastinių funkcijų baltymų sintezėje užtikrinimo, kai kurios potranskripcinės modifikacijos tRNR suteikia savybių, leidžiančių šiai molekulei dalyvauti ir kituose ląsteliniuose procesuose. Viena iš tokių modifikacijų – prokariotuose aptinkamas nukleozidas 4-tiouridinas (s4U). Kaip ir daugelis kitų modifikacijų, jis didina tRNR stabilumą bei dalyvauja tinkamos struktūros formavime, užtikrinančiame molekulės funkcionalumą. Be to, s4U modifikacija atlieka svarbų vaidmenį bakterijų tRNR kokybės kontrolėje: jo neturinčios molekulės yra degraduojamos. O dėl savo foto reaktyvumo, šis nukleozidas gali veikti kaip ultravioleto (UV) jutiklis, reguliuojantis bakterijų atsako į stresą mechanizmus.

Nors pagal masę tRNR molekulės nesudaro didžiosios visų bakterijų RNR dalies, tačiau jų skaičius kelis kartus viršija bet kokių kitų žinomų RNR rūšių. tRNR molekulės yra santykinai stabilios, tačiau tam tikromis fiziologinėmis sąlygomis gali vykti jų degradacija. Jos metu ląstelės citozolyje ir aplinkoje atsiranda daugybė tRNR irimo produktų – tarp jų ir modifikuotų nukleozidų. Kanoninių nukleozidų metabolizmo keliai yra gerai ištyrinėti, o apie modifikuotų nukleozidų likimą kol kas žinoma dar nedaug. Vis dėlto, pastaraisiais metais keletas fermentų, dalyvaujančių modifikuotų nukleozidų skaidymo keliuose, buvo atrasta.

Vienas iš jų – tiouracilo desulfidazė TudS, kuri katalizuoja 2-tiouracilo ir 4-tiouracilo vertimą kanoniniu uracilu *in vivo*. Išskyrus šias reakcijas, nei TudS fermento substratų spektras, nei galima fiziologinė funkcija nebuvo žinomi iki pradedant tyrimus, aprašytus šioje daktaro disertacijoje. Be to, šis prokariotuose paplitęs fermentas genomuose neretai būna koduojamas sulietas su nežinomos funkcijos domenu 1722 (DUF1722), apie kurio funkciją ir/ar įtaką TudS domenui iki šiol nebuvo sukaupta jokių duomenų.

Šio darbo tikslas buvo tirti TudS ir TudS-DUF1722 (RudS) baltymų biochemines savybes ir jų galimas fiziologines funkcijas.

Darbo uždaviniai:

1. Įvertinti TudS baltymų substratinį specifiškumą.
2. Nustatyti galimą fiziologinę TudS funkciją bakterijose.
3. Identifikuoti RudS (TudS-DUF1722) baltymų fermentinį aktyvumą.
4. Nustatyti RudS baltymų katalizinį mechanizmą.
5. Nustatyti RudS-tRNR sąveikos mechanizmą.
6. Nustatyti galimą fiziologinę RudS funkciją bakterijose.

Mokslinis naujumas:

Šiame darbe biochemiškai charakterizuoti du prokariotuose paplitę TudS domeną turintys baltymai – TudS ir RudS – taip praplečiant fundamentines biochemijos žinias. Be to, pasiūlytos galimos šių baltymų fiziologinės funkcijos. Tyrimo metu parodyta, kad anksčiau netyrinėtas nežinomos funkcijos domeną DUF1722 dalyvauja RudS baltymo sąveikoje su tRNR molekule.

Iki TudS charakterizavimo, apie bakterijų vykdomą tiomodifikuotų nukleozidų katabolizmą žinoma nebuvo. Šio tyrimo metu nustatyta, kad pavienį TudS domeną turintys baltymai yra 4-tio-UMP desulfidazės. Be to, buvo pademonstruota, kad *tudS* geno raiška įgalina bakterijas panaudoti išorinius 4-tiouracilo turinčius junginius kaip uracilo šaltinį. Kadangi kai kurie iš šių junginių yra toksiški bakterijoms, buvo iškelta hipotezė, jog jų vertimas kanoniniais junginiais tuo pačiu veikia ir kaip aplinkos detoksikacija, kas pagrindžia fiziologinę pavienių TudS domenų funkciją: 4-tiomodifikuotų nukleobazių, nukleozidų ir nukleotidų perdirbimą.

Šiame tyrime taip pat charakterizuotas RudS fermentas: TudS ir DUF1722 domeną turintis sulietas baltymas, demodifikuojantis 4-tiouridino tRNR molekulėje. RudS yra mūsų žiniomis pirmasis pasaulyje identifikuotas bakterinis specifiškai veikiantis tRNR demodifikuojantis fermentas. Iki šiol iš fermentų, gebančių demodifikuoti tRNR, buvo žinomos tik eukariotinės demetilazės. Taip pat, šio darbo metu atlikti eksperimentai parodė, kad RudS sutrumpina UV poveikio sukeltą bakterijų augimo delną, kas byloja apie RudS fiziologinę funkciją bakterijų atsake į UV sukeltą stresą.

Praktinė vertė:

Antimikrobinės 4-tiouridino savybės jau buvo žinomos anksčiau (1). Šiame tyrime buvo patvirtinta, kad 4-tiouracilas ir 4-tiouridinas gali sulėtinti

tam tikrų laukinio tipo bakterijų augimą, ir pademonstruota, kad aplinkoje esant 4-tiouridino, *tudS* geno pašalinimas visiškai sustabdo *Bacillus subtilis* augimą. Nustačius TudS inhibitorių ir sukombinavus jį su 4-tiouridinu, ši mišinį būtų galima panaudoti kaip baktericidą arba bakteriostatiką tam tikram bakterijų spektrui kaip alternatyvą dabar naudojamoms priemonėms.

UV spinduliuotė yra plačiai naudojama dezinfekcijos priemonė (2). Šio tyrimo metu identifiкуotas RudS aktyvumas ir galima 4-tiouridino, veikiančio kaip bakterinis UV jutiklis, reguliacija šiuo fermentu siekiant išvengti kenksmingo UV poveikio. Tai galėtų paaiškinti tam tikrų bakterijų didesnę atsparumą UV spinduliuotei. Taip pat, taikant UV spinduliuotę žinomų bakterijų rūšių dezinfekcijai, reikėtų atsižvelgti ir į tai, ar jų genomuose nėra koduojami RudS fermentai: žinant apie tikėtiną didesnę atsparumą UV būtų galima rinktis alternatyvią dezinfekcijos priemonę.

Ginamieji disertacijos teiginiai:

1. TudS baltymai katalizuoja 4-tiouracilo darinių desulfidinimą ir yra aktyviausi su 4-tio-UMP.
2. TudS baltymai leidžia bakterijoms panaudoti 4-tiouracilo darinius kaip uracilo šaltinį.
3. RudS (TudS-DUF1722) baltymai yra tRNR 4-tiouridino demodifikuojantys fermentai.
4. RudS katalizinis mechanizmas atitinka TudS, jo aktyvumas priklauso nuo [4Fe-4S] klasterio.
5. RudS baltyme esantis DUF1722 domenas sąveikauja su tRNR antikodono stiebu ir kilpa, o katalizinis TudS domenas – su kintamąja kilpa, akceptorius stiebu bei D kilpa ir stiebu.
6. RudS baltymas sutrumpina UVA sukeltą augimo delną bakterijose.

3. METODAI

Plazmidiniai vektoriai buvo konstruojami standartiniais molekulinės biologijos metodais, naudojantis komerciniais rinkiniais. Uracilo auktrofinių bakterijų kultivavimas vykdytas minimalioje terpėje, kitų bakterijų kultivavimas vykdytas standartiškai arba su pakeitimais nurodytais disertacijoje. Rekombinantinių baltymų gryninimas vykdytas aerobiškai ir anaerobiškai naudojantis FPLC skysčių chromatografijos sistema. Fermentinis TudS baltymo aktyvumas anaerobiškai buvo matuojamas spektrofotometru arba pasitelkiant didelio efektyvumo skysčių chromatografiją (HPLC). tRNR iš bakterinių kultūrų buvo išskirtos rūgštiniu fenoliu ir išgrynintos FPLC skysčių chromatografijos sistema. tRNR nukleozidai buvo analizuojami hidrolizuojant tRNR ir naudojantis tandeminę masių spektrometriją, matavimų rezultatai buvo normalizuojami pagal detektuoto dihidrouridino kiekį. Western hibridizacija su bakteriniais lizatais buvo atliekama naudojant anti-His-Tag antikūnus. Elektroforezinio judrio poslinkio tyrimas buvo atliekamas neradioaktyviu metodu agaroziniame gelyje. UVA apšvietos tyrimai buvo atliekami uždaroje talpoje naudojant 365 nm UV lempą. Šie metodai detalai aprašyti disertacijoje ir susijusiose publikacijose.

Plazmidžių konstravimui naudotas *Escherichia coli* DH5 α kamienas, rekombinantinių baltymų sintezei naudoti *Escherichia coli* BL21(DE3), *Escherichia coli* BL21(DE3) Δ iscR ir *Pseudomonas putida* KT2440 kamienai. Rekombinantinių TudS ir RudS aktyvumai tirti uracilo auktrofiniame *Escherichia coli* HMS174(DE3) Δ pyrF kamiene. Mutantinių kamienų konstravimui naudotas *Pseudomonas putida* KT2440 kamienas. 4-tiouracilo darinių įtaka bakterijų augimui tirta naudojantis *Bacillus subtilis* subsp. *subtilis* 168 ir *Bacillus subtilis* subsp. *subtilis* 168 Δ ybbK::erm kamienus. Tiriamieji TudS ir RudS koduojantys genai buvo klonuoti iš *Pseudomonas* sp. MIL9, *Pseudomonas* sp. MIL19, *Pseudomonas putida* KT2440, *Salmonella enterica* subsp. *enterica* serovar *Typhimurium* LT2 Δ pyrF ir *Thermus thermophilus* HB8. RudS_{vir} koduojantis genas buvo susintetintas Thermo Fisher Scientific (JAV).

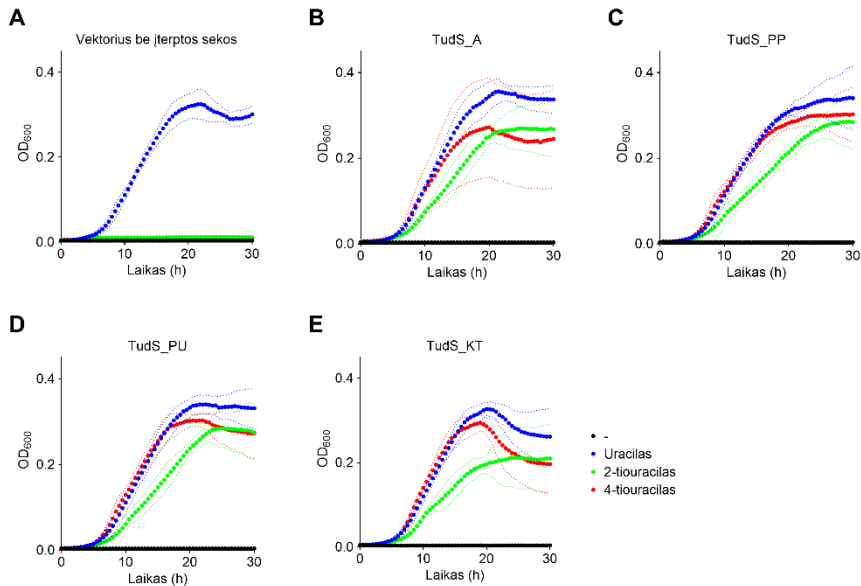
4. REZULTATAI

4.2 TudS funkcijos tyrimas

Ankstesnių tyrimų metu Dr. A. Aučynaitė ir kolegės nustatė nežinomos funkcijos domenų 523 (DUF523) turinčių baltymų aktyvumą verčiant 2-tiouracilą ir 4-tiouracilą uracilu. Buvo nustatyta metagenominėse bibliotekose aptikto DUF523 iš *Aeromonas* sp. kristalinė struktūra, šis fermentas pavadintas TudS (šiam darbe – TudS_A). Siekiant patvirtinti, kad 2-tiouracilo ir 4-tiouracilo desulfidinimas yra bendra TudS baltymų savybė, trys papildomi TudS koduojantys genai buvo klonuoti iš laboratorijoje turimų *Pseudomonas* sp. bakterijų (1 lentelė).

1 lentelė. Tirti TudS baltymai.

Baltymas	Šaltinis	GeneBank nr. (189)	Geno ID
TudS_A	<i>Aeromonas</i> sp.	6Z92_A (146)	-
TudS_PP	<i>Pseudomonas</i> sp. MIL19	JAPVVG010000016	N1078_RS18190
TudS_PU	<i>Pseudomonas</i> sp. MIL9	JAFEHE010000014	JQF37_RS12420
TudS_KT	<i>Pseudomonas putida</i> KT2440	AE015451	PP_5158



1 pav. *E. coli* HMS174 $\Delta pyrF$ uracilo auksotrofinių augimo kreivės terpėje esant uracilo, 2-tiouracilo arba 4-tiouracilo. **A:** bakterijos neprodukuojančios rekombinantinio TudS (neigiama kontrolė). **B:** bakterijos produkuojančios TudS_A (teigiama kontrolė). **C:** bakterijos produkuojančios TudS_PP. **D:** bakterijos produkuojančios TudS_PU. **E:** bakterijos produkuojančios TudS_KT.

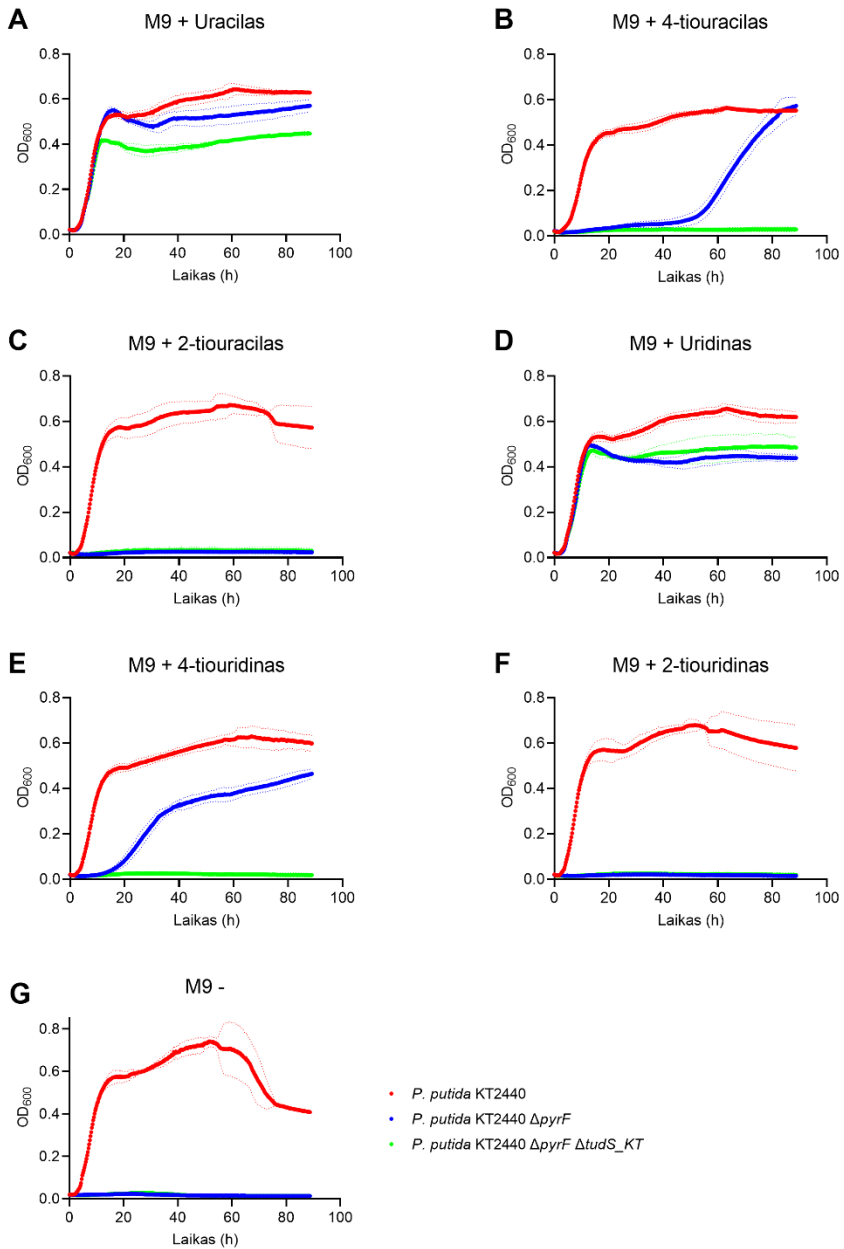
TudS homologus koduojančių genų fenotipai buvo tirti *E. coli* HMS174 $\Delta pyrF$ uracilo auktrofiniame kamiene. Šio bakterinio kamieno augimas yra priklausomas nuo išorinio uracilo šaltinio. Ankstesniuose tyrimuose buvo pademonstruota, kad TudS_A produkavimas leidžia šioms bakterijoms augti pasinaudojant 2-tiouracilu ir 4-tiouracilu kaip uracilo šaltiniu. Atlikus heterologinę tiriamųjų TudS homologus koduojančių genų raišką, visų bakterijų augimo fenotipas atitiko TudS_A fenotipą (1 pav.).

Norint išsiaiškinti fiziologinę TudS funkciją, tyrimams buvo pasirinktas *Pseudomonas putida* KT2440 kamienas, savo genome koduojantis *tudS* ir *tudS-DUF1722* genus. Darbo metu buvo sukurti 6 mutantiniai *P. putida* KT2440 kamienai, pateikti 2 lentelėje. Šie kamienai naudoti ir bandymams, aprašytiems tolimesniuose skyriuose.

2 lentelė. Sukurti *Pseudomonas putida* KT2440 mutantiniai kamienai.

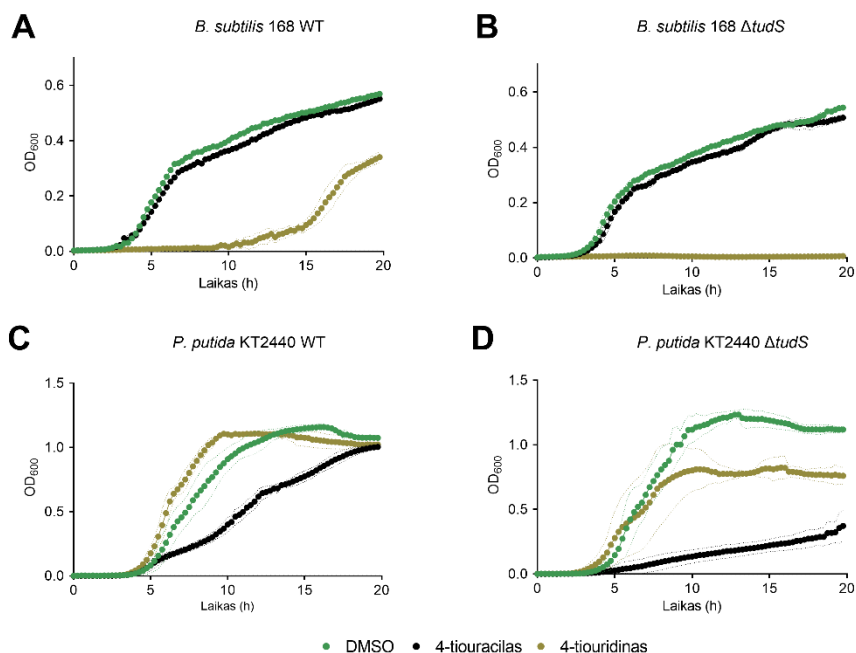
Kamienas	Savybės
<i>P. putida</i> KT2440 $\Delta thil$	Kamienas nesintetinis s4U
<i>P. putida</i> KT2440 $\Delta tudS$	Kamienas neturintis <i>tudS</i> geno
<i>P. putida</i> KT2440 $\Delta tudS-DUF1722$	Kamienas neturintis <i>tudS-DUF1722</i> geno
<i>P. putida</i> KT2440 $\Delta tudS-DUF1722 \Delta tudS$	Kamienas neturintis <i>tudS</i> ir <i>tudS-DUF1722</i> genų
<i>P. putida</i> KT2440 $\Delta pyrF$	Uracilo auktrofas
<i>P. putida</i> KT2440 $\Delta pyrF \Delta tudS$	Uracilo auktrofas neturintis <i>tudS</i> geno

Po bandymų *E. coli* uracilo auktrofuose su padidinta rekombinantinių TudS koduojančių genų raiška, siekta išsiaiškinti ar endogeninė *tudS* geno raiška yra pakankama uracilo auktrofų augimui panaudojant egzogeninį 2-tiouracilą arba 4-tiouracilą. Šiam tyrimui buvo panaudoti uracilo auktrofai su TudS baltymą koduojančiu genu ir be jo. Atkartojant ankstesniame skyriuje aprašytas sąlygas, *P. putida* KT2440 $\Delta pyrF$ ir *P. putida* KT2440 $\Delta pyrF \Delta tudS$ mutantiniai kamienai buvo auginti minimalioje terpėje su tiouracilo dariniais. Uracilo auktrofai koduojantys *tudS* geną gebėjo augti panaudojant 4-tiouracilą ir 4-tiouridiną kaip uracilo šaltinį, tačiau priešingai nei anksčiau tirti *E. coli* auktrofai, 2-tiouracilo darinių nepanaudojo (2 pav.).



2 pav. Laukinio tipo *P. putida* KT2440 (raudona), *P. putida* KT2440 $\Delta pyrF$ (mėlyna) ir *P. putida* KT2440 $\Delta pyrF \Delta tudS_KT$ (žalia) augimo kreivės minimalioje terpėje su: **A:** uracilu (teigiama kontrolė); **B:** 4-tiouracilu; **C:** 2-tiouracilu; **D:** uridinu; **E:** 4-tiouridinu; **F:** 2-tiouridinu; **G:** be priedų (neigiama kontrolė).

Apie antimikrobines 4-tiouridino savybės yra žinoma nuo seno (1). Norint išsiaiškinti, ar *tudS* geno delecija turi įtakos toksiškam 4-tiouracilo ir 4-tiouridino efektui, buvo stebimas laukinio tipo ir *tudS* geno deleciją turinčių *P. putida* KT2440 ir *B. subtilis* 168 bakterijų augimas. Tyrimo metu pastebėtas toksiškas 4-tiouridino efektas *B. subtilis* 168 bakterijoms ir toksiškas 4-tiouracilo efektas *P. putida* KT2440, pasireiškiantis augimo sulėtėjimu. Šis efektas buvo labiau išreikštas *tudS* geno neturinčiuose *P. putida* KT2440 bakterijose. *B. subtilis* 168 bakterijos su pašalintu *TudS* koduojančiu genu terpėje su 4-tiouridinu neaugo iš viso (3 pav.).



3 pav. *Pseudomonas putida* KT2440 ir *Bacillus subtilis* 168 bakterijų augimo kreivės LB terpėje esant DMSO (tirpiklis, žalia), 100 μ M 4-tiouracilo (juoda) arba 100 μ M 4-tiouridino (chaki). **A:** laukinio tipo *B. subtilis* 168 augimo kreivė. **B:** *B. subtilis* 168 $\Delta tudS$ augimo kreivė. **C:** laukinio tipo *P. putida* KT2440 augimo kreivė. **D:** *P. putida* KT2440 $\Delta tudS$ augimo kreivė.

Nors esant *TudS* baltymus koduojančių genų raiškai stebimas tiouracilo ir tiouridino panaudojimas *in vivo*, šių fermentų substratinis specifiskumas buvo nenustatytas. Atlikus preliminarinius aktyvumo tyrimus *in vitro*, pastebėta, kad iš turimų *TudS* baltymų, *TudS*_{PP} yra labiausiai tinkamas grynimui ir charakterizavimui. Dėl geležies–sieros klasterio jautrumo deguoniui, šis baltymas buvo gryninamas griežtai anaerobinėmis sąlygomis. Išgrynintas baltymas pasižymėjo $[4Fe-4S]^{2+}$ būdingoms spektro savybėms, vidutiniškai turėjo 2.99 ± 0.23 molius geležies vienam moliiui baltymo ir gelfiltracijos

chromatografijos metodu buvo nustatyta 19.6 ± 0.1 kDa TudS_PP molekulinė masė, atitinkanti monomerinę baltymo sandarą (teorinė baltymo masė ≈ 18.5 kDa).

Tyrimo metu pastebėta, kad TudS_PP fermentinis aktyvumas su 2-tiouracilu in vitro yra nespecifinis ir neatitinka Michaelis-Menten kinetikos. Didžiausią specifiškumą šis fermentas pademonstravo (mažėjimo tvarka): 4-tio-UMP, 4-tio-UTP, 4-tiouridinui ir 4-tiouracilui. TudS_PP kinetiniai parametrai, kartu su TudS_A kinetiniais parametrais išmatuotais kolegų, yra pateikti 3 lentelėje.

3 lentelė. TudS_PP ir TudS_A kataliziniai parametrai.

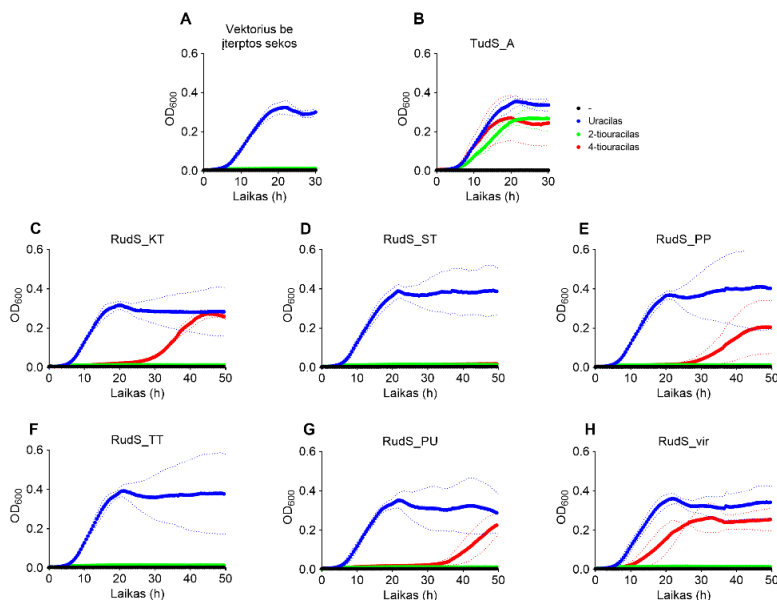
Fermentas	Substratas	k_{cat} (s^{-1})	K_m (mM)	k_{cat}/K_m ($M^{-1} s^{-1}$)	V_{max} (U mg^{-1})
TudS_A TudS_P	4-tiouracilas	0.70 \pm 0.05 4.93 \pm 0.43	0.24 \pm 0.03 1.49 \pm 0.27	2.90×10^3 3.27×10^3	2.4 \pm 0.2 15.9 \pm 1.4
TudS_A TudS_P	4-tiouridinas	8.8 \pm 0.9 19.9 \pm 4.7	3.1 \pm 0.6 0.2 \pm 0.09	2.88×10^3 1.03×10^5	30.1 \pm 3.1 64.3 \pm 15.3
TudS_A TudS_P	4-tiouridino monofosfatas	293 \pm 44 138 \pm 16	0.038 \pm 0.013 0.020 \pm 0.007	7.77×10^6 7.63×10^6	1000 \pm 149 447 \pm 51
TudS_A TudS_P	4-tiouridino trifosfatas	68.6 \pm 3.4 52.3 \pm 2.4	0.100 \pm 0.023 0.117 \pm 0.026	6.85×10^5 4.48×10^5	234 \pm 12 168 \pm 8

4.2 RudS funkcijos tyrimas

Rezultatai pateikti ankstesniuose skyriuose parodė, kad visi tirti TudS homologai pasižymi fenotipu leidžiančiu uracilo auksotrofams augti panaudojant išorinį 2-tiouracilą ir 4-tiouracilą kaip uracilo šaltinį. Norint patikrinti ar TudS-DUF1722 (RudS) baltymai pasižymi tokiomis pačiomis savybėmis kaip TudS, 5 RudS koduojantys genai buvo klonuoti iš bakterijų genomų ir 1 virusinės kilmės genas buvo susintetintas pasinaudojant duomenų bazėje anotuota fago genomo seka. Tirtų RudS baltymų sąrašas pateiktas 4 lentelėje.

4 lentelė. Tirti RudS baltymai.

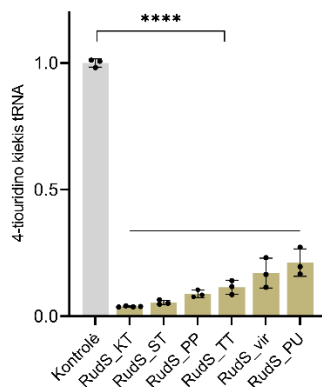
Baltymas	Šaltinis	GeneBank nr. (189)	Geno ID
RudS_KT	<i>Pseudomonas putida</i> KT2440	AE015451	PP_0741
RudS_TT	<i>Thermus thermophilus</i> HB8	AP008227	TTHB112
RudS_ST	<i>Salmonella enterica</i> subsp. <i>enterica</i> LT2	AE006468	STM1389
RudS_PU	<i>Pseudomonas</i> sp. MIL9	JAFEHE010000014	JQF37_16640
RudS_PP	<i>Pseudomonas</i> sp. MIL19	JAPPVG010000016	N1078_12140
RudS_vir	<i>Escherichia</i> phage 1H12	NC_049947	H3V29_gp66



4 pav. *E. coli* HMS 174 $\Delta pyrF$ produkuojančių RudS augimo kreivės. **A:** Rekombinantinių baltymų neprodukuojančios bakterijos (neigiama kontrolė). **B:** TudS_A produkuojančios bakterijos (teigiama kontrolė). **C:** RudS_KT produkuojančios bakterijos. **D:** RudS_ST produkuojančios bakterijos. **E:** RudS_PP produkuojančios bakterijos. **F:** RudS_TT produkuojančios bakterijos. **G:** RudS_PU produkuojančios bakterijos. **H:** RudS_vir produkuojančios bakterijos.

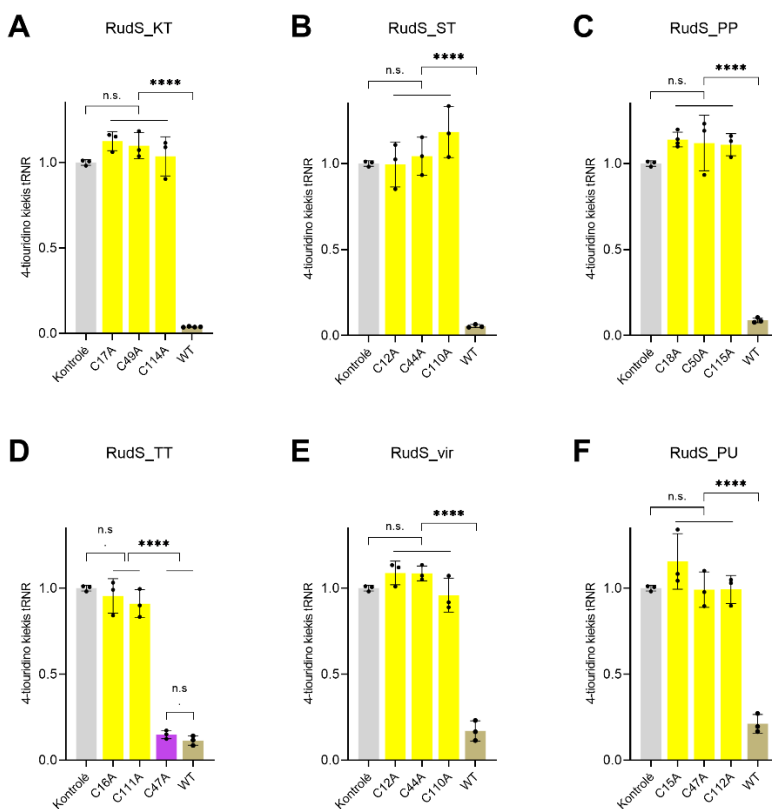
Norint palyginti TudS ir RudS fenotipus, rekombinantinius RudS baltymus produkuojantys uracilo auktrotrofai buvo auginti minimalioje terpėje į ją pridėdant 2-tiouracilo ir 4-tiouracilo. Rezultatai parodė, kad skirtingus RudS baltymus produkuojančios bakterijos pasižymėjo skirtingais fenotipais (4 pav.). Atvirkščiai nei TudS baltymų atveju, nei vienas tirtasis RudS nesugebėjo atstatyti augimo fenotipo terpėje esant 2-tiouracilui. Taip pat, RudS_ST ir RudS_TT nesugebėjo atstatyti augimo fenotipo ir su 4-tiouracilu. Likusius RudS baltymus produkuojančios bakterijos sugebėjo panaudoti 4-uracilą. RudS_vir eksponentinę augimo fazę su 4-tiouracilu pasiekė greičiausiai, o RudS_KT, RudS_PP ir RudS_PU produkuojančios bakterijos eksponentinę augimo fazę pasiekė gerokai vėliau, nei produkuojančios TudS_A. Šie rezultatai parodo, kad RudS baltymai turi tik dalinai į TudS panašų fenotipą arba jo iš viso neturi.

Kadangi TudS ir RudS pasižymi skirtingais fenotipais, iškelta hipotezė, kad šie baltymai turi turėti skirtingas funkcijas in vivo. Kadangi RudS baltymai turi TudS domeną, o 4-tiouridinas randamas tik prokariotinėje tRNR, buvo nuspresta patikrinti ar RudS turi įtakos tRNR 4-tiouridino kiekiui in vivo. Atlikus heterologinę RudS koduojančių genų raišką *E. coli* bakterijose, buvo išskirta jų suminė tRNR. Suminėje tRNR esančius nukleozidus kvantifikavus masių spektrometrijos metodu, pastebėta, kad bakterijų produkuojančių RudS baltymus tRNR žymiai sumažėja 4-tiouridino kiekis (5 pav.).



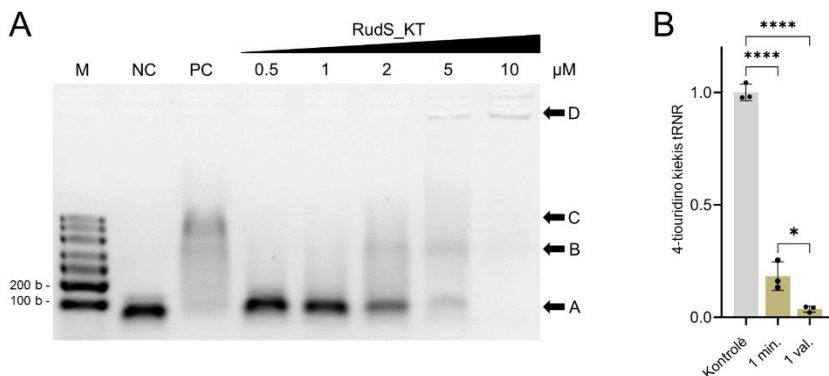
5 pav. 4-tiouridino kiekis *E. coli* BL21(DE3) bakterijos vyktant RudS koduojančių genų raišką. ****: $p < 0.0001$ lyginant su kontrole (vektorius be įterptos sekos) vienkrypte ANOVA su Dunnet pataisa.

Atsižvelgiant į TudS katalizinį mechanizmą, RudS aktyvumui taip pat turėtų būti būtinas [4Fe-4S] klasteris. RudS baltymų sekų palyginimas su TudS parodė, kad visi tiriami RudS baltymai turi konservatyvius cisteinus, randamus TudS homologueose ir formuojančius geležies–sieros klasterius. Tam, kad būtų patikrinta ar šių cisteinų liekanos yra būtinos ir RudS aktyvumui, visuose tiriamuose RudS baltymuose buvo atlikti vienos aminorūgšties pakeitimai keičiant konservatyvius cisteinus į alaninus. Mutantiniai baltymai produkuoti *E. coli* bakterijose, po to analizuotas 4-tiouridino kiekis šių bakterijų suminėje tRNR. Nukleozidų analizė parodė, kad beveik visais atvejais įvykdžius konservatyvių cisteinų pakeitimus į alaninus buvo prarastas RudS aktyvumas (6 pav.).



6 pav. 4-tiouridino kiekis *E. coli* BL21(DE3) bakterijų tRNR vyktant RudS su konservatyvių cisteinų pakeitimais genų raišką. ****: $p < 0.0001$, n.s. $p \geq 0.05$: lyginant su kontrole (vektorius be įterptos sekos) arba laukinio tipo (WT) baltymu vienkrypte ANOVA su Bonferroni pataisa.

Rekombinantinis RudS_KT fermentas pasižymėjo didžiausiu aktyvumu in vivo, taigi buvo nuspręsta jį išgryninti. Aerobiškai išgrynintas rekombinantinis RudS_KT baltymas pasižymėjo $[4\text{Fe-4S}]^{2+}$ būdingoms spektro savybėms, vidutiniškai turėjo $1,01 \pm 0,13$ molius geležies vienam moliui baltymo ir gelfiltracijos chromatografijos metodu buvo nustatyta $37,1 \pm 0,7$ kDa RudS_KT molekulinė masė, atitinkanti monomerinę baltymo sandarą (teorinė baltymo masė ≈ 39 kDa). Tiesioginė RudS_KT ir tRNR sąveika buvo pademonstruota elektroforezinio judrio poslinkio tyrimu (7 pav.). Vykdamt tRNR 4-tiouridino desulfidavimo reakciją in vitro su *E. coli* tRNR, 4-tiouridino kiekis tRNR per valandą sumažėjo ~ 95 proc. (7 pav.).

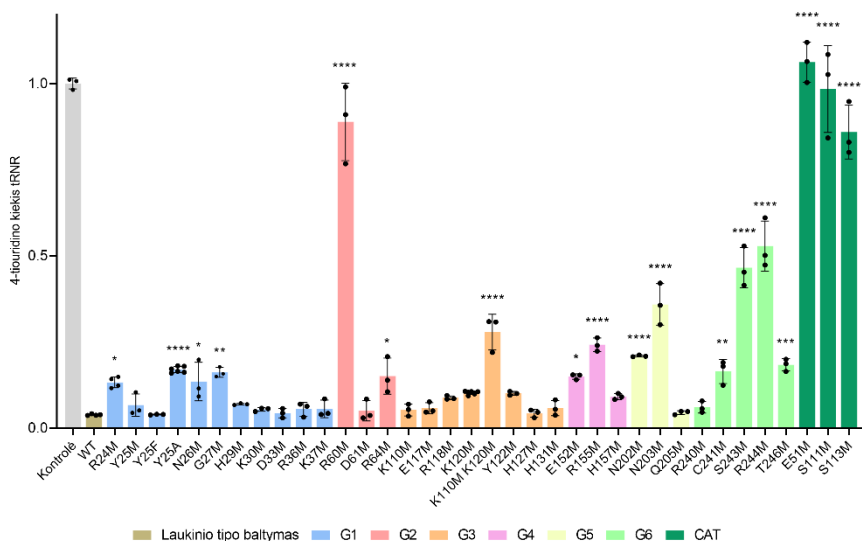


7 pav. A: RudS_KT ir tRNR elektroforezinio judrio poslinkio tyrimas. M – RNR masės standartas, NC – tRNA kontrolė, PC – teigiama poslinkio kontrolė (tRNR ir pseudouridino sintazė TruB 1:6 moliniu santykiu); 0.5–10 μM RudS_KT atitinka 1:1-1:20 tRNR-RudS_KT molinį santykį. Rodyklės: A – nesąveikavusi tRNR; B – tRNR-RudS_KT kompleksas. C: tRNR-TruB kompleksas. D: gelio šulinėliai. **B:** RudS_KT aktyvumas in vitro. ****: $p < 0.0001$, *: $p < 0.05$ vienkrypte ANOVA su Bonferroni pataisa.

RudS_KT sąveikos su tRNR ir už tai atsakingų aminorūgščių tyrimui įgyvendinti, RudS_KT–tRNR kompleksas buvo sumodeliuotas bioinformatiškai bei pasiūlytos už sąveiką su tRNR ir katalizę atsakingos aminorūgštys nurodytos 5 lentelėje. Bioinformatinę analizę atliko dr. Audrius Laurynėnas.

5 lentelė. Septynios bioinformatiniai metodais identifikuotos aminorūgščių grupės, potencialiai dalyvaujančios sąveikoje su tRNR ir/arba katalizėje.

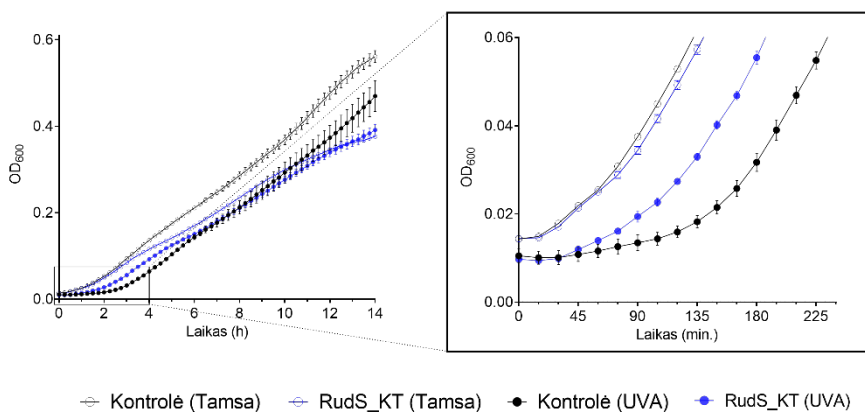
G1	G2	G3	G4	G5	G6	CAT
Arg24	Arg60	Lys110	Glu152	Asn202	Arg240	Glu51
Tyr25	Asp61	Glu117	Arg155	Asn203	Cys241	Ser111
Asn26	Arg64	Arg118	His157	Gln205	Ser243	Ser113
Gly27		Lys120			Arg244	
His29		Tyr122			Thr246	
Lys30		His127				
Asp33		His131				
Arg36						
Lys37						



8 pav. 4-tiouridino kiekis *E. coli* BL21(DE3) bakterijose vyktant RudS su aminorūgščių pakeitimais genų raišką. ****: $p < 0.0001$, ***: $p < 0.001$, **: $p < 0.01$, *: $p < 0.05$ lyginant su laukinio tipo (WT) baltymų vienkrypte ANOVA su Dunnett pataisa.

Buvo atlikti visų 5 lentelėje nurodytų aminorūgščių pakeitimai, mutantinių RudS_KT aktyvumas buvo patikrintas anksčiau minėtu metodu. Kiekvienoje iš tiriamųjų grupių buvo bent po vieną aminorūgštį, kurios pakeitimas sukėlė statistškai reikšmingą pokytį RudS_KT aktyvume. Konservatyvių aminorūgščių dalyvaujančių RudS vykdomoje katalizėje pakeitimas (Grupė CAT), paveikė RudS_KT aktyvumą labiausiai (8 pav.).

Norint išsiaiškinti galimą RudS baltymų fiziologinę funkciją buvo tiriamas tRNR 4-tiouridino demodifikacijos poveikis bakterijoms patiriančioms UVA apšvietą. Tyrimas rėmėsi hipoteze, jog demodifikavus 4-tiouridina, kuris veikia kaip UVA jutiklis bakterijų tRNR, bus sumažinta bakterijų augimo delsa po jų apšvietos UVA bangomis. Tiriamosios *E. coli* BL21(DE3) bakterijos produkuojančios ir neprodukuojančios RudS_KT buvo apšviestos apytiksliai 100 kJ/m² UVA doze.



9 pav. UVA sukelta *E. coli* BL21(DE3) augimo delsa ir jos sutrumpėjimas produkuojant RudS_KT. Pilnaviduriais simboliai pažymėtos UVA apšvitintų bakterijų augimo kreivės, tuščividuriais atinkamą laiką tamsoje laikytų bakterijų augimo kreivės. RudS_KT produkuojančių bakterijų kreivės melnyos, vektorių be įterptos sekos turinčių bakterijų kreivės juodos (neigiama kontrolė).

Kontrolines bakterijas apšvitinus UVA buvo stebima augimo delsa, kuri truko apie 105 minutes. Apšvitinus bakterijas produkuojančias RudS_KT augimo delsa sutrumpėjo iki 45 minučių (9 pav.).

5. IŠVADOS

1. TudS baltymai katalizuoja 4-tiouracilo darinių desulfidinimą ir yra aktyviausi su 4-tio-UMP.
2. TudS baltymai leidžia bakterijoms panaudoti 4-tiouracilo darinius kaip uracilo šaltinį.
3. TudS koduojantis genas *P. putida* ir *B. subtilis* bakterijose atsakingas už aplinkos detoksikaciją ir sumažina jų augimo inhibiciją 4-tiouracilo dariniais.
4. RudS (TudS-DUF1722) baltymai yra tRNR 4-tiouridiną demodifikuojantys fermentai.
5. RudS katalizinis mechanizmas atitinka TudS, jo aktyvumas priklauso nuo [4Fe-4S] klasterio.
6. RudS baltyme esantis DUF1722 domenas sąveikauja su tRNR antikodono stiebu ir kilpa, o katalizinis TudS domenas su kintamąja kilpa, akceptoriaus stiebu bei D kilpa ir stiebu.
7. RudS sintezė *E. coli* bakterijose sutrumpina UVA sukeltą augimo delną.

NOTES

NOTES

Vilniaus universiteto leidykla
Saulėtekio al. 9, III rūmai, LT-10222 Vilnius
El. p. info@leidykla.vu.lt, www.leidykla.vu.lt
bookshop.vu.lt, journals.vu.lt
Tiražas 15 egz.